

## Modelling

### Key points

- Empirical models have been developed to address the relationship between hourly mean  $\text{NO}_2$  and  $\text{NO}_x$  concentrations and annual mean  $\text{NO}_2$  and  $\text{NO}_x$  concentrations. The latter have had major application in air quality policy development with respect to achieving the annual mean air quality objective for  $\text{NO}_2$ .
- The validity of the cause and effect relationships implied in the national scale empirical model have been verified in physically-based process models and shown to result from the conversion of  $\text{NO}$  to  $\text{NO}_2$  by reaction with  $\text{O}_3$  and from the direct primary emission of  $\text{NO}_2$ .
- Comparisons between the national empirical model and dispersion models have been undertaken for locations in London. However, London is a special case in terms of geographical extent, emissions, high concentrations of  $\text{NO}_2$  and number of monitoring sites which has allowed optimum development of empirical schemes. Thus the conclusions of such comparisons may not be valid in other major cities where the empirical formulations may be based on very few monitoring sites. It is recommended that further comparisons should be performed in major cities with the highest annual average  $\text{NO}_2$  concentrations. It is recognised that such comparisons would be enhanced by more rural sites measuring both  $\text{NO}_x$  and  $\text{O}_3$ .
- There are a number of uncertainties that should be taken into account in assessing the policy conclusions concerning  $\text{NO}_2$  and  $\text{NO}_x$  based on empirical, dispersion and other physically-based process models. Emission estimates are a crucial source of uncertainty, particularly the mass fraction of  $\text{NO}_x$  emitted as  $\text{NO}_2$  and the likely future split between vehicle-kilometres travelled by petrol and diesel cars. Difficulties remain in representing urban influences on dispersion of primary  $\text{NO}_2$  and in representing the 3-dimensional distribution of  $\text{O}_3$  in urban areas which drives secondary  $\text{NO}_2$  formation.
- There remains uncertainty as to the detailed spatial distribution of  $\text{NO}_x$  and  $\text{NO}_2$  close to streets or junctions adjacent to buildings. There is a need for improved parameterisations in practical models which may be based on advanced building-resolving numerical models and measurements. There remains a basic incompatibility between the outputs derived from traffic counts and models, and the basic traffic input requirements of both emission and dispersion models. Emission and dispersion models require disaggregated data not just by type of vehicle (for example, passenger car, vans, heavy goods vehicles etc), but by fuel type, engine size and most significantly by vehicle age. It is these parameters, combined with vehicle speed, that are used to characterise the emissions associated with individual vehicles. Existing automated traffic counts and assignment models routinely provide traffic data in terms of axle counts and vehicle length subdivided into a number of vehicle length bins. The translation of these counts into corresponding emission categories undoubtedly introduces additional uncertainty.

- Advanced Eulerian and computational fluid dynamics (CFD) models complement the simpler deterministic and empirical models. The advanced models require very much greater computational resources, time, and data, but assist in the understanding of the complex interactions between processes that determine ground-level concentrations of NO<sub>2</sub>. For example, CFD examines the effect of the shape and separation of buildings, while the larger-scale models allow study of regional processes, the response of ground-level concentrations to vertical mixing and the development of the urban boundary layer.

## 5.1 Introduction

**468.** This chapter describes techniques for modelling and mapping pollutant concentrations at local, urban and regional scales. Although air quality monitoring generally provides reliable data on ambient concentrations of pollutants, monitored data only represent measurements that are made at specific locations at specific times. As such, these data alone provide limited information about the spatial extent of pollutant concentrations and how pollutant concentrations may change in the future. Policy requirements therefore necessitate some form of modelling to be undertaken to address these limitations and to fulfil the following roles:

- providing increased understanding of the relative importance of the different physical and chemical processes that result in NO<sub>2</sub> pollution levels. This includes both increased understanding of transport and dispersion and of the NO<sub>2</sub> to NO<sub>x</sub> relationships identified in the data;
- providing an assessment of NO<sub>2</sub> air quality through the generation of pollutant concentration maps for screening purposes for planned road and other development schemes, for example, using the approach in the Design Manual for Roads and Bridges (DMRB);
- interpolating NO<sub>2</sub> air quality data between monitoring sites and to map NO<sub>2</sub> air quality data over extended local, urban and regional scales;
- providing modelling tools to project NO<sub>2</sub> concentrations into the future and to study policy options and management activities for future NO<sub>x</sub> emission reductions;
- providing indirect verification or otherwise of emission inventories for NO<sub>x</sub>.

### 5.1.1 Modelling approaches

**469.** The Expert Group has not relied on one particular modelling approach but has used a variety of approaches and techniques depending on specific requirements. These requirements relate to the purpose of the exercise in terms of the level of accuracy required and the temporal and spatial scales under investigation.

**470.** Modelling methodologies can be categorised into two general types, namely empirically-based statistical models and physical process-based deterministic models. Deterministic models are based on mathematical formulations which describe the physical and chemical processes operating within the atmosphere, and which can be expressed at different levels of complexity. Some models combine both approaches; for example using a deterministic approach for the transport and dispersion of pollution, but statistical or empirically-based formulations to derive NO<sub>2</sub> concentrations from NO<sub>x</sub> concentrations. Each modelling approach is associated with a set of advantages and disadvantages which are discussed in greater detail in the individual sections within this chapter.

**471.** This diversity of models provides a pragmatic route forward because it is not practical in one model to cover all spatial scales from as small as a metre up to the national scale, and all timescales from less than an hour to annual. There is neither the UK-specific input data necessary to drive such a model, nor are there computers approaching the required capacity to run it. In the paragraphs below, a short introduction is given to a range of different models, followed by a more detailed description of their features and application in the UK to the development of air quality policy on NO<sub>x</sub>.

### 5.1.2 Empirically-based statistical models

**472.** Empirical models are based largely on air quality data. With the dramatic increase in the number of automatic continuous NO<sub>x</sub> monitoring sites during the 1990s, empirical models have become more robust and their coverage of the urban environments has become more extensive. They have been used extensively for policy support through their application to mapping current NO<sub>2</sub> levels and the exceedences of air quality targets and to the projections into the future of such levels and exceedences. The assumptions that correlations represent cause and effect and that regression parameters remain constant into the future, are their main weaknesses.

**473.** Although empirical models can be used for short-term predictions based on correlations between pollutant concentrations and meteorological variables these types of models are most reliable for longer term averages (for example, annual averages). In view of speed of calculation and reasonable accuracy they have been used extensively to model annual average concentrations of NO<sub>2</sub> across the UK. Specifically, for annual average NO<sub>x</sub> concentrations the large number of monitoring sites now available has allowed the contribution to the NO<sub>x</sub> concentration at a specific point to be modelled as three components:

- (i) a background based on rural data;
- (ii) an urban background component based on a regression analysis of dispersion modelling of relatively local emissions together urban background monitoring data;
- (iii) a roadside component which can be based on empirically derived formulations.

**474.** An alternative approach has also used dispersion modelling for the roadside component of the NO<sub>x</sub>, from which annual average NO<sub>2</sub> are then derived using empirically based formulae as discussed in section 5.2.2. This is the approach used by the screening model in the Design Manual for Roads and Bridges (DMRB) (Highways Agency, 2003).

**475.** Surface concentration modelling is a particular form of empirically-based modelling referring to the process of mapping continuous surface data solely from point-based measurements using interpolation procedures. This approach enables monitoring data to be used in exposure assessments in relation to both long-term patterns and short-term events, such as air pollution episodes. Interpolation procedures are also implicit in a number of other empirical models and dispersion models. As with the other modelling procedures outlined in this chapter, there is no universally agreed procedure to estimate concentration surfaces and the robustness of the method for a particular parameter depends on the nature of that parameter and the characteristics of the measurements made (for example, siting characteristics, sample locations and sample numbers). However, there are a number of techniques that are commonly employed to map the spatial distributions of air quality data and these are outlined later in the chapter.

### 5.1.3 Deterministic models

- 476.** Deterministic models range enormously in sophistication, type and application and include Gaussian plume models, Eulerian grid models, Lagrangian trajectory models and computational fluid dynamics (CFD) models.
- 477.** Gaussian plume models based on simple solutions of the diffusion equation are commonly used within the UK. They offer a practical and physically-based treatment of the dispersion of  $\text{NO}_x$  emitted from large point sources, such as power stations; from area-based sources, such as commercial, industrial and domestic sources; and from linear sources, such as motor vehicle traffic, using fixed plume geometries. They can represent many of the important chemical conversion processes and can treat most of the important spatial and temporal scales. Furthermore, their output in the form of maps provides a ready visualisation of the impacts of  $\text{NO}_x$  control policies on  $\text{NO}_2$  levels and air quality target exceedences. They are used extensively for local policy applications in the UK but have limited utility at the national scale due to computational and data requirements.
- 478.** Lagrangian trajectory models simulate the advection of individual air parcels by a three-dimensional wind flow. These models offer the prospect of a more detailed representation of the turbulence, convection and chemical processes influencing urban air quality. They share many of the advantages and disadvantages of complex deterministic models. They require large amounts of input data and the results of their model validation and verification studies are difficult to interpret. Most studies conducted so far with this type of model have represented motor vehicle sources at the 1 km x 1 km scale and this scale is too coarse to represent the detailed structure in the spatial distribution of  $\text{NO}_2$ .
- 479.** The most commonly used model type for urban air quality calculations in North America are numerical Eulerian grid models. Such models are also used for policy related assessment in Europe. These generally include both meteorological models to calculate mean flow and turbulence, and transport and diffusion models. These models generally require large amounts of input data and computer time and also produce large volumes of output data that can be difficult to interpret. Computer capacities currently limit the smallest horizontal grid sizes that can be utilised to about 1 km x 1 km, whilst integration periods are generally limited to a few days so that is not practical to calculate long term averages. The advantage of these models is their ability to include time varying meteorology in a detailed manner that allows analysis of pollutant episodes. This approach is also compatible with sophisticated chemistry routines.
- 480.** CFD models also solve the fluid dynamic equation, however their focus is on the detailed modelling of complex structure at the small scale (for example, street canyons). They are thus able to aid in understanding of local processes but are not appropriate for calculating concentrations of pollutant right across an urban area.
- 481.** The following sections of this chapter consider both empirical and deterministic models used in studies in the UK. These include widely used methodologies (for example, the National empirical model and ADMS-Urban) through to sophisticated models which have been used for particular case studies (for example, LRTCM trajectory models in London and UAM in Birmingham). A detailed discussion on  $\text{NO}_x$ : $\text{NO}_2$  relationships is also presented.

**482.** Table 5.1 describes some of the modelling techniques used in the UK by practitioners, policy makers and researchers. The table does not give model sub classes or version numbers but lists basic names only. Details of model version/developers/suppliers etc. may be found from the reference and/or from the web sites. Most European models are listed on the Model Documentation System: [http://air-climate.eionet.eu.int/databases/mds\\_search.html](http://air-climate.eionet.eu.int/databases/mds_search.html). US and some other models are also presented on the US-EPA web site: <http://www.EPA.gov/scram001/tt22.htm>.

**Table 5.1** Description of the main models and modelling techniques used in the UK for modelling NO<sub>2</sub> air quality<sup>1</sup>.

| Model  | Basic description  | Meteorology   | Transport and dispersion   | Chemistry                                      | Spatial scale   |
|--|--|---|--|--|---|
| <b>1. Empirical models, long term (annual) averages only</b> |  |   |  |  |   |
| DMRB (2003)<br>Highways Agency (2001)                        | Screening model for road traffic emissions and air quality | Fixed, at 2 m s <sup>-1</sup> equally distributed from all directions | Incorporates a fixed empirically adjusted Pasquill stability category  | NO <sub>x</sub> :NO <sub>2</sub> relationships | Local   |
| ERG<br>Carslaw <i>et al.</i> (2001)                          | All emission types; set-up for London                      | Different statistical analyses for different years                    | Regression analysis based on ADMS 3 calculations and monitoring data   | NO <sub>x</sub> :NO <sub>2</sub> relationships | Urban down to local scale including spatial variation at local street scale |
| NETCEN<br>Stedman <i>et al.</i> (2002)                       | All emission types   | Different statistical analyses for different years                    | Regression analysis based on ADMS 3 calculation and monitoring data for urban background; simple formulation for representative calculation on road segments | NO <sub>x</sub> :NO <sub>2</sub> relationships | National to suburban scale representative concentrations for road segments  |

<sup>1</sup> This table is intended only to indicate some of the different modelling techniques and models available. It makes no attempt to be exhaustive, and some commercial models have not been included. Omission of a model should not be inferred as conveying any opinion by the Air Quality Expert Group and, equally, inclusion does not constitute an endorsement by the Group.

| Model   | Basic description  | Meteorology                          | Transport and dispersion  | Chemistry  | Spatial scale  |
|---|--|--------------------------------------|---|--|--|
| 2. Models employing analytic expressions for concentration (for example, Gaussian models); long and short term average concentrations |  |                                      |   |  |  |
| ADMS<br>McHugh <i>et al.</i><br>(1997)  | Models for stationary source emissions and/or road traffic emissions | Hourly sequential data from one site | Quasi Gaussian type model using $h/M_{MO}$ parameterisation of boundary layer. Also includes trajectory model and canyon model based on OSPM approach | Generic reaction set   | Urban down to local, including spatial variation at local street scale |
| AERMOD<br>Lee <i>et al.</i> (1996)<br>US-EPA<br><a href="http://www.epa.gov/scram001">www.epa.gov/scram001</a>                        | Stationary source emissions  | Hourly sequential data from one site | Quasi Gaussian type model. $h/L_{MO}$ parameterisation of boundary layer  | O <sub>3</sub> limiting method                               | About 50 km down to local  |
| AIRVIRO   | All emission types   | Hourly sequential data or fields     | Gaussian plume model and Eulerian grid model for pollutant advection and dispersion   | Limited  | Urban to local   |
| CALINE<br>Benson (1979)<br>US-EPA<br><a href="http://www.epa.gov/scram001">www.epa.gov/scram001</a>                                   | Road traffic emissions   | Hourly sequential data               | Gaussian model. Pasquill parameterisation of boundary layer   | Discreet parcel method for NO <sub>2</sub> for some versions | Local  |
| CAR   | Road traffic emissions   |                                      |   |  | Street scale   |
| OSPM<br>Berkowicz <i>et al.</i><br>(1997)   | Road sources in street canyons                                       | Hourly sequential data               | Two component model – direct plume component and recirculation component  | Various  | Street canyon scale  |

| Model  | Basic description  | Meteorology  | Transport and dispersion  | Chemistry                                      | Spatial scale   |
|--|--|--|---------------------------|--|---|
| 3. Numerical models.   |  |  |                           |  |   |
| MM5-CMAQ/<br>Models 3  | Advanced nesting air quality model – US community model for air quality with focus on O <sub>3</sub> | MM5  | CMAQ                      | SMVGEAR model based on CBM-IV                  | Minimum 1 km resolution                               |
| EURAD  | Nested mesoscale transport model   | Mesoscale MM5  | Bott Advection scheme     | RADM2, CBM4.                                   | Grid size 2 to 80 km                                  |
| LRTC<br>Derwent (1999)   | Lagrangian column trajectory model   | Hourly sequential for 1995   | Trajectory model          | NO + O <sub>3</sub>                            | 1 x 1 km resolution                                   |
| MEMO   | Simulation of mesoscale air motion and passive pollution dispersion at local to regional scale       | Non hydrostatic model  | TVD scheme                | None   | Grid resolution 500-10,000 m<br>domain size 10-500 km |
| NAME   | Mesoscale model for pollutant dispersion   | Mesoscale model  | Lagrangian particle model | NO <sub>x</sub> :NO <sub>2</sub> relationships | 15 km x 15 km   |
| UAM  | Urban air quality model  | Generally requires mesoscale model as driver   | Eulerian scheme           | CBMIV  | Minimum 1 x 1 km                                      |
| 4. Computational fluid dynamics  |  |  |                           |  |   |
| For example,<br>CFX<br>FLUENT<br>STAR-CD<br>Galpin <i>et al.</i><br>(1985) | General purpose CFD  | Meteorology represented as 'upstream' profiles, finite volume techniques, range of turbulence parameterisation | Eulerian transport model  | Reaction schemes available                     | Local scale   |

## 5.2. Empirical models of NO<sub>x</sub> and NO<sub>2</sub> concentrations across the UK

### 5.2.1 The UK National Scale Empirical Model of NO<sub>2</sub> and NO<sub>x</sub>

#### 5.2.1.1 Introduction to the National Scale Empirical Model

**483.** Empirical models have been used by netcen to estimate both background and roadside annual mean NO<sub>x</sub> and NO<sub>2</sub> concentrations across the UK for the purposes of policy development within the UK. They are therefore relevant only to the conditions of the UK and to the time periods appropriate to the observations employed. Maps for 2001 have been prepared for the assessment of ambient concentrations in the UK required under the first Air Quality Daughter Directive (AQDD1) and can be projected to years such as 2005 and 2010 for baseline analysis and scenario testing (see section 7.3). Detailed descriptions of the modelling methods are available from earlier publications (Stedman *et al.*, 1997; Stedman *et al.*, 2001a; b; Stedman and Bush, 2000; Stedman *et al.*, 2002). A summary of the approach is provided here along with details of key aspects of the method. The methods used to calculate site-specific projections at monitoring site locations are also described.

**484.** A map of annual mean background NO<sub>x</sub> concentrations in 2001 has been built-up from contributions from:

- distant sources (characterised by the rural background concentration);
- large point sources;
- local area sources.

**485.** Hence, at locations away from busy roads NO<sub>x</sub> concentrations has been estimated as:

**Estimated background NO<sub>x</sub> concentration (µg m<sup>-3</sup>, as NO<sub>2</sub>) = corrected rural NO<sub>x</sub> concentration (µg m<sup>-3</sup>, as NO<sub>2</sub>) + contributions from major point sources (µg m<sup>-3</sup>, as NO<sub>2</sub>) + contributions from area sources (µg m<sup>-3</sup>, as NO<sub>2</sub>)**

**486.** At locations close to busy roads an additional roadside contribution is added to account for contributions to total NO<sub>x</sub> from road traffic sources.

**487.** Empirically derived conversion factors are then used to estimate the NO<sub>2</sub> concentrations from modelled NO<sub>x</sub> concentrations.

#### 5.2.1.2 Empirical relationships between NO<sub>x</sub> and NO<sub>2</sub> at background locations

**488.** The following relationships have been derived from monitoring data from 1998 to 2001 inclusive and are presented in Figures 5.1 and 5.2.

**Rural Background NO<sub>2</sub> [µg m<sup>-3</sup>] = 0.7835.NO<sub>x</sub> [µg m<sup>-3</sup>, as NO<sub>2</sub>]**

**(Elsewhere) Background NO<sub>2</sub> [µg m<sup>-3</sup>] = 1.9301.(NO<sub>x</sub> [µg m<sup>-3</sup>, as NO<sub>2</sub>])<sup>0.6887</sup>**

**Central London Background NO<sub>2</sub> [µg m<sup>-3</sup>] = 2.28.(NO<sub>x</sub> [µg m<sup>-3</sup>, as NO<sub>2</sub>])<sup>0.6887</sup>**

**489.** At rural background locations, the majority of NO<sub>x</sub> is present as NO<sub>2</sub>, because such areas are generally distant from sources, and oxidant (O<sub>3</sub>) is available in excess. In urban areas however, annual mean NO<sub>2</sub> concentrations are more limited by the availability of oxidant. From Figure 5.2 it is also notable that measured NO<sub>2</sub> concentrations in Central London are higher than in other

urban areas. This is thought to be due to the large size of the urban area, which enables relatively aged NO<sub>x</sub> from other parts of London to contribute to NO<sub>2</sub> in Central London.

**Figure 5.1** Relationship between annual mean NO<sub>x</sub> and NO<sub>2</sub> concentrations measured at rural background sites in the AURN 1998-2001.

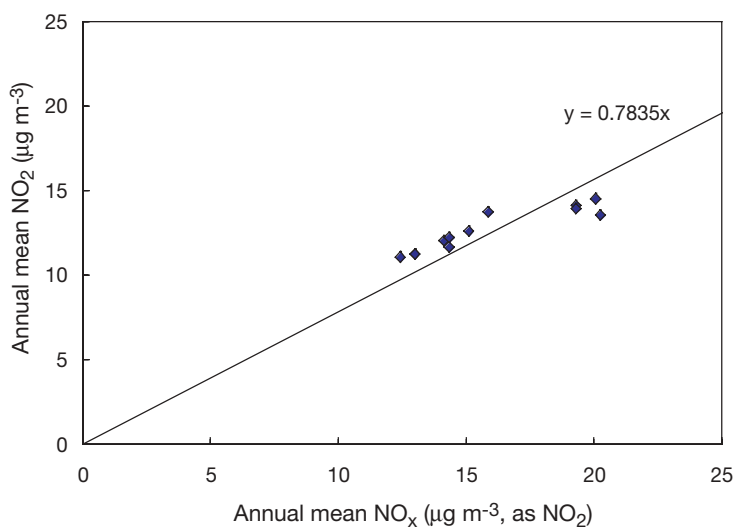
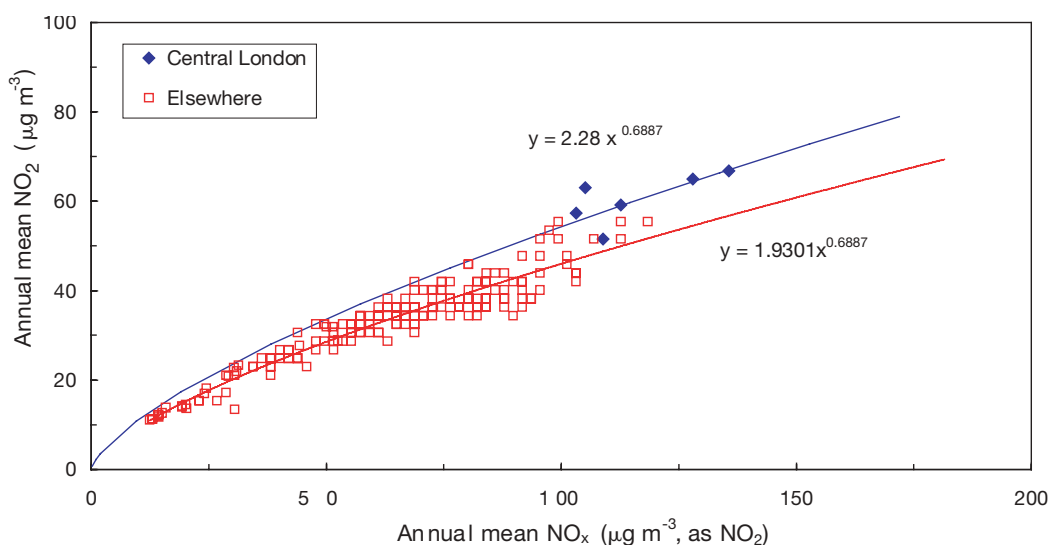


**Figure 5.2** Relationship between annual mean NO<sub>x</sub> and NO<sub>2</sub> concentrations measured at background sites in the AURN 1998-2001 with at least three years data.



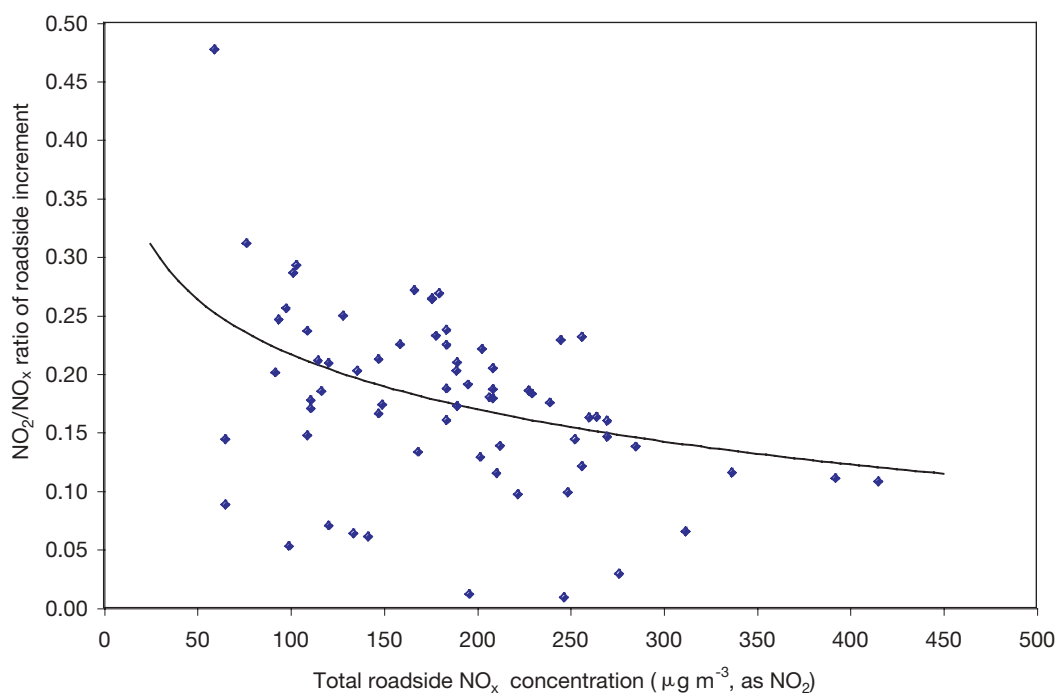
### 5.2.1.3 NO<sub>x</sub> to NO<sub>2</sub> relationships at roadside locations

**490.** Estimates of annual mean roadside NO<sub>2</sub> concentration have been calculated as the sum of the modelled background NO<sub>2</sub> concentration and an NO<sub>2</sub> roadside increment derived from a modelled NO<sub>x</sub> roadside increment using the following equation:

$$\text{NO}_2 \text{ Roadside increment } (\mu\text{g m}^{-3}) = \text{NO}_x \text{ Roadside increment } (\mu\text{g m}^{-3}, \text{ as NO}_2) \cdot (0.53 - 0.068 \cdot \ln(\text{total roadside NO}_x \text{ concentration } (\mu\text{g m}^{-3}, \text{ as NO}_2)))$$

**491.** This method (developed by Laxen and Wilson (2002b) from a method proposed by Stedman *et al.* (2001a)) takes into account that the  $\text{NO}_2/\text{NO}_x$  ratio at high  $\text{NO}_x$  locations (close to major roads) will be lower than the same ratio at lower  $\text{NO}_x$  areas as a result of oxidant limiting. The  $\text{NO}_x$  to  $\text{NO}_2$  relationship for the roadside increment is based on a natural logarithmic best-fit curve as shown in Figure 5.3. Thus the percentage of the roadside increment of  $\text{NO}_x$  represented by  $\text{NO}_2$  falls from about 25% at low total  $\text{NO}_x$  concentrations to about 10% at the highest concentrations close to busy roads in large urban areas.

**Figure 5.3** Relationship between the  $\text{NO}_x/\text{NO}_2$  ratio of the roadside increment and total roadside  $\text{NO}_x$  concentration at AURN and TRL road and kerbside sites 1999-2001.



#### 5.2.1.4 Detailed descriptions of the individual contributions from point sources

**492.** Contributions to ground level annual mean  $\text{NO}_x$  concentrations from point sources have been estimated by modelling each source explicitly using an atmospheric dispersion model (see Section 5.3). The contribution to annual mean  $\text{NO}_x$  concentrations from  $\text{NO}_x$  point sources with >250 tonnes per annum emission, was modelled using ADMS 3.1. Contributions from  $\text{NO}_x$  point sources with <250 tonnes per annum release were modelled using a dispersion matrix approach, at a 1 km receptor resolution. Each source was assumed to emit into a nominal 1 km x 1 km x 50 m volume.

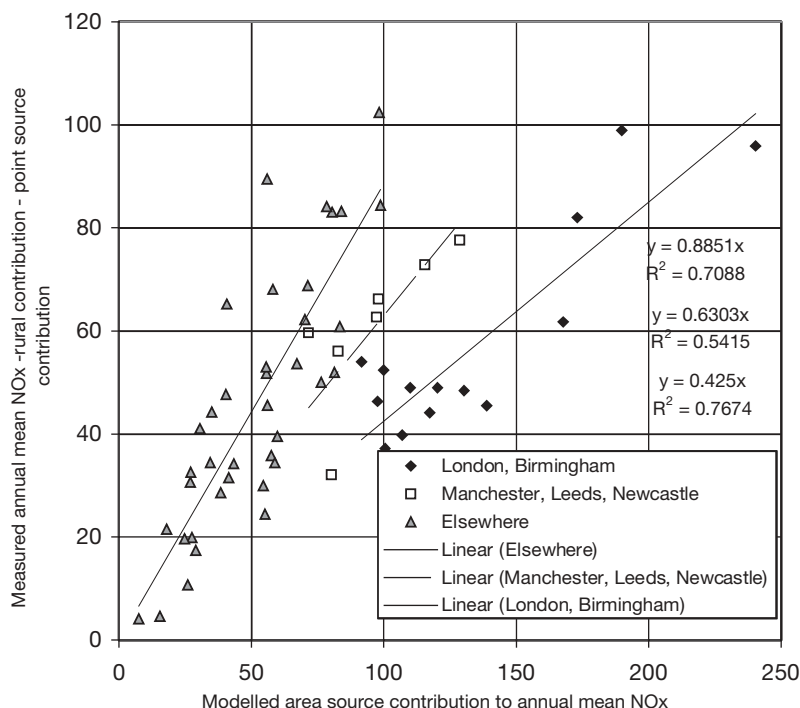
#### 5.2.1.5 Rural concentrations

**493.** Diffusion tube measurement data from the Acid Deposition Monitoring Network (Hayman *et al.*, 2001) were used to estimate rural annual mean background  $\text{NO}_2$  concentrations. In a number of instances, measurements from this network are influenced by contributions from nearby point and area sources. Care has been taken to avoid double counting these contributions. The contributions from point sources (as modelled explicitly) and area sources (estimated using the area source modelling methods described below but coefficients derived from earlier work) were subtracted prior to interpolation to obtain estimates of corrected regional background concentrations throughout the UK (section 5.6.4).

5.2.1.6 Area sources

494. An empirical model based method has been adopted to estimate the contribution to ambient concentrations from area sources. An ADMS-derived dispersion matrix has been applied to weight emissions from area sources within a 35 x 35 km square surrounding each monitoring site according to distance and direction of the emissions from the central receptor. 10-year average meteorological data from Heathrow has been used to construct this dispersion matrix and represents the contribution from unit emission in each 1 km x 1 km square to concentrations at the receptor. An example calibration plot for this area source model for 2001 is shown in Figure 5.4. The modelled point source and corrected rural NO<sub>x</sub> concentrations have been subtracted from the measured annual mean NO<sub>x</sub> concentration at background sites. This is compared with the modelled area source contribution to annual mean NO<sub>x</sub> concentration. Emissions from traffic sources have been dispersed from a volume source of height 10 m and stationary area sources have been dispersed from a volume source of height 30 m. Estimates of NO<sub>x</sub> emissions for 2000 have been adjusted to values for 2001 using UK sector total emission estimates for 2000 and 2001 available from the NAEI. The modelled area source contribution is therefore directly comparable with the measured concentrations in 2001.

Figure 5.4 Calibration of NO<sub>x</sub> area source model for 2001 (µg m<sup>-3</sup>, as NO<sub>2</sub>).

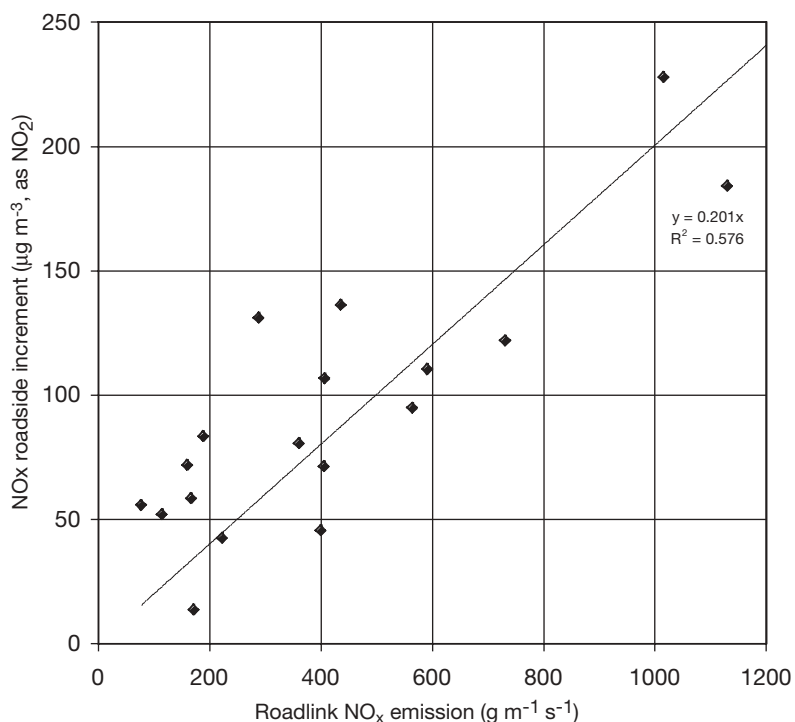


495. The study utilised the air quality model ADMS-Urban. Non airport sources were treated in a standard way as discussed in Chapter 5. Airport sources, including take-off and climb-out, landing, loading bays and taxi areas are represented as a series of volume sources. The calculated concentrations are dependent on the number of individual sources specified and the height and width of these sources. In particular there is considerable model sensitivity to the specified height of the ground level volume sources representing take-off roll and landing. A height of 50 m is used in this study.

- 496.** Examination of figure 5.4 shows that the monitoring sites fall into three groups related to the size of urban area:
- London and Birmingham;
  - Manchester, Leeds and Newcastle;
  - elsewhere.
- 497.** The elsewhere slope is close to unity, showing that in these locations the un-calibrated model is quite successful in predicting the concentration. The other slopes are lower, reflecting the different meteorological and dispersion conditions in larger cities. Meteorological data from Heathrow is not expected to be representative of central London, for example. The effective roughness in large urban areas is also greater than in rural or smaller urban areas, leading to more efficient dispersion of pollutants.
- 498.** The modelled area source contribution can be multiplied by the relevant empirical coefficient to calculate the calibrated area source contribution for each grid square in the country. The corrected rural and point source contributions are then added, resulting in a map of background  $\text{NO}_x$  concentrations. A map of background  $\text{NO}_2$  concentrations can then be calculated from this  $\text{NO}_x$  map using the  $\text{NO}_x$  to  $\text{NO}_2$  relationships listed above.

#### 5.2.1.7 Roadside concentrations

- 499.** The annual mean concentration of  $\text{NO}_x$  at a roadside location can be made up of two parts: the background concentration (as described above) and a roadside increment:
- roadside  $\text{NO}_x$  concentration = background  $\text{NO}_x$  concentration +  $\text{NO}_x$  roadside increment**
- 500.** The NAEI provides estimates of  $\text{NO}_x$  emissions for major road links in the UK for 2000 derived from traffic counts carried out at a 'census point' alongside each link (Goodwin *et al.*, 2001). The estimates for 2000 have been adjusted to provide estimates of emissions in 2001. Figure 5.5 shows a comparison of the roadside increment of annual mean  $\text{NO}_x$  concentrations at roadside or kerbside national automatic monitoring sites with  $\text{NO}_x$  emission estimates for the individual road links alongside which these sites are located. The background  $\text{NO}_x$  component at these roadside monitoring sites was derived from the map described above. This comparison provides an empirical dispersion coefficient, which can be used to calculate estimates of the roadside increment of annual mean  $\text{NO}_x$  concentrations from road link-specific emission estimates. This empirical model is calibrated using data from roadside or kerbside national automatic monitoring sites, so the estimated roadside concentration will be representative of the places in which the monitoring sites are located (typically 5 m from the kerb, see section 4.7). Thus a single estimate of the roadside concentration is calculated for each major road link in the UK. This is in contrast to more detailed local air quality modelling studies, which typically provide estimates of concentrations at a range of receptor points adjacent to an individual road link.

**Figure 5.5** Calibration of NO<sub>x</sub> roadside increment model for 2001 ( $\mu\text{g m}^{-3}$ , as NO<sub>2</sub>).

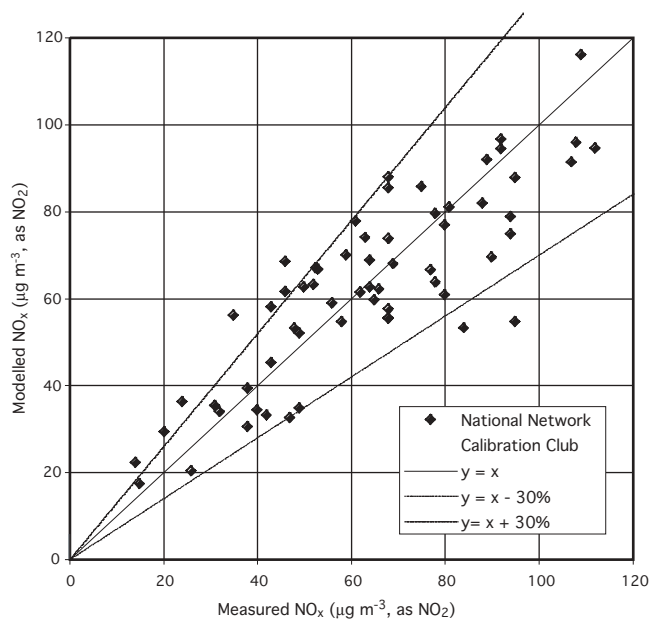
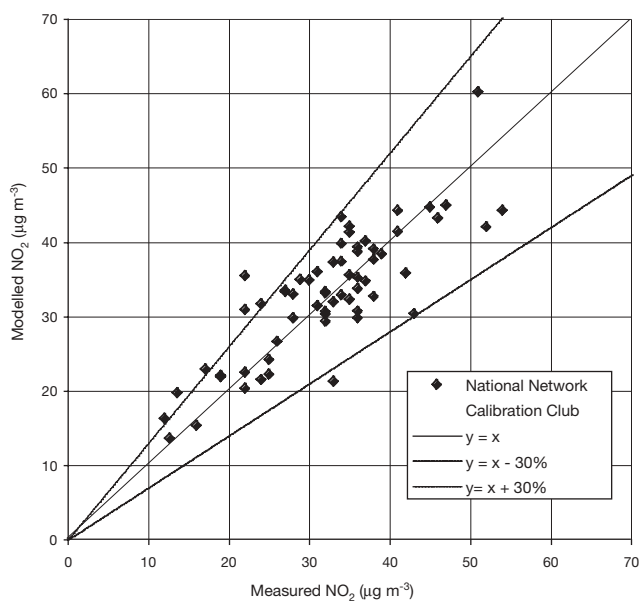
**501.** The roadside increments of annual mean NO<sub>x</sub> concentrations adjacent to motorways and non-built-up dual carriageways are considerably smaller per unit emissions than for built-up roads in urban areas. This is due to a combination of the wider traffic lanes, faster speeds and the more open aspects typically found on this type of road. An empirically derived factor of 0.25 was therefore applied to emissions from motorways and non-built-up dual carriageways prior to inclusion in the calibration. No attempt has been made to calculate roadside concentrations for non-built-up single carriageway roads.

**502.** The roadside increment of NO<sub>2</sub> can be calculated from the roadside increment of NO<sub>x</sub> using the relationships described above. This is then added to the mapped background NO<sub>2</sub> concentration:

$$\text{roadside NO}_2 \text{ concentration} = \text{background NO}_2 \text{ concentration} + \text{NO}_2 \text{ roadside increment}$$

#### 5.2.1.8 Verification of mapped values

**503.** Figures 5.6 and 5.7 show comparisons of modelled and measured annual mean NO<sub>x</sub> and NO<sub>2</sub> concentration in 2001 at background monitoring site locations and Figures 5.8 and 5.9 show similar comparisons for roadside sites. Both the national network sites used to calibrate the models and the Calibration Club sites (and other sites quality assured by netcen) which provide an independent verification of the modelled concentrations are shown. Lines representing  $y = x - 30\%$  and  $y = x + 30\%$  are also shown.

**Figure 5.6** Verification of background  $\text{NO}_x$  model for 2001.**Figure 5.7** Verification of background  $\text{NO}_2$  model for 2001.

**Figure 5.8** Verification of roadside NO<sub>x</sub> model for 2001.

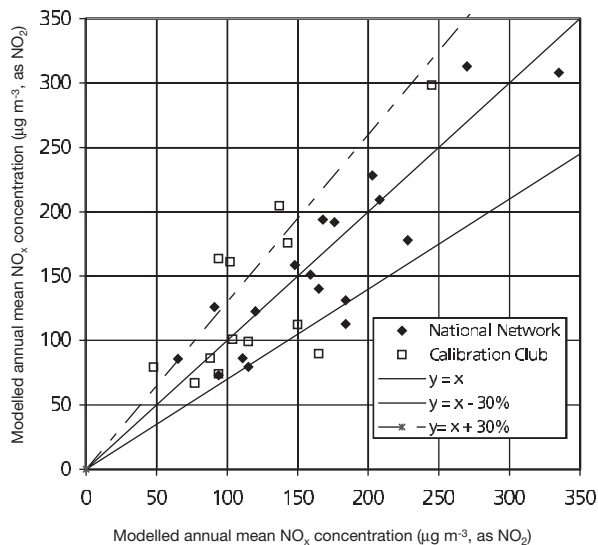
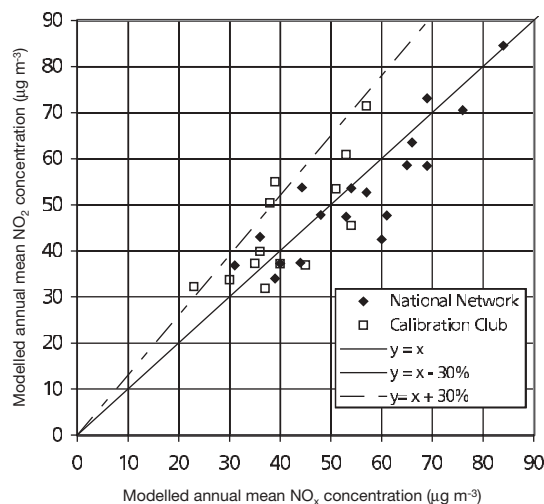


**Figure 5.9** Verification of roadside NO<sub>2</sub> model for 2001.



**504.** Summary statistics for the comparison between modelled and measured NO<sub>x</sub> and NO<sub>2</sub> concentrations are listed in Tables 5.2 and 5.3. Comparisons of modelled and measured NO<sub>x</sub> concentrations provide an additional check on the reliability of modelled estimates of NO<sub>2</sub>. This is because the non-linear relationships between NO<sub>x</sub> and NO<sub>2</sub> tend to cause modelled NO<sub>2</sub> concentrations to be relatively insensitive to errors in the dispersion modelling of NO<sub>x</sub>.

**Table 5.2** Summary statistics for comparison between modelled and measured NO<sub>x</sub> and NO<sub>2</sub> concentrations at background sites (µg m<sup>-3</sup>, as NO<sub>2</sub>).

|                  |                 | Mean of measurements | Mean of model estimates | r <sup>2</sup> | Number of sites |
|------------------|-----------------|----------------------|-------------------------|----------------|-----------------|
| National Network | NO <sub>x</sub> | 63.3                 | 62.6                    | 0.72           | 62              |
| Calibration Club | NO <sub>x</sub> | 51.3                 | 61.0                    | 0.77           | 25              |
| National Network | NO <sub>2</sub> | 32.1                 | 33.0                    | 0.70           | 62              |
| Calibration Club | NO <sub>2</sub> | 27.1                 | 32.2                    | 0.55           | 25              |

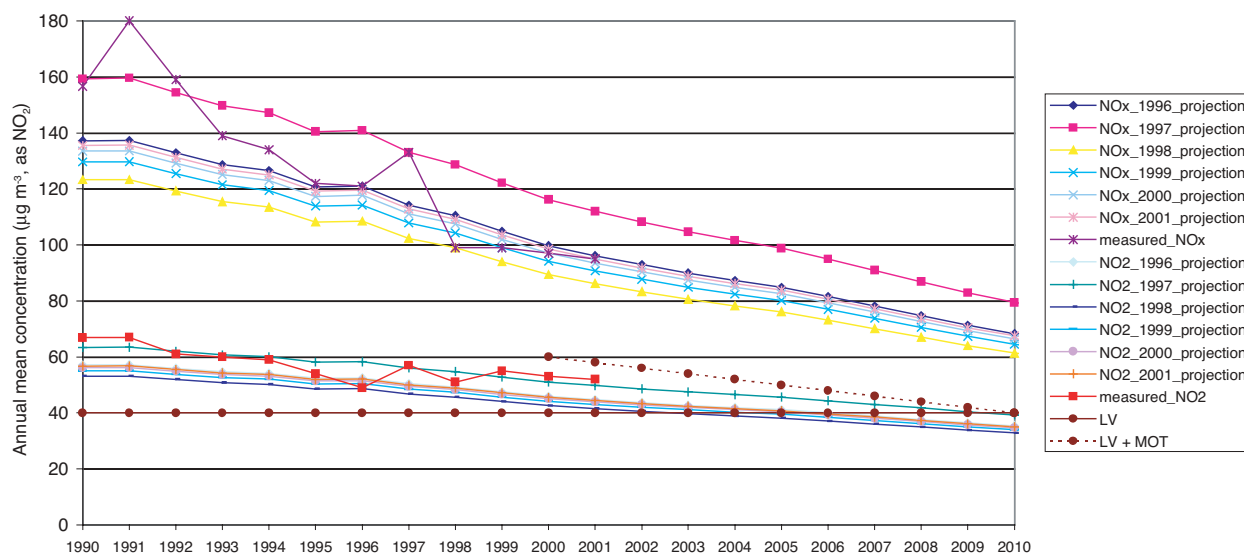
**Table 5.3** Summary statistics for comparison between modelled and measured NO<sub>x</sub> and NO<sub>2</sub> concentrations at roadside sites (µg m<sup>-3</sup>, as NO<sub>2</sub>).

|                  |                 | Mean of measurements | Mean of model estimates | r <sup>2</sup> | Number of sites |
|------------------|-----------------|----------------------|-------------------------|----------------|-----------------|
| National Network | NO <sub>x</sub> | 168.0                | 160.5                   | 0.79           | 18              |
| Calibration Club | NO <sub>x</sub> | 120.2                | 131.7                   | 0.55           | 13              |
| National Network | NO <sub>2</sub> | 55.3                 | 42.4                    | 0.79           | 18              |
| Calibration Club | NO <sub>2</sub> | 41.4                 | 45.1                    | 0.57           | 13              |

#### 5.2.1.9 Site-specific projections of NO<sub>2</sub> concentrations

- 505.** Site-specific projections of annual mean NO<sub>x</sub> and NO<sub>2</sub> concentrations have also been calculated using empirical models derived from the national mapping models. These projections provide a valuable tool for the rapid assessment of the impact of a range of possible policy options on ambient concentrations. Concentrations can also be projected backwards and the comparison with historical measured concentrations can provide useful insights into the reasons for the observed trends in addition to some verification of the model predictions. The site-specific projections also have the advantage of reducing the uncertainties associated with the empirical or dispersion modelling of concentrations.
- 506.** Figure 5.10 shows an example of site-specific projections for the West London monitoring site. The empirical models described above have been used to assign the measured annual mean NO<sub>x</sub> concentration in a range of base years to different emission sectors (rural background, traffic, industry, domestic, etc). The contribution for each sector in different years is then calculated using emission statistics and projections from the NAEI. These are then summed to calculate the predicted NO<sub>x</sub> concentration in each year. Annual mean NO<sub>2</sub> concentrations are then calculated from the NO<sub>x</sub> estimates using the empirical relationships described above.

**Figure 5.10** Site-specific projections of annual mean NO<sub>x</sub> and NO<sub>2</sub> concentrations at West London



### 5.2.1.10 Advantages and disadvantages of the National Empirical Model

**507.** The disadvantages of the empirical modelling methods include the following. The models do not attempt a full physical description of the processes taking place in the atmosphere and there is a risk that the empirical calibration of model results could hide errors that tend to cancel out. It is also assumed that any empirical relationships or coefficients will remain valid for other locations or at other times, such as projections to 2010. It is not always straightforward to incorporate adjustments to empirical models to take into account factors such as changes in oxidant concentrations, or primary NO<sub>2</sub> emissions. The spatial resolution of the model outputs is also limited and is restricted to estimates for background and roadside locations. No treatment of concentrations at locations intermediate between roadside and background or at complex locations such as junctions is attempted.

**508.** The first attempts to map NO<sub>2</sub> concentrations across the UK used a combination of diffusion tube data and population density as a surrogate for NO<sub>x</sub> emission estimates at a high spatial resolution (Campbell *et al.*, 1994; QUARG, 1993). The UK scale empirical models have since been extensively developed in a number of important areas and these highlight some of the advantages of empirical modelling methods. NAEI maps of UK emissions at a 1 km x 1 km resolution are now used along with emissions estimates on an individual road link basis for the major road network. This avoids the uncertainties that surround using surrogate statistics other than emission estimates for the empirical modelling. The models are calibrated using automatic monitoring data, which are now available from extensive networks in the UK. A dispersion matrix approach has been adopted to model the contribution from area sources to ambient concentrations. This enables the model to be calibrated directly in ‘concentration units’, improving the transparency of the calibration compared with calibrating the relationships between emissions and concentrations directly. This has the additional advantage that the models derived for a base year for which measured concentrations and emissions inventory estimates are available can be applied to calculate estimates of concentrations for alternative scenarios or projections by revising the emission inventory inputs. Another advantage of empirical modelling methods is that they are generally very computationally efficient in comparison with more complex modelling methods.

## 5.2.2 Screening models

### 5.2.2.1 Introduction to the screening models

- 509.** Screening models are designed to provide an initial estimate of pollutant concentrations arising from specific sources. The main characteristic of all screening models is that they require relatively simple inputs, with the results being generated rapidly and with a minimum of computer processing. The predictions are usually used to determine the need for a more detailed assessment. In general screening models are often simplified versions of more sophisticated approaches, which omit or simplify various input parameters such as meteorology. Although screening models are designed to be quick and simple to use, the assumption that they are inaccurate is not necessarily valid but they do take a generally precautionary approach.
- 510.** Screening models are available from the United States Environmental Protection Agency support centre for regulatory air models web site ([www.epa.gov/scram001/tt22.htm](http://www.epa.gov/scram001/tt22.htm)). All of these models incorporate Gaussian dispersion functions, and are applicable for the determination of relatively conserved species such as CO. In general, NO<sub>2</sub> concentrations are derived from predicted NO<sub>x</sub> concentrations, the latter quantity remaining relatively stable in the immediate vicinity of a source. The functions used to convert NO<sub>x</sub> to NO<sub>2</sub> are based on empirical relationships derived from simultaneous ambient measurements of the two pollutants.

### 5.2.2.2 The DMRB Screening Method

- 511.** With respect to UK road transport, one of the most widely used screening approaches is that contained within volume 11 of the Design Manual for Roads and Bridges (DMRB) (Highways Agency, 2003). The DMRB provides guidance on the Environmental assessment requirements for highway schemes in the UK, and has also become an important tool within the local authority review and assessment process for air quality, which is a requirement under the Environment Act 1995. This method was originally developed in the early 1980s, and is broadly based upon the TRL PREDCO Gaussian dispersion model. The approach, originally restricted to the estimation of CO concentrations, has subsequently been revised and extended in 2002 to include NO<sub>2</sub>, PM<sub>10</sub>, benzene and 1,3-butadiene (Boulter *et al.*, 2002a). The recent revision incorporates the latest UK road transport emission data (Barlow *et al.*, 2001), the vehicle fleet composition model from the 2000 National Atmospheric Emission Inventory (NAEI), a re-evaluation of roadside pollutant dispersion curves (Hickman *et al.*, 2002), the relationships between annual mean concentrations and other metrics relevant to the air quality objectives, and revised empirical relationships to estimate NO<sub>2</sub> from NO<sub>x</sub> concentrations.
- 512.** Prior to the revision, the official DMRB method had taken the form of a series of paper-based tables and graphs, and incorporated a step-by-step procedure for calculating the contribution of road traffic to both area-wide emissions and concentrations of air pollutants at a specified location. The method now takes the form of an Excel spreadsheet (DMRB, 2003).
- 513.** In previous versions of the DMRB, the method for deriving NO<sub>2</sub> concentrations near to a road involved the estimation of the background concentration of NO<sub>x</sub>, adding this to a NO<sub>x</sub> contribution from the road, then converting to NO<sub>2</sub> using a best-fit relationship between measured NO<sub>2</sub> and NO<sub>x</sub> based on data from a wide variety of national monitoring sites. The method now employed to derive NO<sub>2</sub> from NO<sub>x</sub> is that proposed by Laxen and Wilson (2002b). This approach assumes that concentrations near to roads are made up of two components: (i) NO<sub>2</sub> from the road traffic and (ii) NO<sub>2</sub> from the background air. The relationship between the atmospheric NO<sub>2</sub> and NO<sub>x</sub> concentrations due to road traffic was examined by subtracting the corresponding background values of NO<sub>2</sub> and NO<sub>x</sub> from the measured values at monitoring

sites. In the simplest terms, the road traffic contribution to NO<sub>2</sub> can be treated as being a constant proportion (approximately 16 %) of road traffic NO<sub>x</sub>. However, the actual proportion is dependent on the total amount of NO<sub>x</sub>. Hence, a variable factor is preferred because it provides a more logical fit to the measured data. The equation used to estimate total annual mean NO<sub>2</sub> is therefore (see section 5.2.1.3 and Figure 5.3):

$$\text{NO}_2 \text{ total} = \text{NO}_2 \text{ background} + \text{NO}_2 \text{ road}$$

Where NO<sub>2</sub> road is given by:

$$\text{NO}_2 \text{ road} = \text{NO}_x \text{ road} \times [-0.068 \ln(\text{NO}_x \text{ total}) + 0.53]$$

This approach has been tested and refined using data for a large number of sites throughout the UK for 1999, 2000 and 2001.

- 514.** An important element of the DMRB revision has been the calibration and adjustment of the method by comparison of predicted annual mean NO<sub>2</sub> concentration with measured concentration using data from 27 roadside monitoring sites between 1998 and 2001. Although such comparisons have been conducted in the past (for example, Mann *et al.*, 2001), the 2002 revision represents the first consideration and incorporation of such results in the development of the method itself.
- 515.** Pollutant concentrations tended to be overestimated by the model. There was found to be a good relationship between the annual average daily traffic flow (AADT), or AADT weighted by distance if more than one road was present, and the overestimation of the contribution of road traffic emissions to pollutant concentrations. The differences between the predicted and measured concentrations were then integrated into the spreadsheet model itself as a series of adjustments. However, although the application of the adjustment factors substantially improved the prediction accuracy of the method at the sites that were considered, a thorough verification of the model at other sites remains a task for the future (Boulter *et al.*, 2002a).

## 5.2.3 Empirical models of NO<sub>x</sub> and NO<sub>2</sub> concentrations in London

### 5.2.3.1 Introduction to the empirical models for London

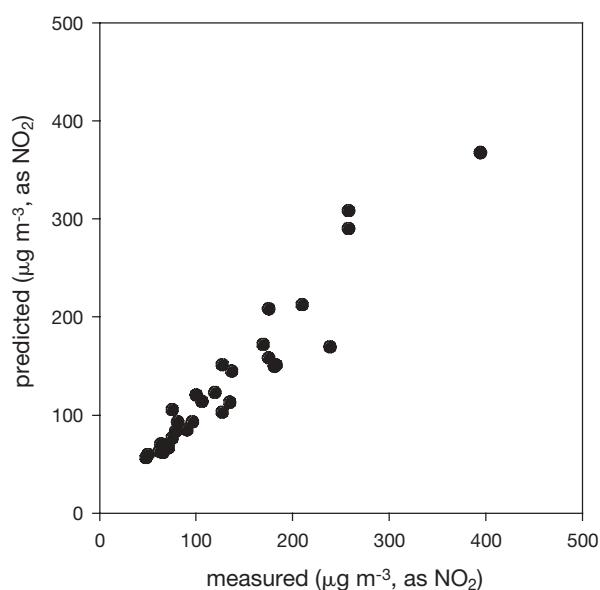
- 516.** Empirical techniques have been used to predict annual mean concentrations of NO<sub>x</sub> and NO<sub>2</sub> in London by the Environmental Research Group at King's College London (ERG). These predictions have been used by the GLA in their development of the Mayor's Air Quality Strategy (GLA, 2002) and for many local authorities in London as part of their responsibilities to review and assess air pollution under the National Air Quality Strategy.
- 517.** The most significant issue affecting predictions of air pollutants in London is the size and complexity of the London conurbation. For this reason, it is not possible to model each source explicitly taking account of hourly to seasonal changes in emissions: it is necessary to make simplifying assumptions. In the ERG model a distinction is made between emissions from the local road network and other sources. The approach uses a dispersion model together with empirical relationships derived from air pollution measurements. The approach aims to address the issue of the partitioning of different source types through a multiple regression using measurements from the LAQN and the AURN. A dispersion model is used to make predictions; the multiple regression with measurements is simply a refinement of the technique. The annual mean concentration of NO<sub>x</sub> at a monitoring site is described by a linear regression:

$$\text{NO}_x = A.\text{NO}_x[\text{roads}] + B.\text{NO}_x[\text{other}] + C$$

Where A, B and C are constants to be derived from the multiple regression,  $\text{NO}_x[\text{roads}]$  is the contribution from the local road network (defined and modelled within 500 m of a monitoring site) and  $\text{NO}_x[\text{other}]$  is the contribution from more distant sources of  $\text{NO}_x$  i.e. beyond 500 m of a monitoring site.

- 518.** Emissions from the road network within 500 m of each monitoring site are modelled in a detailed way. The road network is split up into 10 m sections to take account of the geographic variation in the actual road network. Careful treatment of the road network is necessary because of the steep gradient in concentrations of  $\text{NO}_x$  close to roads.
- 519.** All other sources of  $\text{NO}_x$  (except Part A industrial processes, which are modelled explicitly as point sources) and road network emissions greater than 500 m from a monitoring site are represented as shallow volume sources of varying dimension depending on their source characteristics.
- 520.** Emissions from gas combustion (domestic and commercial; the second most important emissions category for  $\text{NO}_x$  after road transport) are released from a wide range of source heights. Furthermore, the type of building can also influence the release of emissions. This feature of these sources makes it difficult to model them in a consistent way. For example, emissions from these sources are greatest in central London, but they are generally released from a greater height, thus reducing their ground-level impact. At present, there is insufficient information to warrant a more detailed treatment of these sources. However, it is important to recognise that emissions from these sources will be diluted in a very different way to road transport emissions. The regression technique described above aims to use the additional information provided by measurements to assist in the partitioning of ground-level  $\text{NO}_x$  from these different source types.
- 521.** The effect of the multiple regression is that more emphasis is placed on local road network emissions than would have been the case if each source type were modelled directly. Concentrations of  $\text{NO}_x$  in London therefore respond very well to changes in the emissions from road transport. A comparison between measured and modelled annual mean  $\text{NO}_x$  concentrations is shown in Figure 5.11.

**Figure 5.11** Comparison between measured and modelled annual mean  $\text{NO}_x$  concentration in 1999 in London ( $r_2=0.89$ ).

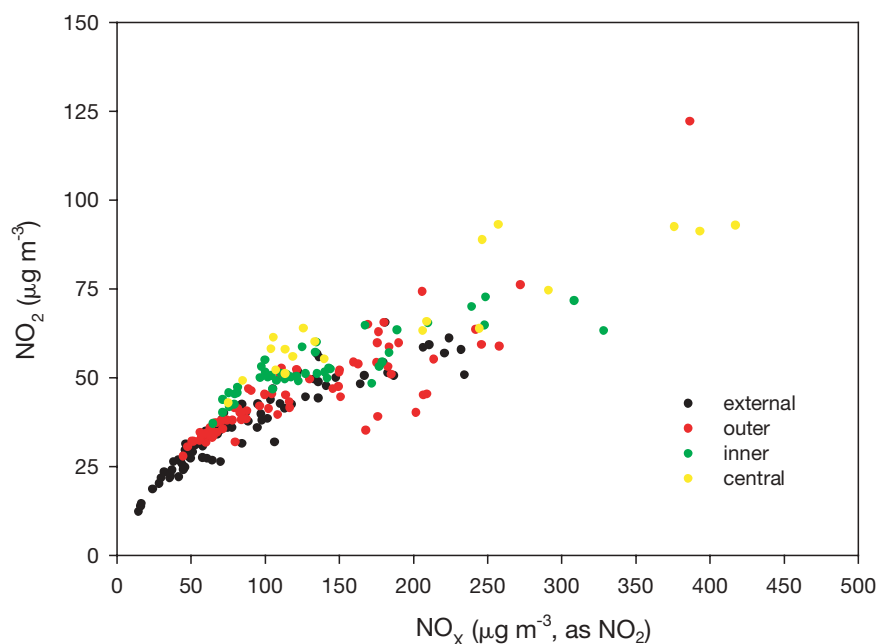


### 5.2.3.2 Empirical relationships between $\text{NO}_2$ and $\text{NO}_x$ in London

**522.** One potential approach to developing a relationship between annual mean  $\text{NO}_x$  and  $\text{NO}_2$  is to plot the annual mean  $\text{NO}_x$  against the annual mean  $\text{NO}_2$ , as has been done for most empirical approaches, for example, as used in the national modelling described in section 5.2.1. In the past, it has been difficult to distinguish between different  $\text{NO}_2$  environments because of a lack of data. However, in London there is now sufficient monitoring to consider one urban area in isolation. Figure 5.12 shows the annual mean  $\text{NO}_x$ - $\text{NO}_2$  relationship for sites in and close to London for measurements between 1996-2000. For convenience central is defined as within 5 km of Bloomsbury, inner between 5-10 km, outer between 10-20 km and external > 20 km.

**523.** Figure 5.12 shows higher  $\text{NO}_2$  concentrations in central and inner London for a particular value of  $\text{NO}_x$ . Central London locations receive emissions from all wind directions, thus allowing time for chemistry to occur and emissions to be mixed into incoming trajectories. The other principal difference is between background and roadside/kerbside locations, where the latter always shows a lower  $\text{NO}_2/\text{NO}_x$  ratio for a particular  $\text{NO}_x$  concentration compared with background locations. Again, this observation reflects the time available for chemistry to occur and the relatively high background  $\text{NO}_2$  concentrations that are observed. Figure 5.12 also encompasses the localised effects of higher direct emissions of  $\text{NO}_2$ , which will affect some locations more than others.

**Figure 5.12** Annual mean  $\text{NO}_x$  vs.  $\text{NO}_2$  by location in London (1996-2000).



**524.** One difficulty with approaches that rely on the relationships between annual mean  $\text{NO}_x$  and  $\text{NO}_2$  is that some assumptions must be made to describe how  $\text{NO}_2$  concentrations respond to decreasing concentrations of  $\text{NO}_x$ . For example, there are no central London sites at low  $\text{NO}_2$  concentrations: these have to be interpolated. This interpolation must either include sites in other locations, for example, outer London, or some other guess as to how the curve reaches the origin. The risk is that there is no direct information on which to base future predictions of  $\text{NO}_2$  in central London. Specifically, this approach does not provide the concentration of  $\text{NO}_x$  that must be reached in order that the  $\text{NO}_2$  objective is met at a particular site.

- 525.** An alternative approach described below aims to provide some information on how  $\text{NO}_2$  might be expected to decline at different sites in London. More information can be found in Carslaw *et al.* (2001).
- 526.** The relationship between hourly  $\text{NO}_x$  and  $\text{NO}_2$  concentrations can be investigated by plotting each hourly value of  $\text{NO}_x$  against the corresponding  $\text{NO}_2$  concentration in a scatter plot, as shown for the Bloomsbury site in Figure 5.13. Derwent and Middleton (1996) found that the relationship between  $\text{NO}_x$  and  $\text{NO}_2$  could be usefully summarised by plotting  $\text{NO}_2$  against  $\text{NO}_x$  in different  $\text{NO}_x$  'bins'. The mean  $\text{NO}_2$  concentration is averaged according to different ranges of  $\text{NO}_x$  concentration. Figure 5.14a shows the effect of summarising data in this way for the Bloomsbury site in 1998. However, the precise relationship is always both year- and site-dependent.
- 527.** The  $\text{NO}_x$ - $\text{NO}_2$  relationship and the frequency distribution shown in Figure 5.14 can be multiplied together and divided by the number of measurements in one year to derive the annual mean  $\text{NO}_2$  concentration. The  $\text{NO}_2$  concentration derived in this way is identical to the measured annual mean  $\text{NO}_2$  concentration. Of more use in a predictive sense, is the calculation of the annual mean  $\text{NO}_2$  based on a new concentration of  $\text{NO}_x$ , for example, the expected annual mean  $\text{NO}_2$  concentration for a 50 % reduction in  $\text{NO}_x$ .

**Figure 5.13** The relationship between hourly  $\text{NO}_x$  and  $\text{NO}_2$  concentrations for the Bloomsbury site (1998).

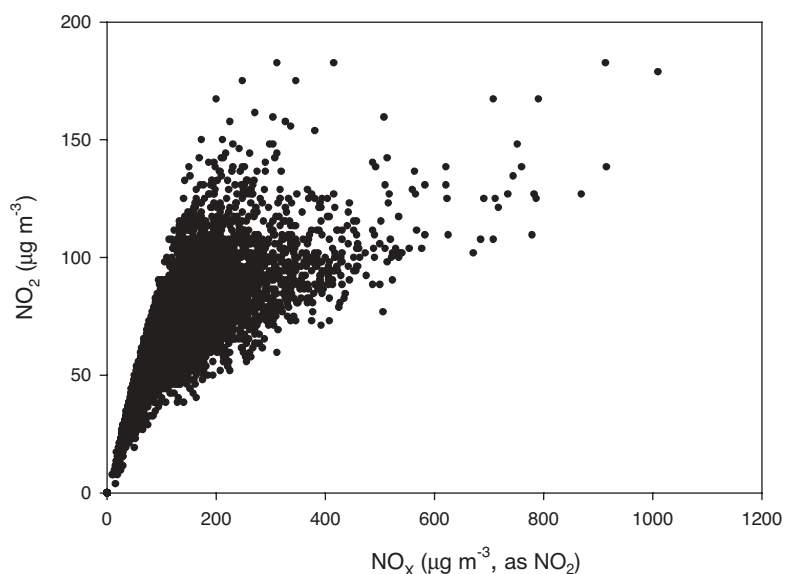
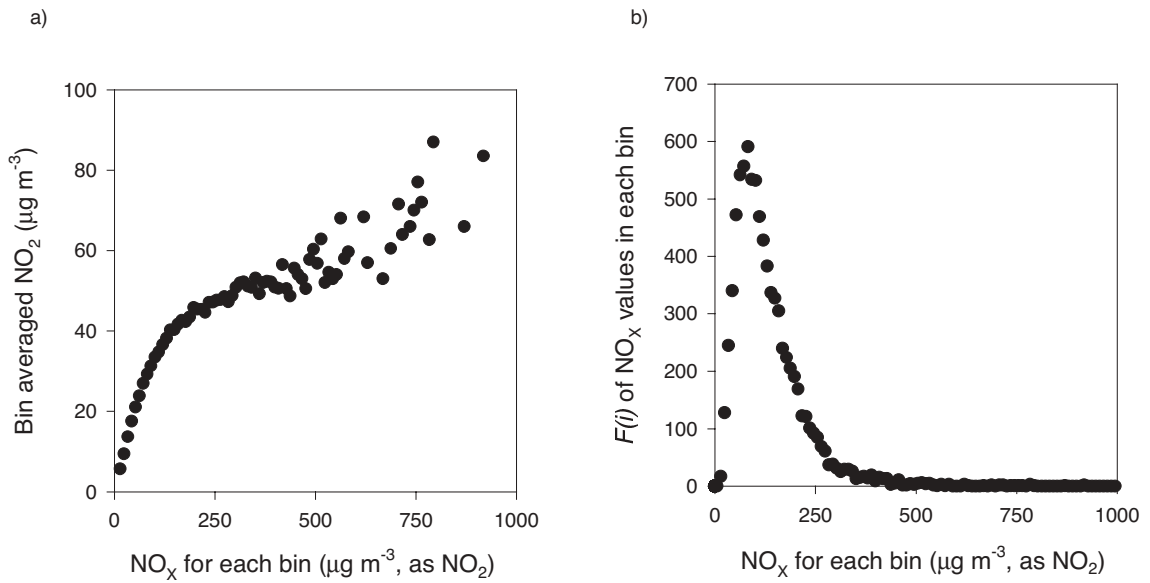
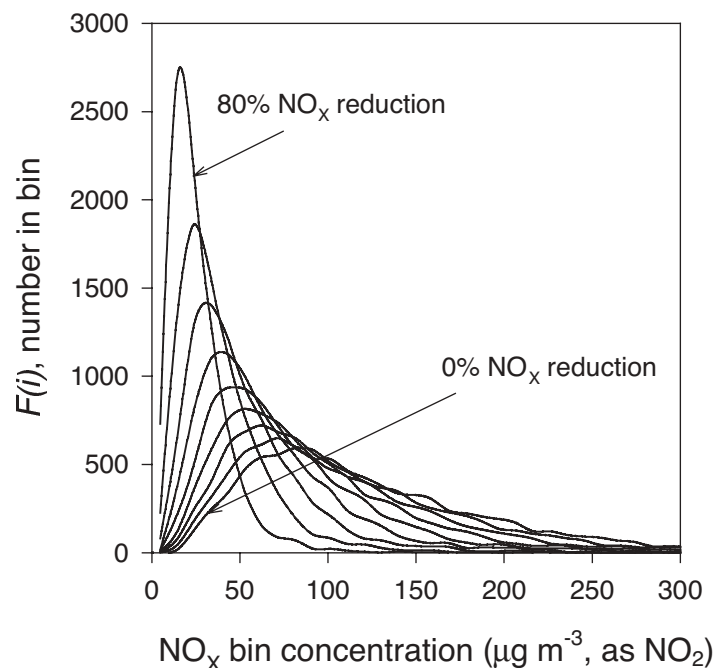


**Figure 5.14 (a)** The hourly  $\text{NO}_x$ - $\text{NO}_2$  relationship at Bloomsbury for 1998 showing the bin averaged  $\text{NO}_2$  concentrations after sorting into  $10 \mu\text{g m}^{-3}$   $\text{NO}_x$  bins and **(b)** the corresponding  $\text{NO}_x$  frequency distribution  $F(i)$  showing the number of points averaged in each bin.



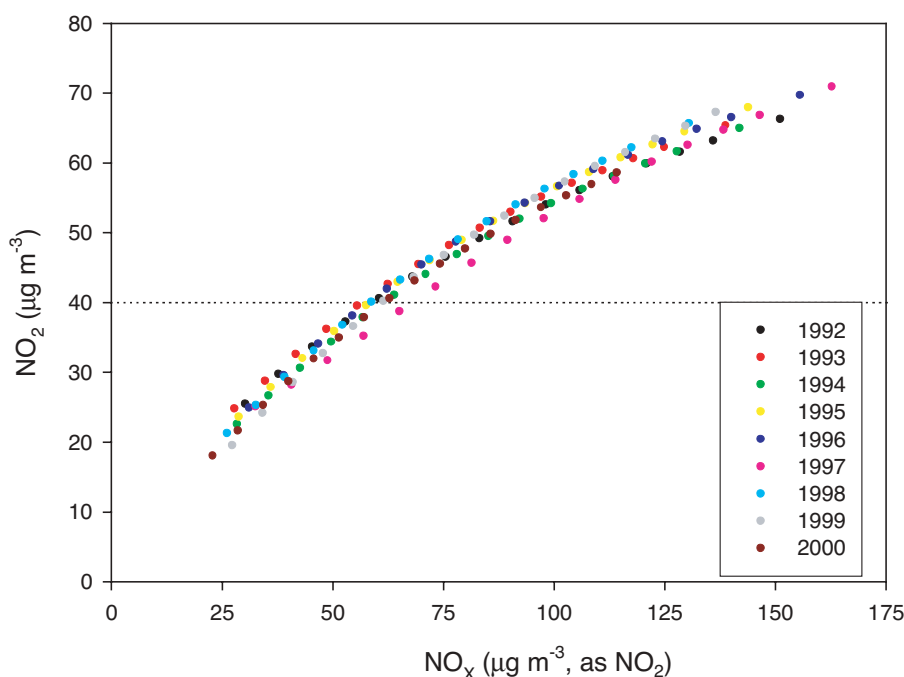
**528.** Different  $\text{NO}_x$  reductions can be considered by re-calculating the hourly values of  $\text{NO}_x$  for different percentage reductions in  $\text{NO}_x$  from 0 to 80% in 5% intervals, reducing the annual mean  $\text{NO}_x$  accordingly, and then sorting to find the new frequency distribution. The revised frequency distributions for  $\text{NO}_x$  are multiplied by the  $\text{NO}_2$  vs.  $\text{NO}_x$  relationship to provide a new estimate of the annual mean  $\text{NO}_2$  concentration. Figure 5.15 shows how the frequency distribution changes with reductions in  $\text{NO}_x$ . The shape of the relationship becomes increasingly narrow and tall as  $\text{NO}_x$  values migrate to lower concentrations, with increased reductions in  $\text{NO}_x$ . Second, as the  $\text{NO}_x$  concentration is reduced an increased number of points move to the  $\text{NO}_x$ -limited regime.

**Figure 5.15** The effect on the  $\text{NO}_x$  frequency distribution,  $F(i)$ , at the Bloomsbury site as  $\text{NO}_x$  concentrations are reduced in 10% intervals from 0 to 80% reduction (1998).



**529.** By multiplying successive  $\text{NO}_x$  frequency distributions shown in Figure 5.15 with the  $\text{NO}_x$ - $\text{NO}_2$  relationship shown in Figure 5.14a and dividing by the number of observations, it is possible to derive an *annual mean*  $\text{NO}_x$ - $\text{NO}_2$  relationship at a site. This approach indicates how  $\text{NO}_2$  concentrations might change as  $\text{NO}_x$  is reduced at a *single site*. Furthermore, the technique is based on hourly measurements of  $\text{NO}_x$  and  $\text{NO}_2$ , which is essential if the change in future  $\text{NO}_2$  concentrations is to be predicted.

**Figure 5.16** Annual mean  $\text{NO}_x$  vs.  $\text{NO}_2$  (1992-2000) for the Bloomsbury site derived using the ERG approach. The different points for each year show the estimated effect of different % reductions in  $\text{NO}_x$ .



**530.** Figure 5.16 shows the results of applying the technique to the Bloomsbury site over 9 different years covering a range of annual mean  $\text{NO}_x$  and  $\text{NO}_2$  concentrations. In general, these derived curves show consistency between the years and indicate that to achieve a  $\text{NO}_2$  concentration of  $40 \mu\text{g m}^{-3}$ ,  $\text{NO}_x$  must reduce to approximately  $60\text{--}70 \mu\text{g m}^{-3}$  at this site. 1997 stands out as one year where the relationship is slightly different, although the reasons for this are not properly understood (there were a large number of wintertime pollution episodes during 1997). The advantage of the approach is that it provides predicted concentrations of  $\text{NO}_2$  given a concentration of  $\text{NO}_x$ , say from a dispersion model.

### 5.2.3.3 Advantages and disadvantages of the empirical model for London

**531.** Many of the advantages and disadvantages of the modelling approach described are the same as those described for the national modelling. The aim of the modelling has been to describe ‘typical’ concentrations expected at different locations. However, it is recognised that actual concentrations depend upon many factors that cannot adequately be described using the techniques described above. These factors include:

- Factors affecting local dispersion that cannot be adequately described using existing dispersion models, for example, locations in a ‘mixed’ setting surrounded by buildings of various heights. Most urban locations do not simply fit into ‘open’ or ‘street canyon’ descriptions. The empirical approach only recognises that concentrations tend to be enhanced in urban locations where many buildings are present compared with open locations.

- Local variation in emissions of  $\text{NO}_x$ . No account is taken of the variation in emissions along each road link. It would generally be expected that emissions (and therefore concentrations) would be higher close to locations with queuing traffic, for example, near junctions. Again, the techniques provide predictions that represent average or typical conditions.
- Local variation in direct emissions of  $\text{NO}_2$ . The approach inherently accounts for the local contribution to direct emissions of  $\text{NO}_2$ . This is both an advantage and a disadvantage. The advantage is that some account is taken of direct emissions, which is useful since emission inventories are not currently detailed enough to account for direct emissions of  $\text{NO}_2$ . The disadvantage is that the approach does not currently account separately for direct emissions. It is not possible therefore to consider how these emissions might change in future.
- The calculation of future concentrations of  $\text{NO}_2$  is dependent on several assumptions, most significantly how future concentrations of  $\text{NO}_2$  respond to changes in the concentration of  $\text{NO}_x$ . The only way that these assumptions can be tested is to compare them with approaches that attempt to account for all or most of the processes controlling concentrations of  $\text{NO}_2$ , for example, a Lagrangian model (section 5.4). The approach also does not account for changes in future concentrations of tropospheric  $\text{O}_3$ . The empirical oxidant approach described in section 5.2.4 indicates how  $\text{O}_3$  concentrations can be included in empirical models.

#### 5.2.4 Prediction and interpretation of annual mean $\text{NO}_2$ vs. $\text{NO}_x$ curves by consideration of oxidant sources and chemistry

**532.** As described in detail in section 3.2.1, there is a strong chemical coupling between the  $\text{NO}_x$  species and  $\text{O}_3$ . Because of this, the consideration of  $\text{NO}$ ,  $\text{NO}_2$  and  $\text{O}_3$  as a set of species, rather than  $\text{NO}$  and  $\text{NO}_2$  alone, can provide additional information to assist the prediction and interpretation of how the concentration of  $\text{NO}_2$  varies with  $\text{NO}_x$ . Consistent with the definition explained in section 3.2.1,  $\text{NO}_2$  and  $\text{O}_3$  are collectively considered as oxidant (OX). The method presented here (based on that reported by Clapp and Jenkin, 2001), involves defining (i) how the concentration of OX varies with  $\text{NO}_x$  and (ii) how the fractional contribution of  $\text{NO}_2$  to OX (i.e.,  $\text{NO}_2/\text{OX}$ ) varies with  $\text{NO}_x$ . The product of these two quantities yields the dependence of  $\text{NO}_2$  on  $\text{NO}_x$ .

**533.** Figure 5.17 shows how the annual mean concentrations of OX depend on  $\text{NO}_x$  for the majority of London AURN sites where the required measurements are available, and for Reading and Harwell (as in section 3.3, graphs presenting data for  $\text{O}_3$  and/or OX, exceptionally, make use of the ppb units). The general trend of increasing OX with  $\text{NO}_x$ , superimposed on a background level, may be interpreted in terms of the 'regional' and 'local' contributions to OX, as described in section 3.3.1. Clearly, however, there are some variations in the magnitudes of these contributions from one site to another. This is further illustrated in Figure 5.18, which shows only the data for five selected sites. In each case an associated regression line is presented, based on an intercept (i.e. regional contribution) fixed at a value of 35.7 ppb, derived from analysis of the entire data set in Figure 5.17. Corresponding regression parameters are presented in Table 5.4, for all the sites in Figure 5.17. The assumption here is that variations in levels of OX from one site to another arise primarily from differences in local input (for example, the fraction of  $\text{NO}_x$  emitted as  $\text{NO}_2$ ), but that the regional contribution (resulting from the background  $\text{O}_3$  level) is the same at all sites in a given region.

**Figure 5.17** Variation of annual mean OX mixing ratio with  $\text{NO}_x$  for London sites where  $\text{O}_3$ ,  $\text{NO}$  and  $\text{NO}_2$  are measured, Reading and Harwell. The number of years of available data vary from one site to another, but all displayed data were obtained during 1992-2000. (adapted from Clapp and Jenkin, 2001).

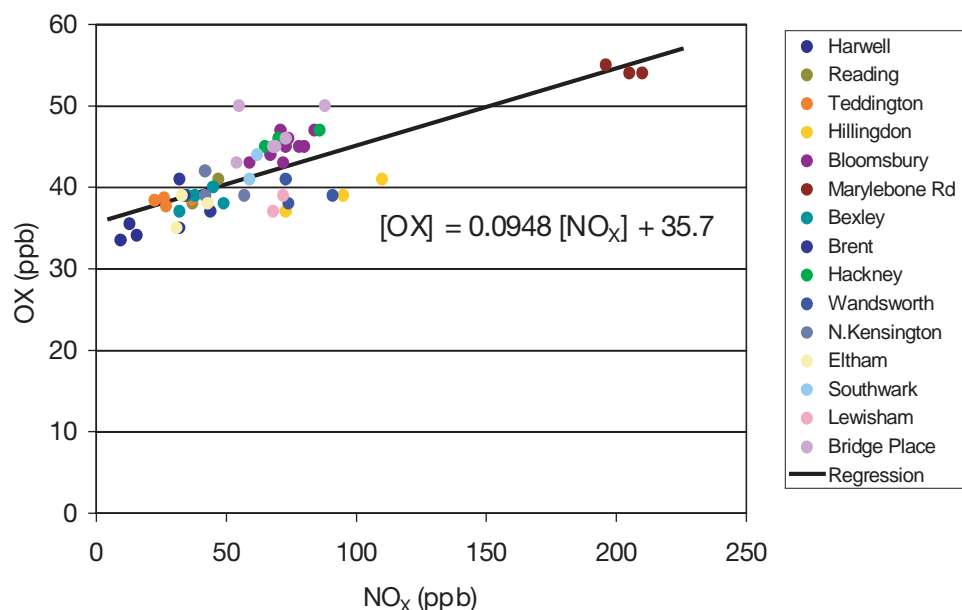


**Table 5.4** Summary of  $[\text{OX}]$  vs  $[\text{NO}_x]$  and  $[\text{NO}_2]/[\text{OX}]$  vs  $[\text{NO}_x]$  relationships, and  $\text{NO}_x$  thresholds derived from the analysis of annual mean data presented in Figures 5.18 and 5.20.

| Site          | Type         | A <sup>1</sup> | $[\text{NO}_2]/[\text{OX}]^2$ | $\text{NO}_x$ threshold <sup>3</sup> , $\mu\text{g m}^{-3}$ as $\text{NO}_2$ (ppb) |                              |
|---------------|--------------|----------------|-------------------------------|--|------------------------------|
|               |              |                |                               | Current method   | Carslaw <i>et al.</i> (2001) |
| Bexley        | Suburban     | 0.0771         | Fit 1                         | 75.4 (39.4)  | –                            |
| Bloomsbury    | Urban Centre | 0.1272         | Fit 1                         | 70.6 (36.9)  | 60.6 (31.7)                  |
| Brent         | Urban BG     | 0.0616         | Fit 1                         | 77.1 (40.3)  | –                            |
| Bridge Place  | Urban BG     | 0.1572         | Fit 1                         | 68.1 (35.6)  | 65.6 (34.3)                  |
| Eltham        | Suburban     | 0.0477         | Fit 1                         | 78.8 (41.2)  | –                            |
| Hackney       | Urban Centre | 0.1391         | Fit 2                         | 77.3 (40.4)  | 66.8 (34.9)                  |
| Hillingdon    | Suburban     | 0.0375         | Fit 2                         | 93.0 (48.6)  | 100.0 (52.3)                 |
| Lewisham      | Urban Centre | 0.0332         | Fit 1                         | 80.7 (42.2)  | 76.7 (40.1)                  |
| Marylebone Rd | Kerbside     | 0.0914         | Fit 2                         | 83.2 (43.5)  | 71.9 (37.6)                  |
| N Kensington  | Urban BG     | 0.0873         | Fit 1                         | 74.2 (38.8)  | 70.6 (36.9)                  |
| Reading       | Urban BG     | 0.1121         | Fit 2                         | 80.4 (42.0)  | –                            |
| Southwark     | Urban Centre | 0.1129         | Fit 1                         | 71.8 (37.5)  | 68.7 (35.9)                  |
| Teddington    | Urban BG     | 0.0902         | Fit 1                         | 74.1 (38.7)  | –                            |
| Wandsworth    | Urban Centre | 0.0449         | Fit 2                         | 91.5 (47.8)  | 89.0 (46.5)                  |

1 Linear  $[\text{OX}]$  vs  $[\text{NO}_x]$  relationships given by  $[\text{OX}] = A \cdot [\text{NO}_x] + B$ , derived from data for each site presented in Figure 5.17.

The regional OX contribution,  $B = 35.7$  ppb, is assumed site-independent and equivalent to that derived from the composite analysis of all sites.

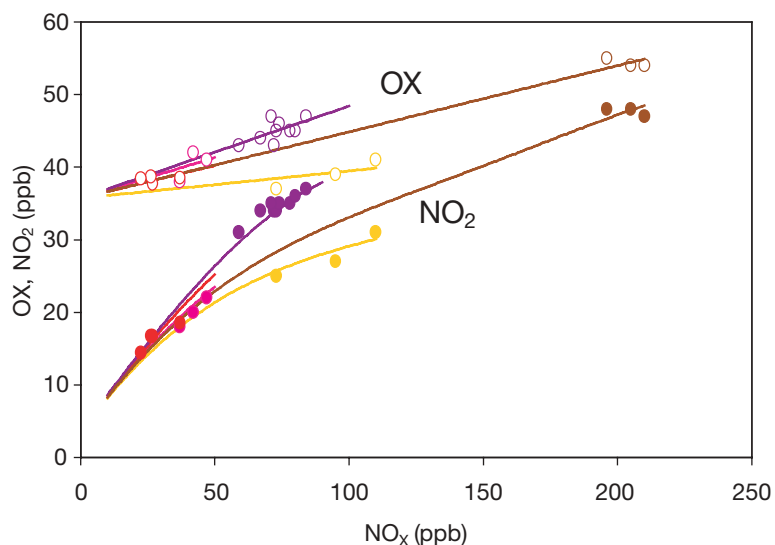
2  $[\text{NO}_2]/[\text{OX}]$  vs  $[\text{NO}_x]$  expressions are polynomial fits to data presented in Figure 5.19:

Fit 1:  $[\text{NO}_2]/[\text{OX}] = (1.015 \times 10^{-1}) + (1.367 \times 10^{-2} [\text{NO}_x]) - (6.127 \times 10^{-5} [\text{NO}_x]^2) - (4.464 \times 10^{-8} [\text{NO}_x]^3)$ : applicable range, 19 – 172  $\mu\text{g m}^{-3}$   $\text{NO}_x$  as  $\text{NO}_2$  (10 – 90 ppb)

Fit 2:  $[\text{NO}_2]/[\text{OX}] = (8.962 \times 10^{-2}) + (1.474 \times 10^{-2} [\text{NO}_x]) - (1.290 \times 10^{-4} [\text{NO}_x]^2) + (5.527 \times 10^{-7} [\text{NO}_x]^3) - (8.906 \times 10^{-10} [\text{NO}_x]^4)$ : applicable range, 19 – 402  $\mu\text{g m}^{-3}$   $\text{NO}_x$  as  $\text{NO}_2$  (10 – 210 ppb).

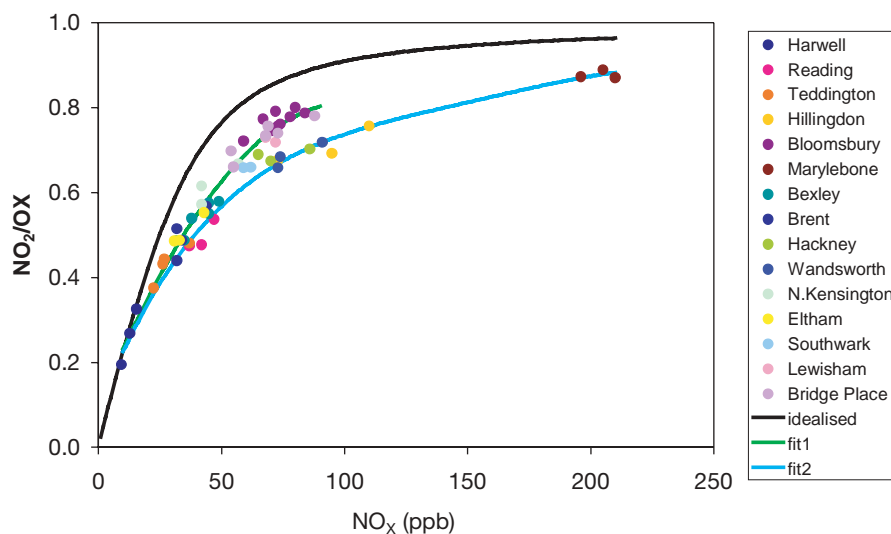
3 Predicted  $\text{NO}_x$  threshold corresponding to an annual mean  $\text{NO}_2$  of 40  $\mu\text{g m}^{-3}$  (21 ppb).

**Figure 5.18** Annual mean OX and NO<sub>2</sub> as a function of NO<sub>x</sub> at Marylebone Rd (●), Bloomsbury (●), Hillingdon (●), Teddington (●) and Reading (●). Open circles refer to OX, full circles to NO<sub>2</sub>. Lines are calculated from the expressions in Table 5.4. (adapted from Clapp and Jenkin, 2001).



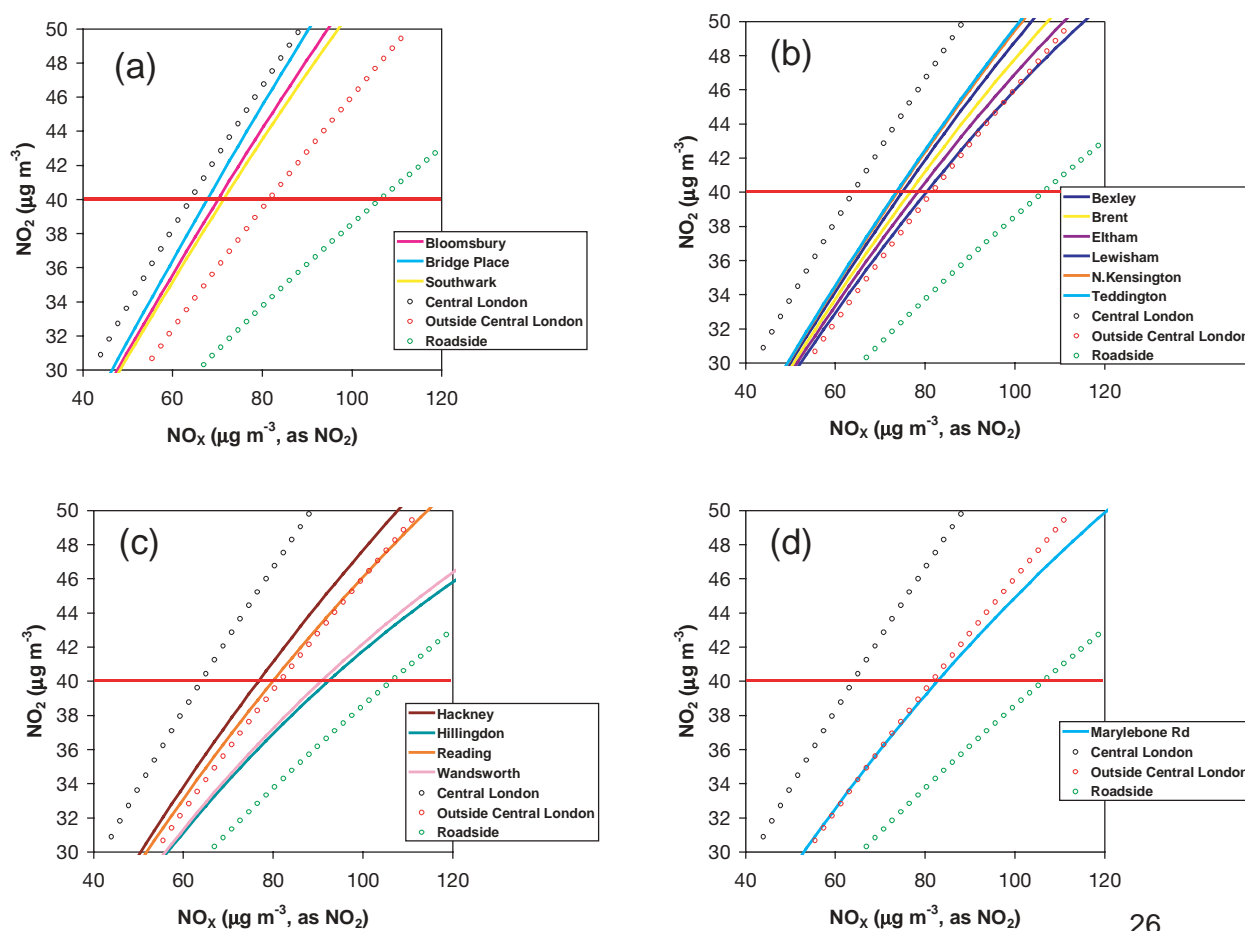
**534.** Figure 5.19 shows the fraction of OX which is in the form of NO<sub>2</sub>, based on the annual average data for the same set of sites. The data appear to fall into two reasonably distinct groups, the first containing Hillingdon, Hackney, Wandsworth, Reading and Marylebone Rd, and the second containing the remaining sites, which generally show higher NO<sub>2</sub>/OX ratios. Such differences in the partitioning of NO<sub>2</sub> and O<sub>3</sub> are likely to relate (at least partially) to the time available for reaction of NO with O<sub>3</sub> to occur, following emission of NO. A short time lag between emission and measurement most likely accounts for the lower ratios in the first group identified above. Marylebone Rd is a kerbside site, and the other four sites are located comparatively close to local traffic sources and therefore have partial roadside character.

**Figure 5.19** Variation of annual mean [NO<sub>2</sub>]/[OX] as a function of NO<sub>x</sub> for London sites where O<sub>3</sub>, NO and NO<sub>2</sub> are measured, Reading and Harwell. The black line is the calculated idealised variation based on the assumption of photostationary state. (adapted from Clapp and Jenkin, 2001).



**535.** An idealised variation of  $\text{NO}_2/\text{OX}$  with level of  $\text{NO}_x$  can be inferred on the basis of the photostationary state relationship (discussed in section 3.2.1). This defines the levels of  $\text{O}_3$ ,  $\text{NO}$  and  $\text{NO}_2$  which co-exist under steady state conditions in a sunlit atmosphere. The variation, calculated with an annual average  $\text{NO}_2$  photolysis rate, is also displayed in Figure 5.19. This qualitatively shows the same trend as the observed points, indicating an increasing proportion of OX in the form of  $\text{NO}_2$  as  $\text{NO}_x$  increases.

**Figure 5.20** Inferred variation of annual mean  $\text{NO}_2$  with annual mean  $\text{NO}_x$  at (a) central London sites, (b) sites outside central London, (c) intermediate sites and (d) roadside sites, based on the parameters given in Table 5.4. In each panel, the generic dependences of Stedman *et al.* (2002) for urban centre and background sites in central London and outside central London are also shown. A generic dependence for roadside sites used previously (Stedman *et al.*, 2001a) is shown for comparison.

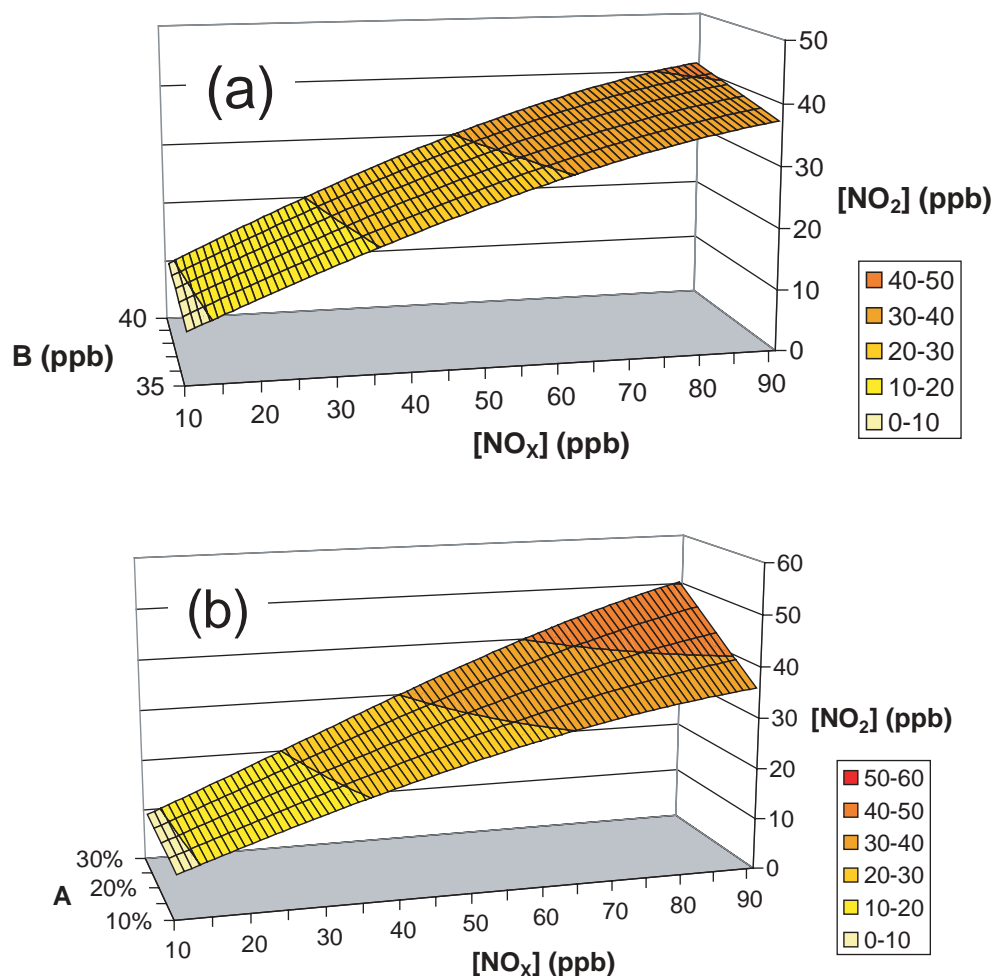


26

**536.** It cannot, however, provide a quantitative description for annual mean data, for two main reasons. First, the idealised dependence describes how the partitioning of the OX components varies for a range of unique levels of  $\text{NO}_x$ , whereas each observed data point represents the mean of a large number of measurements at many  $\text{NO}_x$  levels. If a number of discrete measurements describe a curve of the form shown in Figure 5.19, then the mean of the measurements must lie below the curve. Secondly, the photostationary state relationship assumes there is sufficient time for steady state to be established. As indicated above, this is less likely at sites closer to source and cannot generally be achieved at night. As a result, the idealised curve overpredicts the proportion of OX in the form of  $\text{NO}_2$  on an annual mean basis.

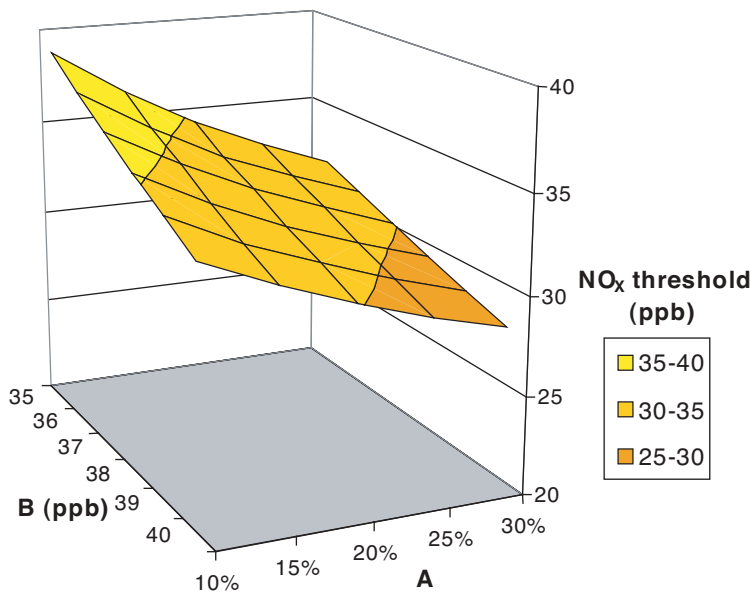
- 537.** The  $\text{NO}_2/\text{OX}$  variation is therefore defined using fitted functions for groups of sites with particular characteristics. The data for the two groups shown in Figure 5.19 yield the two polynomial expressions given in Table 5.4, and illustrated in the figure. In conjunction with the  $\text{OX}$  vs  $\text{NO}_x$  regression parameters, these expressions allow  $\text{NO}_2$  vs  $\text{NO}_x$  curves to be inferred for all 14 urban and suburban sites. These are presented with the observed annual mean data in Figure 5.18 for five selected sites.
- 538.** The calculated variation of annual mean  $\text{NO}_2$  with  $\text{NO}_x$  is also shown for all 14 sites in Figure 5.20, and the inferred  $\text{NO}_x$  thresholds which correspond to an annual mean  $\text{NO}_2$  concentration of  $40 \mu\text{g m}^{-3}$  (21 ppb) are also presented in Table 5.4. The  $\text{NO}_x$  thresholds for the sites considered show significant site-to-site variation, covering the range 35.6 – 48.6 ppb (i.e.,  $68.1 - 93.0 \mu\text{g m}^{-3}$  as  $\text{NO}_2$ ). The results are thus broadly consistent with threshold values derived from the  $\text{NO}_2$  vs.  $\text{NO}_x$  relationships discussed in the previous subsections (Carslaw *et al.*, 2001; Stedman *et al.*, 2002). Those reported by Carslaw *et al.* (2001) for specific sites generally lie slightly below the present values, but in reasonable agreement, as also shown in Table 5.4. Stedman *et al.* (2001a) and Stedman *et al.* (2002) derived three generic expressions to describe the  $\text{NO}_2$  vs.  $\text{NO}_x$  relationship for ‘central London sites’, for ‘sites outside central London’, and for ‘roadside sites’, which are compared with the present expressions in Figure 5.20. The present data for urban centre and background central London sites and sites outside central London are consistent with the expressions of Stedman *et al.* (2002).
- 539.** As discussed above, a number of sites can be classified as ‘intermediate’, as they have partial roadside character, due to the influence of nearby roads. Logically, therefore, the present data for some of these lie at higher  $\text{NO}_x$  than the generic expressions for the urban centre and background sites, but lower than the generic expression for roadside sites. The present data for Marylebone Rd (the only roadside site available for consideration by the analysis method) lie at significantly lower  $\text{NO}_x$  than the generic expression of Stedman *et al.* (2001a). Although the  $\text{NO}_2$ - $\text{NO}_x$  dependence provides a good description of the variation of the currently available narrow range, some systematic error may result from the necessary inclusion of Marylebone Rd in the intermediate grouping in the present analysis.
- 540.** This analysis suggests that consideration of  $\text{NO}$ ,  $\text{NO}_2$  and  $\text{O}_3$  as a set of chemically-coupled species allows variation of (oxidant in the form of)  $\text{NO}_2$  as a function of  $\text{NO}_x$  to be explained on the basis of sources of oxidant and well-understood chemical processes. This allows new insights into the origins of site-to-site variations of  $\text{NO}_2$  vs.  $\text{NO}_x$  curves, by decoupling differences which are due to variations in the time available for chemical processes (for example, the reaction of  $\text{NO}$  with  $\text{O}_3$ ) from those which are due to variations in the sources of oxidant (OX), for example, the fractional contribution of primary  $\text{NO}_2$ . The methodology potentially enables predictions that take account of future changes in regional oxidant (i.e. the background  $\text{O}_3$  level), or local oxidant inputs which might arise, for example, from modifications in vehicle emissions control technologies or fleet composition.

**Figure 5.21** The calculated influence of changing the regional background oxidant level (B) and the local oxidant contribution (A) on the variation of  $\text{NO}_2$  with  $\text{NO}_x$  at London Bloomsbury. Consistent with analysis in Table 5.4, variation with changing B carried out with  $A = 12.72\%$ ; variation of A carried out with  $B = 35.7$  ppb.



**541.** This is illustrated in Figure 5.21, using the London Bloomsbury site as an example. The figure shows the influence of varying the regional background oxidant level (B), and the local oxidant contribution (A) on the calculated  $\text{NO}_2$  vs.  $\text{NO}_x$  curves. In particular, these graphs show that increasing either A or B leads to greater  $\text{NO}_2$  concentrations for a given level of  $\text{NO}_x$ , such that the  $\text{NO}_x$  threshold corresponding to an annual mean  $\text{NO}_2$  concentration of  $40 \mu\text{g m}^{-3}$  (21 ppb) decreases. This is illustrated further in Figure 5.22, for combinations of B (in the range 35-40 ppb) and A (in the range 10-30% of  $\text{NO}_x$ ). The present day reference conditions for Bloomsbury ( $A = 12.7\%$ ;  $B = 35.7$  ppb) correspond to a point close to the high corner of the  $\text{NO}_x$  surface. The lowering of the  $\text{NO}_x$  threshold if and when either A or B (or both) are increased is indicative of the additional  $\text{NO}_x$  reduction that would be required to achieve the annual mean  $\text{NO}_2$  concentration of  $40 \mu\text{g m}^{-3}$  (21 ppb).

**Figure 5.22** The calculated influence of changing the regional background oxidant level (B) and the local oxidant contribution (A) on the NO<sub>x</sub> threshold corresponding to 21 ppb (40 µg m<sup>-3</sup>) NO<sub>2</sub> at London Bloomsbury.



**542.** Although this methodology allows the influence of these factors to be considered, it should be noted that it is limited to sites where measurements of O<sub>3</sub> and NO<sub>x</sub> are co-located. However, it is possible that the NO<sub>2</sub> vs. NO<sub>x</sub> dependence at additional sites possessing similar characteristics (for example, local traffic flows and vehicle fleet composition) may be adequately represented by inference.

### 5.3 Dispersion and small-scale models

#### 5.3.1 Introduction

**543.** The class of ‘Gaussian-type’ models covers a range of model types which are in widespread use across the UK and elsewhere. The main advantage of this general model type is that computer codes can be designed to be relatively straightforward to use by practitioners and they can also be constructed in a way that allows the impact of different physical/chemical factors to be readily understood.

#### 5.3.2 Dispersion processes

**544.** The first such models of this type were constructed to calculate concentrations of a pollutant emitted from a single point source but the general approach is easily extendable to line, area and volume sources and also to multiple sources. The basic Gaussian formulation for concentration *C* due to a pollutant emission rate *Q* in windspeed *U* is derived as a solution of the diffusion equation as

$$C(x, y, z) = \frac{Q}{2\pi U \sigma_y \sigma_z} \exp\left\{-\frac{1}{2}\left(\frac{(y - y_s)^2}{\sigma_y^2} + \frac{(z - z_s)^2}{\sigma_z^2}\right)\right\} \quad (1)$$

$\sigma_y$  and  $\sigma_z$  are the lateral and vertical standard deviations of the concentration distribution and are therefore a measure of its spread or cross section of the plume.

**545.** Strictly the expression (1) for the concentration distribution is only valid in a turbulent flow if it is assumed that turbulent diffusion can be represented by a constant turbulent diffusivity. However, it has been applied successfully in the atmospheric boundary layer where there are

rapid changes in the diffusivity especially with height. The expression is also valid only if  $C$  represents the mean concentration, that is the concentration averaged over times greater than the turbulent time scales but less than that associated with changing meteorology; typically it would be an hourly average concentration. For shorter averaging times the concentration will vary significantly from one averaging period to the next because of the random movement of the plume by turbulence and because of in-plume structure which occurs as the plume mixes with ambient air. Expressions similar to (1) have formed the basis both for discussions of dispersion and of many dispersion models. Referring to (2) we see that it describes the mean concentration in terms of the vertical and horizontal plume spreads, the mean wind speed, and a distribution about a plume centreline ( $y_s, z_s$ ) at downstream distance  $x$ . Since the plume spread and the location of the plume centreline depend on the mean and turbulent wind field the expression provides a mechanism by which concentrations can be approximately quantified in terms of the atmospheric boundary layer variables.

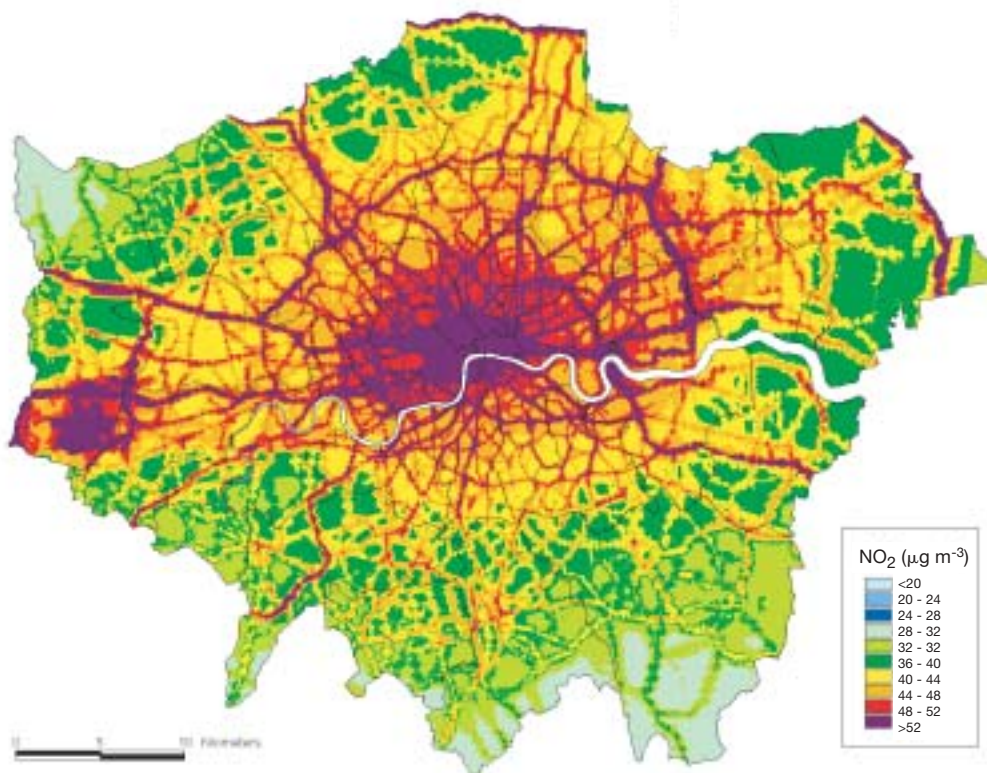
- 546.** In early dispersion models (for example, Pasquill and Smith, 1983; R91, ISC) the boundary layer structure was parameterised in terms of a single parameter, the Pasquill stability category, which typically varied from Category A (very unstable) through to D (neutral) to F or G (very stable). The plume spread parameters ( $z$  and  $y$ ) are then determined analytically as functions of stability category and distance downstream. More recent research has shown that one parameter is not sufficient to describe turbulence mixing satisfactorily since both mean flow and turbulence and hence dispersion vary significantly with plume height in the boundary layer. Thus more recent and advanced models (for example, OML, ADMS, AERMOD) parameterise the boundary layer structure in terms of two length scales, the boundary layer height ( $h$ ) and the Monin Obukhov length ( $L_{MO}$ ) a length scale dependent on mechanical mixing and the surface heat flux. Some models also employ more complex non-Gaussian formulae than (1) to describe the concentration profile normal to the ground. The use of these more physically based parameters ( $h, L_{MO}$ ) rather than Pasquill categories, also has the advantage that other effects on dispersion such as those of complex terrain can be treated within the model in a consistent manner since these effects can also be described in terms of the boundary layer variables.
- 547.** Many validation studies have been performed on dispersion models for point sources (for example, Hanna et al., 2001). These generally show the better performance of the models based on  $h$  and  $L_{MO}$ .

### 5.3.3 Practical dispersion models for calculating $\text{NO}_2$ concentrations

- 548.** Most practical dispersion models have features additional to those required for the dispersion of pollutants emitted from point sources. These include extensions to line source models (analytical or numerical integration of point source models) and sometimes area or volume sources, allowance for deposition and also inclusion of chemical routines. As with the basic formulation for  $\alpha_z, \sigma_y$ , levels of sophistication employed for additional source types vary greatly with, for example, some models employing simple 'virtual' upstream point sources to represent line or volume sources (for example, ISC, AERMOD) whilst others describe dispersion from elements within the source (for example, CALINE, ADMS). Models for dispersion from roads include different formulations for the impacts of street canyons or vehicle-induced turbulence.
- 549.** Models also include chemical schemes of very different levels of sophistication dependent on the intended model application. These range from no scheme, to empirical formulae, to the simple chemical reaction schemes, for example the Generic Reaction Set (GRS) used in ADMS, through to more advanced schemes such as CBM IV used in UAM.

- 550.** An analysis, using ADMS 3, of dispersion from point sources (Carruthers *et al.*, 2002) has shown that the chemical scheme employed can have a large influence on both peak and annual  $\text{NO}_2$  concentrations. For instance, the  $\text{O}_3$  limiting method which assumes all available  $\text{O}_3$  reacts with  $\text{NO}_x$  may result in much higher concentrations of  $\text{NO}_2$  than the GRS scheme which allows for reaction times and photodissociation of  $\text{NO}_2$ . In this study concentrations were also sensitive to the background concentration and the year of the meteorological data.
- 551.** The most advanced models, ADMS-Urban and AIRVIRO, can be used to calculate dispersion at high resolution over large cities. These systems include allowance for a large number of sources of each type, chemical reaction schemes and other advanced options (for example, ADMS-Urban nests the Gaussian-type model with a trajectory model, AIRVIRO offers an Eulerian flow and diffusion scheme as an alternative to a Gaussian model). These models also include emissions database and analysis facilities for manipulating emissions data and calculating emissions from raw activity data. They also usually include GIS functionality for input and display of model output. An example of the annual average  $\text{NO}_2$  concentration across London calculated using ADMS-Urban is shown in Figure 5.23.

**Figure 5.23** Annual average  $\text{NO}_2$  for 1999 across London calculated using ADMS-Urban.



### 5.3.4 Applications and limitations of dispersion models in urban areas

- 552.** The basic Gaussian plume formula (1) assumes that the turbulent flow is stationary, that is, the statistics of the boundary layer flow are assumed to remain constant over time. This means that the formulation is less effective when there are rapid changes in local weather conditions; it also limits the spatial range from sources for which the models might be expected to perform well, with the upper limit typically set at 30-50 km. Puff models or the nesting of Gaussian-type models within trajectory or Eulerian models are methods for overcoming these limitations.
- 553.** As discussed in Chapter 3, in urban areas the local mean flow and turbulence may change over small spatial scales due to the impact of building structure and local heating effects etc. In practical models such effects can be included, for example with variable surface roughness and/or street canyon models, although such parameterisations cannot describe the precise details of flow and dispersion and there is inevitably a degree of approximation at small spatial scales. The most commonly used practical street canyon model (OSPM, Berkowicz *et al.*, 1997) is widely used as a basis for many dispersion models of road traffic emissions in built up areas. This OSPM approach is based on the idealised model of a street as a long road enclosed along its length on both sides by buildings of equal height. The wind passing across the street induces a vortex or recirculating region in the street (Figure 5.24). As the canyon increases in width the vortex is confined to the leeward side of the canyon. The concentration consists of two components, the first resulting from direct emissions that contribute across the whole canyon and represented by a line source formulation, the second of pollutant recirculating in the vortex that of course only contributes in the vortex. OSPM requires only simple data from the user on the street dimensions, and wind strength and direction. The model parameterisation has been optimised and tested against experimental data collected in wind tunnel studies and in field campaigns in long uniform streets. Under these circumstances these models perform quite well.

**Figure 5.24** Example of the capability of computational fluid dynamics to model pollutant concentrations from vehicle exhaust – two-dimensional simulation of street canyon circulation in steady, horizontal incident flow.

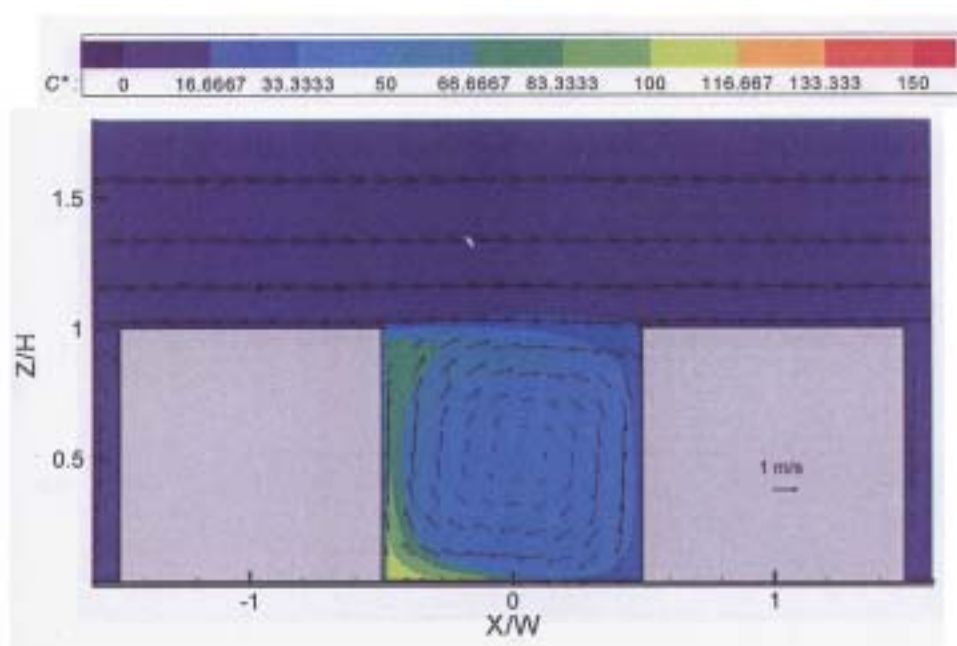
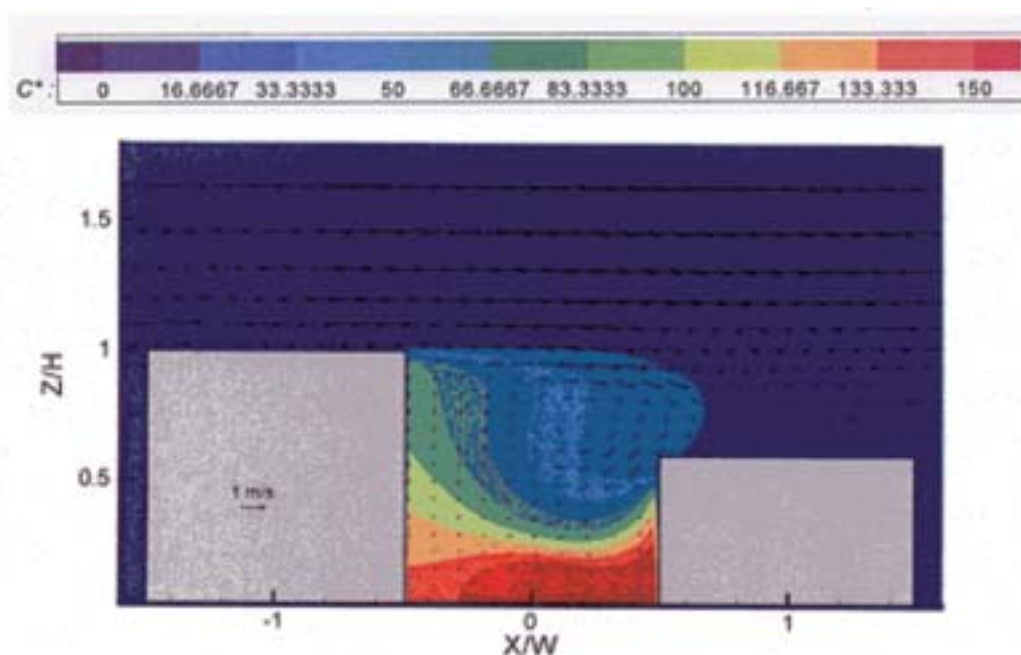


**Figure 5.25** Example of the capability of computational fluid dynamics to model pollutant concentrations from vehicle exhaust – asymmetrical canyon, showing marked influence of asymmetry when compared with Figure 5.24.



- 554.** However, most streets do not conform to these simple idealised forms, with buildings of uniform height along them. They also have intersections and cross-roads with air moving between streets as well as exchanging with air above the urban canopy. The effect of introducing asymmetry in the building heights of a street canyon is illustrated in Figure 5.25, where the vortex has been displaced and distorted, changing the ventilation potential of the street, and in this case enhancing. The 3-dimensional dispersion at, for example, a cross-roads, is even more complex- as illustrated in the work of Scaperdas *et al.* (2000). Here an analysis of the intersection between Marylebone Road and Gloucester Place explained a lot of the observed variability observed at the local monitoring station, but wind tunnel experiments and CFD studies illustrated the sensitivity to slight asymmetries and building configurations.
- 555.** The above illustrations are based on more complex computational fluid dynamics (CFD) modelling solving the detailed equations describing the physical flow and turbulence. Several codes of this type are available, and can treat three dimensional flows round quite complex building and street geometries, but they are computationally very demanding, and require very detailed input. They are also more difficult to interpret. For these reasons and because the evidence of validation (for example, Carruthers *et al.*, 2003) is that approximations used in practical models can be sufficiently accurate for air quality assessments and policy analysis, practical models are routinely used for complex urban environments.

### 5.3.5 Validation and verification of dispersion models and intermodel comparison

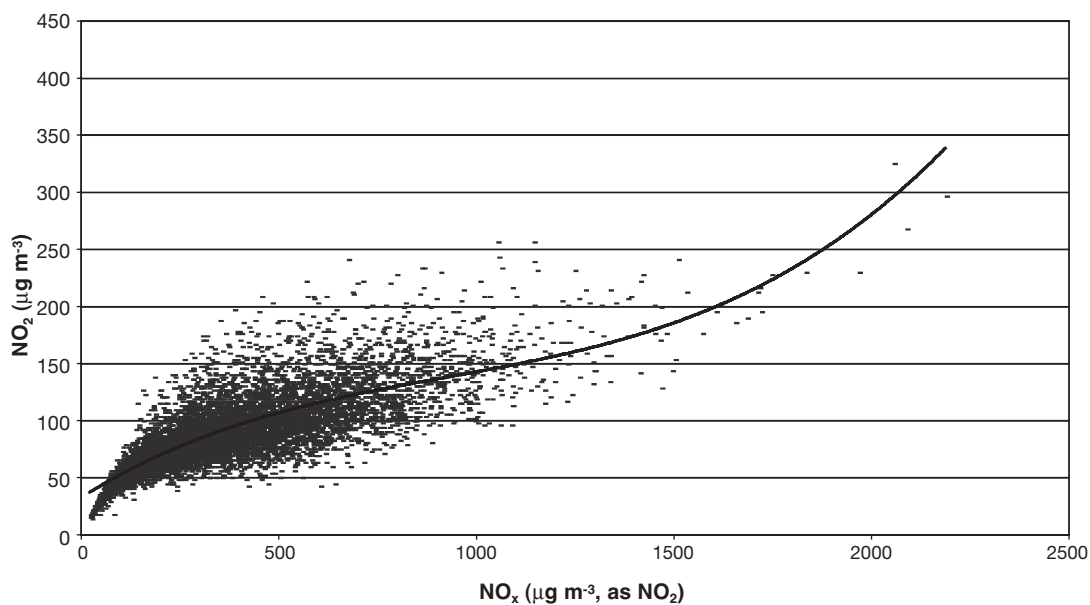
- 556.** It is important to distinguish between model validation and verification. Model validation generally refers to detailed peer-reviewed studies that have been carried out by the model developer or regulatory agency (for example, Environment Agency or USEPA). Models in general use in the UK have been subject to these detailed and documented validation trials.
- 557.** Model verification generally refers to checks on the model performance that are carried out at a local level or application to a study. Such verification studies may result in adjusting input parameters to improve fit with measured data (for example, surface roughness, MO length etc), by improvements to the emissions data, or by selection of the meteorological data.
- 558.** Comprehensive validation and verification is a prerequisite for using models to predict air pollutant concentrations. This section describes validation of ADMS-Urban, a Gaussian-type model which has been used for and on behalf of more than 80 UK local authorities and is currently being used for modelling studies of the major UK conurbations. This process has included validation in London and also comparisons with two empirical models, the national empirical model (Section 5.2.1) and the ERG model (Section 5.2.3).
- 559.** The validation study utilised the latest emission inventory for London which is for 1999, meteorological data recorded at Heathrow airport, and rural background pollution for  $\text{NO}_x$  and  $\text{O}_3$  from sites at Harwell, Rochester, Wicken Fen and Lullington Heath. A detailed validation study including model performance statistics derived from the predicted hour by hour concentrations was conducted using hourly data from the 24 AURN sites across London. Table 5.5 summarises the validation of annual mean concentrations for  $\text{NO}_x$  and  $\text{NO}_2$  calculated from  $\text{NO}_x$  using the GRS scheme. These show the generally good agreement between model and data with all comparisons showing appreciably less than 30% divergence as specified in the Air Quality Daughter Directive. The overall fractional bias showed a 2% underprediction. The model was also able to broadly reproduce the dependence of  $\text{NO}_2$  on the  $\text{NO}_x$  concentration at the monitoring sites; see for example Figure 5.26.

**Table 5.5** Monitored and calculated (ADMS-Urban) average NO<sub>2</sub> and NO<sub>x</sub> concentrations at London sites (1999).

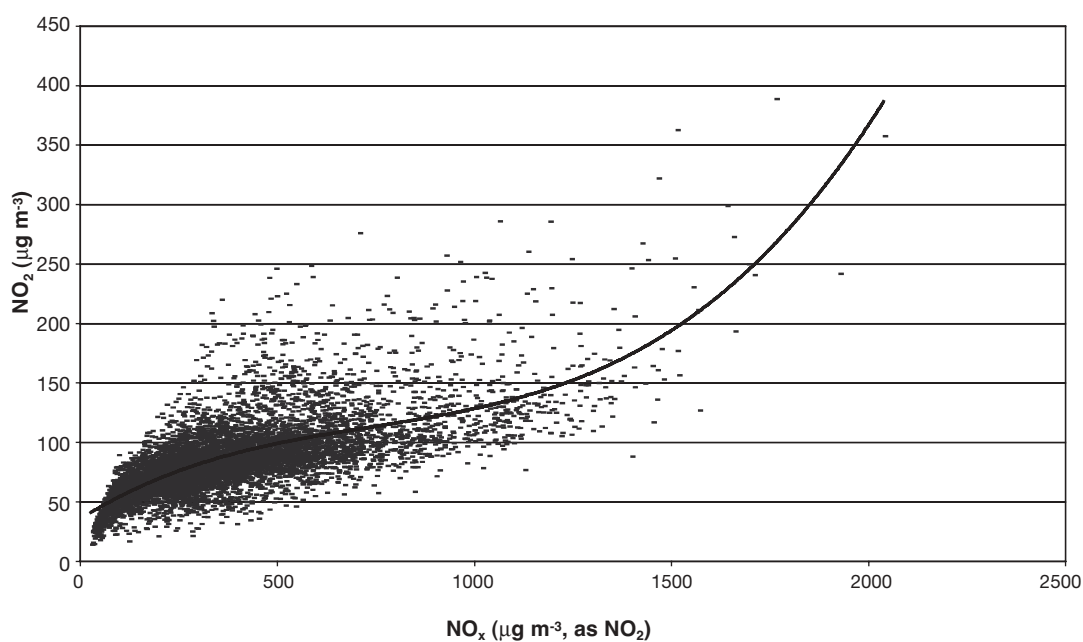
|                        | Annual average NO <sub>x</sub> concentrations (µg m <sup>-3</sup> ) |            | Annual average NO <sub>2</sub> concentrations (µg m <sup>-3</sup> ) |            |
|------------------------|---|------------|---|------------|
|                        | Monitored   | Calculated | Monitored   | Calculated |
| A3                     | 257   | 230        | 58  | 67         |
| Camden                 | 211   | 205        | 66  | 71         |
| Cromwell Road          | 257   | 260        | 93  | 76         |
| Haringey               | 136   | 115        | 51  | 55         |
| Hounslow               | 192   | 132        | 60  | 53         |
| Marylebone Road        | 391   | 385        | 91  | 88         |
| Southwark roadside     | 228   | 186        | 75  | 67         |
| Sutton roadside        | 117   | 77         | 44  | 42         |
| Tower Hamlets          | 241   | 193        | 70  | 71         |
| <b>Roadside mean</b>   | <b>220</b>  | <b>189</b> | <b>68</b>   | <b>66</b>  |
| Bexley                 | 69  | 79         | 37  | 40         |
| Bloomsbury             | 136   | 119        | 67  | 57         |
| Brent                  | 67  | 77         | 37  | 44         |
| Bridge Place           | 105   | 109        | 63  | 53         |
| Eltham suburban        | 65  | 86         | 36  | 44         |
| Hackney                | 136   | 113        | 60  | 55         |
| Hillingdon             | 167   | 207        | 50  | 63         |
| Lewisham               | 140   | 117        | 54  | 55         |
| North Kensington       | 82  | 101        | 46  | 52         |
| Southwark urban centre | 119   | 100        | 56  | 50         |
| Sutton suburban        | 65  | 67         | 35  | 38         |
| Teddington             | 52  | 61         | 32  | 34         |
| Wandsworth             | 142   | 128        | 52  | 59         |
| West London            | 100   | 92         | 55  | 50         |
| <b>Background mean</b> | <b>103</b>  | <b>103</b> | <b>49</b>   | <b>50</b>  |
| <b>Overall mean</b>    | <b>149</b>  | <b>138</b> | <b>56</b>   | <b>56</b>  |

**Figure 5.26** Scatter plots of (a) monitored and (b) calculated hourly average  $\text{NO}_x$  and  $\text{NO}_2$  concentrations for Marylebone Road (1999).

(a) Monitored



(b) ADMS-Urban



**560.** The comparisons show generally good performance of models. However there are significant differences, in particular ADMS shows a greater ratio of  $\text{NO}_2$  to  $\text{NO}_x$  especially for 2005 projections; this results in a greater number of roads showing exceedence of  $40 \mu\text{g m}^{-3}$  in that year, see Table 5.6.

**Table 5.6** Comparisons of annual average NO<sub>2</sub> concentrations for 1999 (µg m<sup>-3</sup>) calculated using ADMS-Urban and the NETCEN and ERG methodologies.

|  |   | Measured Value | ADMS-Urban | NETCEN NAEI Background | NETCEN NAEI Roadside | NETCEN Site Specific | ERG       |
|--|---|----------------|------------|------------------------|----------------------|----------------------|-----------|
| Roadside monitoring sites                | A3 roadside   | 58             | 67         | 41                     | –                    | –                    | 61        |
|  | Camden roadside   | 66             | 71         | 46                     | 69                   | 66                   | 63        |
|  | Cromwell roadside                                       | 93             | 76         | 54                     | 70                   | 92                   | 73        |
|  | Haringey roadside                                       | 51             | 55         | 45                     | 49                   | 48                   | 50        |
|  | Hounslow roadside                                       | 60             | 53         | 44                     | 60                   | –                    | –         |
|  | Marylebone roadside                                     | 91             | 88         | 59                     | 83                   | 92                   | 80        |
|  | Southwark roadside                                      | 75             | 67         | 51                     | 66                   | –                    | –         |
|  | Sutton roadside   | 44             | 42         | 39                     | –                    | 44                   | –         |
|  | Tower Hamlets roadside                                  | 70             | 71         | 48                     | 58                   | 67                   | 61        |
|  | <b>All roadside sites mean</b>                          | <b>68</b>      | <b>66</b>  | <b>–</b>               | <b>–</b>             | <b>–</b>             | <b>–</b>  |
| <b>ERG roadside sites mean</b>           | <b>72</b>   | <b>71</b>      | <b>–</b>   | <b>–</b>               | <b>–</b>             | <b>65</b>            |           |
| Background monitoring sites              | Bexley suburban   | 37             | 40         | 37                     | –                    | –                    | 40        |
|  | Bloomsbury urban centre                                 | 67             | 57         | 63                     | –                    | 67                   | 65        |
|  | Brent urban background                                  | 37             | 44         | 42                     | –                    | –                    | 36        |
|  | Bridge Place urban background                           | 63             | 53         | 57                     | –                    | –                    | 57        |
|  | Eltham suburban   | 36             | 44         | 41                     | –                    | –                    | 40        |
|  | Hackney urban centre                                    | 60             | 55         | 46                     | –                    | –                    | 53        |
|  | Hillingdon suburban                                     | 50             | 63         | 45                     | –                    | –                    | 55        |
|  | Lewisham urban centre                                   | 54             | 55         | 43                     | –                    | –                    | –         |
|  | N Kensington urban background                           | 46             | 52         | 48                     | –                    | –                    | 48        |
|  | Southwark urban centre                                  | 56             | 50         | 47                     | –                    | –                    | 61        |
|  | Sutton suburban   | 35             | 38         | 39                     | –                    | –                    | –         |
|  | Teddington urban background                             | 32             | 34         | 40                     | –                    | –                    | 36        |
|  | Wandsworth urban centre                                 | 52             | 59         | 45                     | –                    | –                    | –         |
|  | West London urban background                            | 55             | 50         | 47                     | –                    | 55                   | 57        |
|  | <b>All background sites mean</b>                        | <b>49</b>      | <b>50</b>  | <b>46</b>              | <b>–</b>             | <b>–</b>             | <b>–</b>  |
| <b>ERG background sites mean</b>         | <b>49</b>   | <b>49</b>      | <b>47</b>  | <b>–</b>               | <b>–</b>             | <b>50</b>            |           |
| Roadside and background monitoring sites | <b>All AURN sites mean</b>                              | <b>56</b>      | <b>56</b>  | <b>46</b>              | <b>–</b>             | <b>–</b>             | <b>–</b>  |
|  | <b>Combined NAEI roadside and background sites mean</b> | <b>56</b>      | <b>56</b>  | <b>52</b>              |                      |                      |           |
|  | <b>All ERG AURN sites mean</b>                          | <b>57</b>      | <b>57</b>  | <b>–</b>               | <b>–</b>             | <b>–</b>             | <b>55</b> |

- 561.** A sensitivity analysis of model performance to input parameters showed relatively little sensitivity to model set-up parameters (minimum Monin Obukhov length, gridded emission source height, surface roughness) but greater sensitivity to changes in the emission inventory, the met data site and the meteorological year – the latter mainly impacted on concentration through significant changes in the pollutant background concentrations.
- 562.** Comparisons between ADMS-Urban, National Empirical Model and ERG methodology have also been conducted at sites across London for both current (1999) emissions and for future projections. Table 5.6 and Figure 5.27 give such a comparison of annual mean  $\text{NO}_2$  for 1999 emissions at both roadside and urban background sites. Table 5.7 presents percentage of road segments exceeding a range of defined concentration thresholds of  $\text{NO}_x$  and  $\text{NO}_2$ , and finally Figure 5.28 presents scatter plots of comparisons of  $\text{NO}_2$  concentrations on road segments calculated by ADMS and ERG methodologies. As detailed in sections 5.2.3 and 5.3, the ERG and ADMS methodologies are able to calculate concentrations at defined receptor points whereas the NETCEN methodology, section 5.2.1, calculates a simple representative value for concentrations close to the road. This is used for both receptor point concentration and concentrations representative of the road segment. Thus care is required in the interpretation of the comparisons.

**Figure 5.27** Comparison of measured 1999 annual average pollutant concentrations with values predicted at AURN Sites by ADMS-Urban, NETCEN and ERG for (a)  $\text{NO}_x$ , (b)  $\text{NO}_2$ .

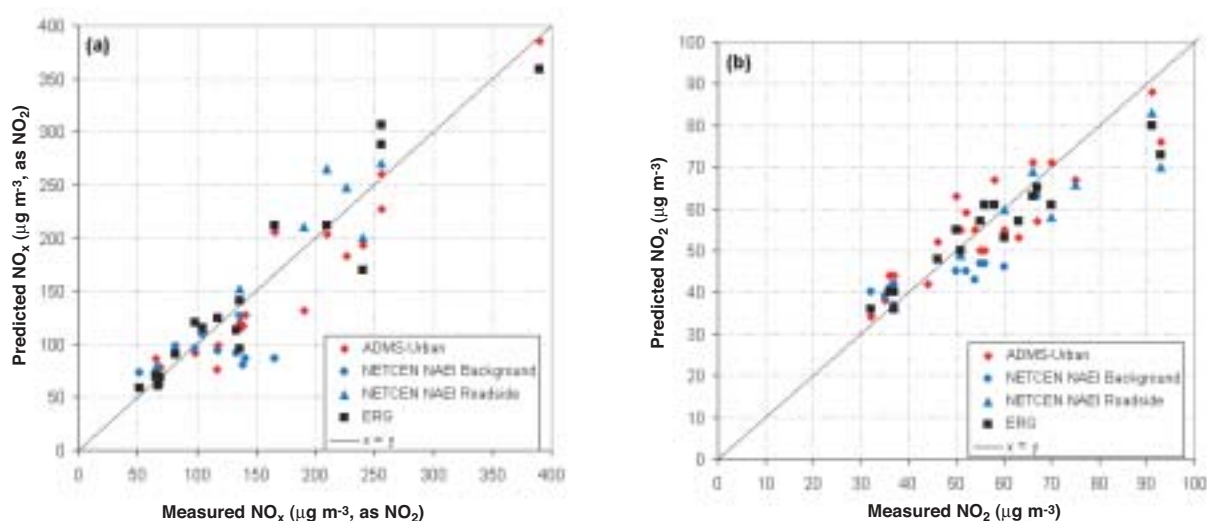
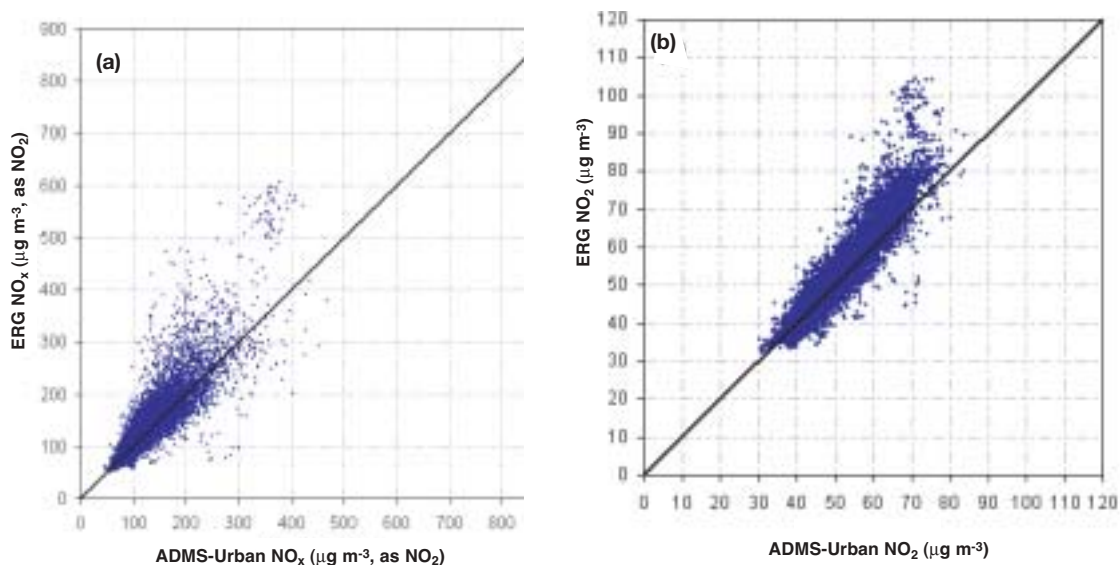


**Figure 5.28** Comparison of annual average NO<sub>x</sub> and (b) NO<sub>2</sub> concentrations predicted on road links between ADMS – Urban and ERG for 1999.



**563.** The comparisons between models and data show generally good performance of models. However there are differences, in particular ADMS shows a greater ratio of NO<sub>2</sub> to NO<sub>x</sub> and somewhat higher NO<sub>2</sub> concentrations at roadside; this results in a greater number of roads showing exceedence of 40 µg m<sup>-3</sup> in that year, see Table 5.7. Further comparisons of the three methodologies are presented in Chapter 7. These show divergence of model predictions for future years and significant differences in the predicted areas of exceedence of the NO<sub>2</sub> annual limit value.

**Table 5.7** Percentage road length exceeding specified annual mean values.

|  | ADMS-Urban |           | ERG  |
|--|------------|-----------|------|
|  | 1999       | 2004/2005 | 1999 |
| NO <sub>x</sub> >30 µg m <sup>-3</sup> | 100        | 100       | 100  |
| NO <sub>x</sub> >40 µg m <sup>-3</sup> | 100        | 98        | 100  |
| NO <sub>x</sub> >50 µg m <sup>-3</sup> | 99         | 83        | 100  |
| NO <sub>x</sub> >60 µg m <sup>-3</sup> | 90         | 56        | 98   |
| NO <sub>2</sub> >20 µg m <sup>-3</sup> | 100        | 100       | 100  |
| NO <sub>2</sub> >30 µg m <sup>-3</sup> | 100        | 97        | 100  |
| NO <sub>2</sub> >40 µg m <sup>-3</sup> | 87         | 59        | 84   |
| NO <sub>2</sub> >50 µg m <sup>-3</sup> | 39         | 16        | 42   |

## 5.4 Applications of Lagrangian trajectory models

### 5.4.1 The LRCTM Model for NO<sub>2</sub> in London

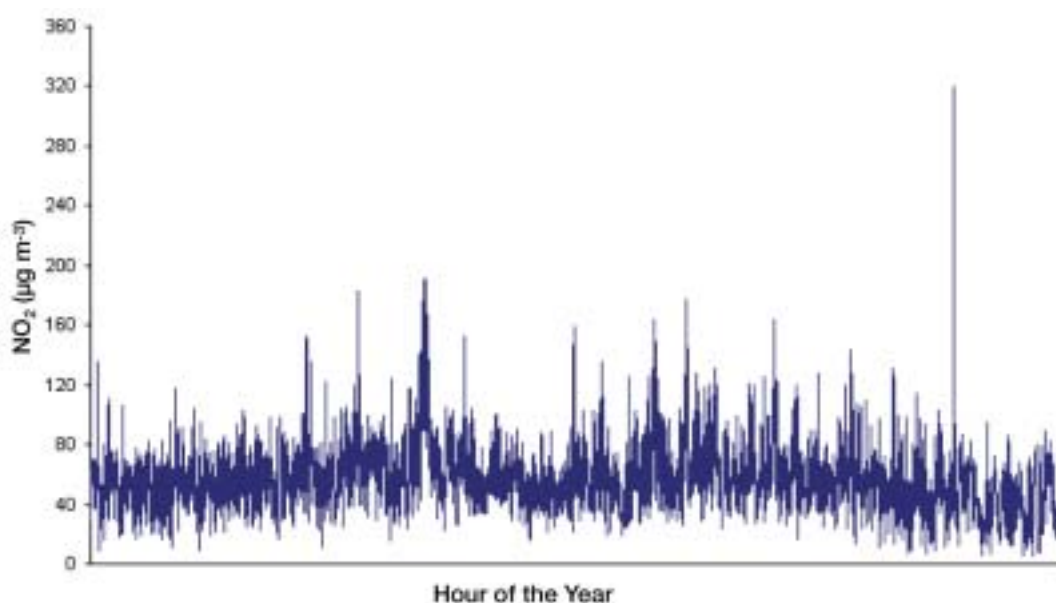
**564.** The London Routine Column Trajectory Model LRCTM (Derwent, 1999) adopts a Lagrangian trajectory approach in which a column of air is advected into an arrival point within the London conurbation. The column of air is divided into 21 layers in the vertical and is advected along a 6-hour trajectory using sequential meteorological data for Heathrow Airport for 1995. Trajectories are initialised using hourly O<sub>3</sub> data for Harwell, Lullington Heath and Sibton for each

day of 1995. The model includes dry deposition and chemistry and describes the height and spatial distributions of NO, NO<sub>2</sub> and O<sub>3</sub> at a spatial scale of 1 km x 1 km across London using either the NAEI or ERG-GLA LAEI NO<sub>x</sub> emission inventories for 1999, 2005 and 2010.

**565.** The LRCTM model identifies and describes in some detail the following major sources of NO<sub>2</sub> in London:

- direct emission of NO<sub>2</sub> from NO<sub>x</sub> sources, assumed to be 5% by volume in the base case model;
- oxidation of NO by O<sub>3</sub> advected into the model from the northern hemisphere baseline or from regional-scale photochemical pollution events;
- oxidation of NO in the NO + NO + O<sub>2</sub> reaction in local-scale wintertime stagnation events.

**Figure 5.29** Annual time series of model calculated NO<sub>2</sub> concentrations for an urban background location in central London using 1999 LAEI NO<sub>x</sub> emissions.

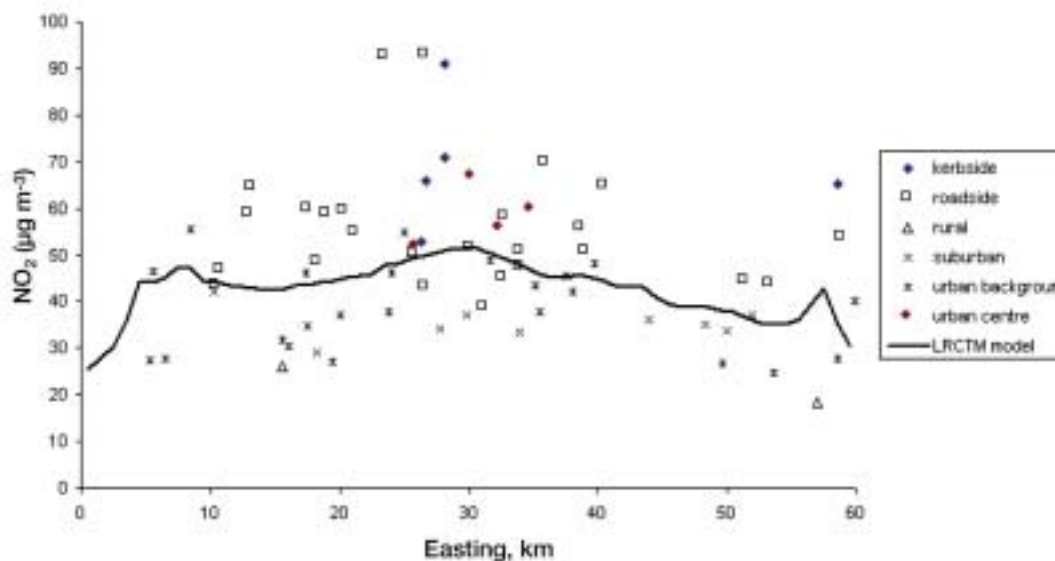


**566.** Figure 5.29 presents the annual time series of model hourly NO<sub>2</sub> concentrations for a typical urban background location in central London in the base case model using the 1999 LAEI NO<sub>x</sub> emission inventory. The plot illustrates the presence of both a local-scale wintertime stagnation event, which occur particularly during November and December and the summertime regional-scale O<sub>3</sub> transport episodes, particularly during the period May to August.

#### 5.4.2 Model validation

**567.** The LRCTM results on an annual average basis have been carefully compared with observations of NO<sub>2</sub> in Figure 5.30 for a selection of sites which form a west-east transect across London. The comparison has been made for the model surface level by averaging the results across a 10 km width, centred on Westminster. The model is well able to account for the observed variations in NO<sub>2</sub> concentrations along the transect, showing the step up from the rural values on the fringe of the London conurbation. The influence of the M25 corridor is clear at the easterly and westerly ends of the transect, with the peak at the westerly end somewhat higher; reflecting the added influence of Heathrow Airport. The model curve rises towards the centre of London and shows a significant portion of the transect above the 40 µg m<sup>-3</sup> annual NO<sub>2</sub> air quality standard.

**Figure 5.30** Observed annual mean  $\text{NO}_2$  concentrations for 1999 at various sites and the model results for a 10 km wide transect from west to east across London, centred on Westminster using the 1999 LAEI  $\text{NO}_x$  emission inventory.



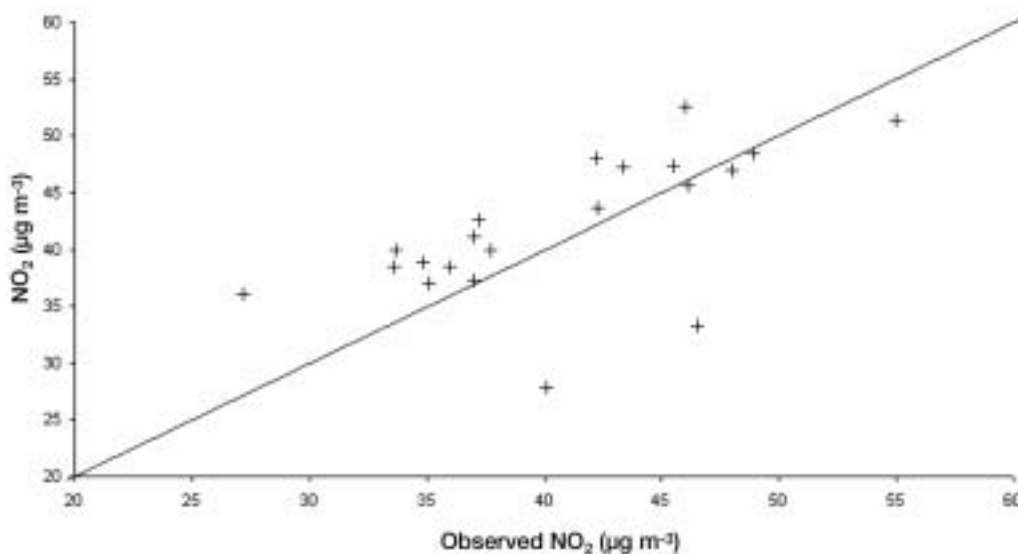
**568.** The model results appear to overestimate considerably the majority of the observed  $\text{NO}_2$  concentrations for the sites marked as suburban and rural, and to underestimate the concentrations for the sites marked as roadside and kerbside sites. Model performance appears much better against the urban background sites. These comparisons are entirely consistent with the model's use of a 1 km x 1 km  $\text{NO}_x$  emission inventory. The model appears to be able to describe many of the major features of the observed distribution of  $\text{NO}_2$  at urban background locations across London.

**569.** Table 5.8 describes a more detailed evaluation of the model predictions for suburban and urban background sites against the available observations for 1999. The mean model  $\text{NO}_2$  concentrations was  $42.9 \mu\text{g m}^{-3}$  compared with the observed concentrations of  $41.4 \mu\text{g m}^{-3}$ . The mean bias was therefore about  $1.5 \mu\text{g m}^{-3}$ , representing a mean percentage bias of 3.7%. The normalised mean square error was 0.02 and all of the points fell within a factor of two of the observations. The scatter plot of model vs. observations is illustrated in Figure 5.31 and was characterised by a correlation coefficient,  $r_2$  of 0.51, indicating a good correlation between model and observation. Altogether these comparisons indicate a satisfactory level of model performance and indicate that the LRCTM model is able to describe the major features influencing the distribution of  $\text{NO}_2$  across London.

**Table 5.8** Comparison of observed and model calculated annual mean NO<sub>2</sub> concentrations for a range of suburban and urban background sites for 1999.

| Site Name                              | Category         | Observed ( $\mu\text{g m}^{-3}$ ) | Model ( $\mu\text{g m}^{-3}$ ) |
|--|------------------|-----------------------------------|--------------------------------|
| Bexley 2 – Belvedere                   | Suburban         | 33.7                              | 40.0                           |
| Bexley 5 – Bedonwell                   | Suburban         | 35.1                              | 37.0                           |
| Enfield 1 – Bushhill Park              | Suburban         | 33.6                              | 38.5                           |
| Haringey 2 – Priory Park               | Suburban         | 37.2                              | 42.6                           |
| Hounslow 2 – Cranford                  | Suburban         | 42.2                              | 48.0                           |
| London Bexley                          | Suburban         | 37.0                              | 37.3                           |
| London Eltham                          | Suburban         | 36.0                              | 38.5                           |
| Brentwood – Town Hall                  | Urban background | 40.1                              | 27.8                           |
| Ealing 1 – Ealing Town Hall            | Urban background | 46.0                              | 45.7                           |
| Enfield 3 – Salisbury School           | Urban background | 37.7                              | 39.9                           |
| Harrow – Stanmore                      | Urban background | 34.8                              | 38.9                           |
| Heathrow Airport                       | Urban background | 55.4                              | 60.7                           |
| Hertsmere Background<br>(Borehamwood ) | Urban background | 27.2                              | 36.1                           |
| Islington – Upper Street               | Urban background | 48.9                              | 48.4                           |
| London Brent                           | Urban background | 37.0                              | 41.1                           |
| London N. Kensington                   | Urban background | 46.0                              | 52.6                           |
| Three Rivers Background                | Urban background | 46.5                              | 33.4                           |
| Tower Hamlets – Bethnal Green          | Urban background | 43.4                              | 47.3                           |
| Tower Hamlets 1 – Poplar               | Urban background | 45.5                              | 47.4                           |
| Waltham Forest – Dawlish Road          | Urban background | 42.3                              | 43.7                           |
| West London                            | Urban background | 55.0                              | 51.4                           |
| Newham Tant Avenue                     | Urban background | 48.0                              | 46.9                           |

**Figure 5.31** Scatter plot of model predicted annual mean NO<sub>2</sub> concentrations and the observed concentrations at suburban and urban background sites during 1999.

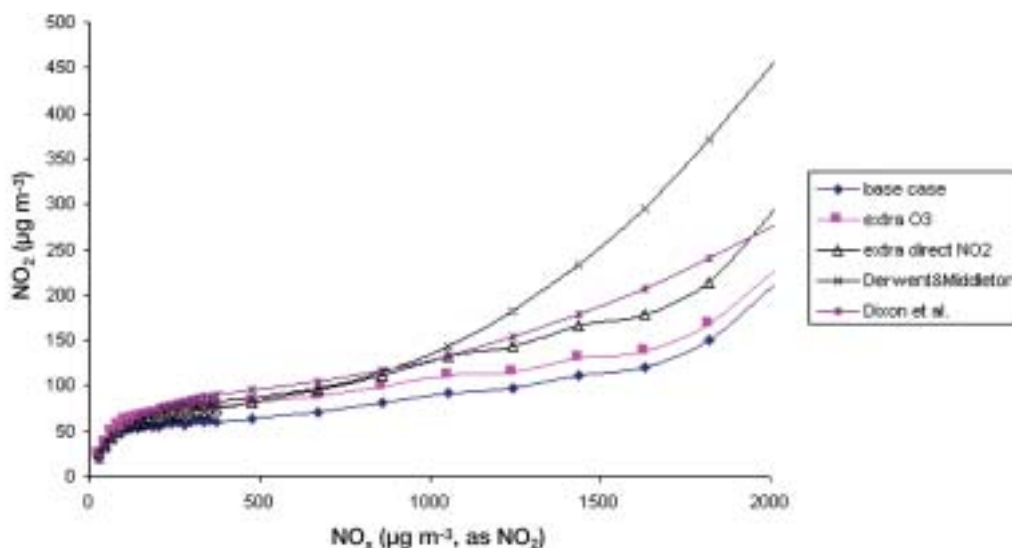


### 5.4.3 Comparison with empirical models

**570.** An important application of the LRCTM model has been to provide some underpinning to the empirical models used in policy formulation. An important feature of the observations of NO<sub>2</sub> and NO<sub>x</sub> has been that there appears to be a simple relationship between the amount of NO<sub>2</sub> that is present in a polluted air mass and the NO<sub>x</sub> concentration. Empirical curves have been derived of the ‘so-called’ NO<sub>2</sub> vs. NO<sub>x</sub> relationship (Derwent and Middleton, 1996; Dixon *et al.*, 2001). These empirical curves have been derived by sorting the hourly NO<sub>x</sub> concentrations in ascending order and determining the mean NO<sub>2</sub> concentrations for each NO<sub>x</sub> concentration. Plots of the resulting NO<sub>2</sub> vs. NO<sub>x</sub> relationship from the data are shown in Figures 5.32 and 5.33. Here the observed NO<sub>2</sub> vs. NO<sub>x</sub> relationship for Exhibition Road, London during the annual period which contained the 1991 pollution episode, is presented together with the relationship obtained by combining all the sites and years between 1991 and 1997 in London and the West Midlands.

**571.** Also shown in Figure 5.32 is the NO<sub>2</sub> vs. NO<sub>x</sub> relationship obtained by sorting the model results in exactly the same manner as the observations. There is a clear similarity in shape and form between the model and observed NO<sub>2</sub> vs. NO<sub>x</sub> relationships.

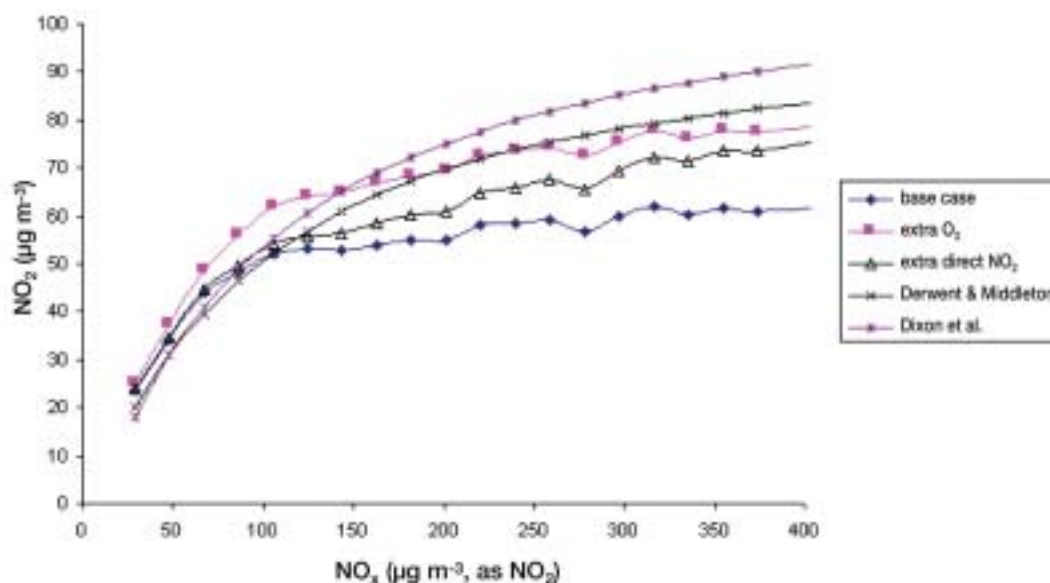
**Figure 5.32** Observed and model derived NO<sub>2</sub> vs. NO<sub>x</sub> relationships across the entire range of hourly NO<sub>x</sub> concentrations.



**572.** To illustrate the main source of  $\text{NO}_2$  in London, Figure 5.32 and 5.33 show two additional model sensitivity cases in addition to the base case model results. The sensitivity case marked 'extra  $\text{O}_3$ ' addresses the difficulties associated with initialising the  $\text{O}_3$  concentrations in the air parcels before they enter the London conurbation. Although it is straightforward to initialise the surface  $\text{O}_3$  concentrations using observed rural concentrations, it is difficult to know how to initialise the  $\text{O}_3$  concentrations throughout the vertical profile. Undoubtedly there is more  $\text{O}_3$  aloft than close to the surface but there are no observed  $\text{O}_3$  vertical profiles with which to initialise the model accurately. In the sensitivity case, an extra  $20 \mu\text{g m}^{-3}$  of  $\text{O}_3$  was added across the vertical profile and this produced a dramatic shift in the  $\text{NO}_2$  vs.  $\text{NO}_x$  relationship derived from the model results. Figures 5.32 and 5.33 show the results from the base case and the 'extra  $\text{O}_3$ ' sensitivity cases across the entire range of  $\text{NO}_x$  concentrations.

**573.** The second sensitivity case in Figures 5.32 and 5.33 shows the impact of doubling the fraction by volume of the  $\text{NO}_x$  emitted as  $\text{NO}_2$  from 5 to 10% by volume. Again this sensitivity case generates a different shape  $\text{NO}_2$  vs.  $\text{NO}_x$  relationship to the base case, indicating the importance of the direct emission of  $\text{NO}_2$  in determining the model-calculated  $\text{NO}_2$  concentrations. Clearly the model fit is improved at the highest  $\text{NO}_x$  concentrations with the higher direct emissions of  $\text{NO}_2$ . However, there is little information with which to fix this important model input parameter.

**Figure 5.33** Observed and model derived  $\text{NO}_2$  vs.  $\text{NO}_x$  relationships across the lowest range of hourly  $\text{NO}_x$  concentrations.



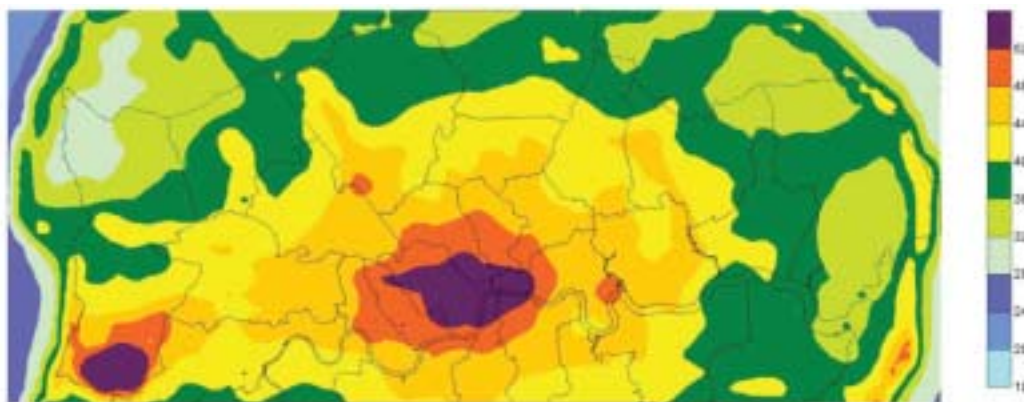
**574.** The close similarity between the  $\text{NO}_2$  vs.  $\text{NO}_x$  relationships derived from the model and from observations provides strong confirmation that the model is able to describe quantitatively the magnitudes of the sources of  $\text{NO}_2$  in London. Sensitivity studies point to the importance of direct emission of  $\text{NO}_2$  and oxidation by  $\text{O}_3$  as the two most important sources of  $\text{NO}_2$  in London. A third source becomes active under wintertime stagnation conditions through the  $\text{NO} + \text{NO} + \text{O}_2$  reaction.

#### 5.4.4 Assessment of current $\text{NO}_2$ air quality across London

**575.** The LRCTM model can be used to calculate the spatial distribution of annual mean  $\text{NO}_2$  concentrations at a spatial resolution of  $1 \text{ km} \times 1 \text{ km}$  across London as is shown in Figure 5.34. The mapped area contains 1560 grid squares of which 686 (44%) exceeded the  $40 \mu\text{g m}^{-3}$  annual mean air quality target. Exceedences are found in the vicinity of Heathrow Airport and across much of the centre of London. Peak model annual mean  $\text{NO}_2$  concentrations of

67  $\mu\text{g m}^{-3}$  are found in the vicinity of Heathrow Airport and 57  $\mu\text{g m}^{-3}$  in central London using the LAEI 1999  $\text{NO}_x$  emission inventory.

**Figure 5.34** Distribution of annual mean  $\text{NO}_2$  concentrations in  $\mu\text{g m}^{-3}$  calculated with the LRCTM model using 1999  $\text{NO}_x$  emissions from the LAEI inventory.



## 5.5 Eulerian grid modelling

### 5.5.1 Modelling $\text{NO}_x$ and $\text{O}_3$ using the urban airshed model

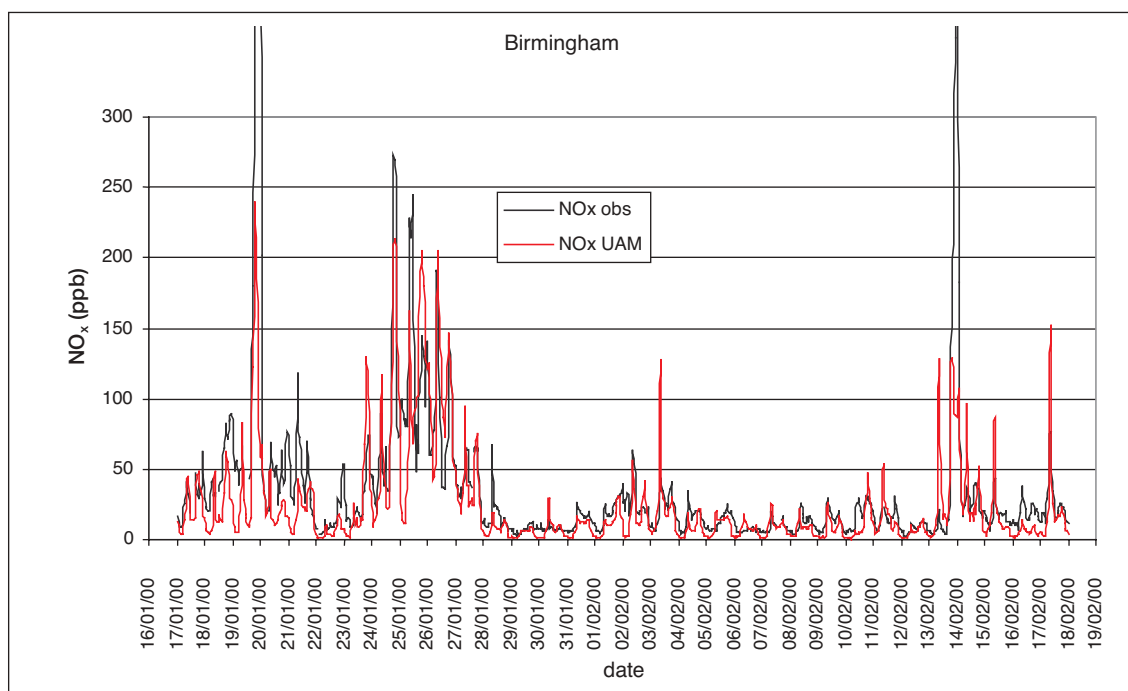
**576.** The Urban Airshed Model (UAM-IV) is an Eulerian air quality model developed in the United States for the prediction of  $\text{O}_3$  within polluted urban regions. The University of Birmingham has applied the model to predict primary and secondary pollutant concentrations across the West Midlands conurbation.

**577.** The model requires detailed hourly three-dimensional meteorological fields which were provided through running the Colorado State University RAMS (Regional Atmospheric Modelling System) model using two nested domains, the outer one covering much of England, whilst the inner one covering the West Midlands conurbation with a horizontal spatial resolution of 2 km and 31 vertical levels. For each 2 x 2 km grid square and each vertical level, the RAMS model predicts variables such as air temperature, pressure, wind speed, wind direction and turbulent kinetic energy (TKE). The calculation requires the meteorological information on the boundaries of the outer domain together with spatially disaggregated information on topography and land use types within the domain of the model. The RAMS model was validated in detail against measured data and provides an excellent simulation of hourly meteorological data. The depth of the atmospheric boundary layer was diagnosed from the vertical profile of TKE. The UAM model uses the meteorological fields of the inner domain.

**578.** In addition to meteorological drivers, the UAM model requires data on primary emissions of pollutants and the 1998 1 x 1 km inventory from the National Atmospheric Emissions Inventory was used across the modelled domain of the West Midlands. Diurnal variations in emissions from major sources such as road traffic were imposed on the inventory. Since the model relies upon an Eulerian formulation, for each time step, pollutants which are emitted and those already within the atmosphere are dispersed according to the level of turbulence and transferred between grid boxes in the model according to the three dimensional wind vectors predicted by the RAMS meteorological model.

- 579.** In addition to the advection and diffusion of primary pollutants, the model needs to account for atmospheric chemical change and accordingly it contains the CBM IV chemical scheme which is a highly condensed scheme using surrogate species to describe carbon bond types and molecules of similar behaviour. It was run with a horizontal resolution of 2 x 2 km and six vertical layers, four of which were in the boundary layer. For each time step in the model, the chemical scheme computes pollutant degradation and formation within each grid box, and the pollutants are then transferred between grid boxes at the end of the time step, as for unreactive primary pollutants. The model computes the atmospheric chemical changes in each 2 x 2 km grid box and for each of the six vertical levels as well as transferring materials between the boxes in response to the results of the meteorological model. Such simulations are highly computationally intensive.
- 580.** It was found particularly important to provide the model with hourly upwind boundary conditions representing pollutant concentrations on the upwind edge of the model domain. These were taken from campaign measurements where available and elsewhere from the nearest available National Network rural monitoring station.
- 581.** The model was run in order to simulate the results of monitoring campaigns which took place over periods of one-month duration in the summer of 1999 and the winter of 1999/2000. The predictions of NO<sub>x</sub> were generally good, with a slight under prediction in the summer and a very good reflection of true concentration magnitudes in the winter. The model had difficulty in reproducing exactly the hour-to-hour variation in NO<sub>x</sub>, but produced excellent simulations of average diurnal behaviour and reasonable representations of specific episodic conditions. The results for the winter campaign appear in Figure 5.35. In both summer and winter the model predicts rather lower NO<sub>2</sub>/NO<sub>x</sub> ratios than are actually observed, despite simulations of O<sub>3</sub> being generally good.

**Figure 5.35** Model and observed NO<sub>x</sub> concentrations at the Birmingham East site during January 2000.



**582.** Further examples of model output appear in Figures 5.36 and 5.37. In Figure 5.36, predictions of concentrations NO of at the Pritchatts Road site in south Birmingham over the period 24-28 January 2000 are compared with measurements. Also shown are measurements of atmospheric boundary layer depth (Zi) which clearly show the build-up of high NO concentrations when the boundary layer depth was low (200 m), with much reduced concentrations when the boundary layer deepened, especially towards the end of the monitoring period. Figure 5.37 shows the spatial distribution of NO, NO<sub>2</sub> and O<sub>3</sub> across the model domain at 16.00 on 24 June 1999, when the wind was in an easterly sector. Clear O<sub>3</sub> decrements and corresponding NO<sub>2</sub> formation are seen across central Birmingham and the Black Country corresponding to O<sub>3</sub> removal by reaction with traffic-generated NO<sub>x</sub>. Also clearly visible are O<sub>3</sub> decrements in the plumes downwind of major point sources to the east of the conurbation, together with NO<sub>2</sub> enhancements.

**Figure 5.36** Measured and modelled nitric oxide and boundary layer depths in Birmingham, 24-28 January 2000 from UAM.

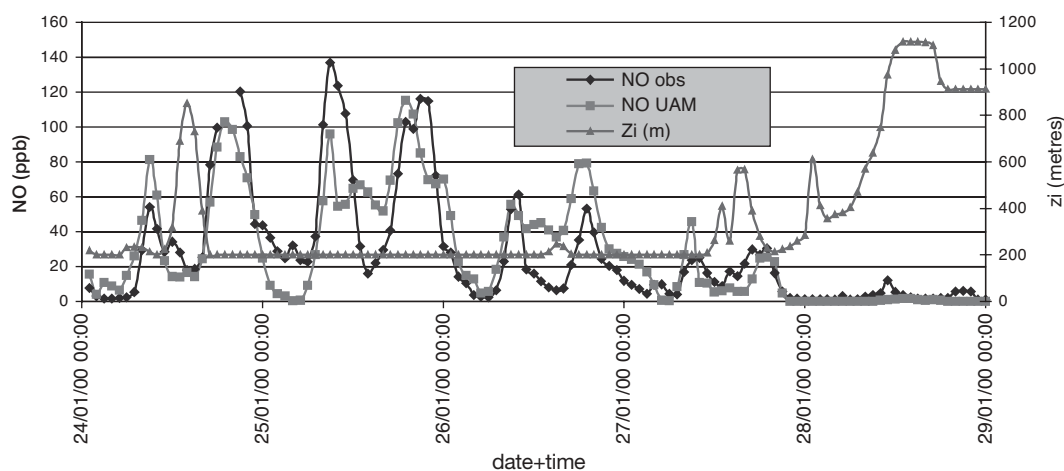
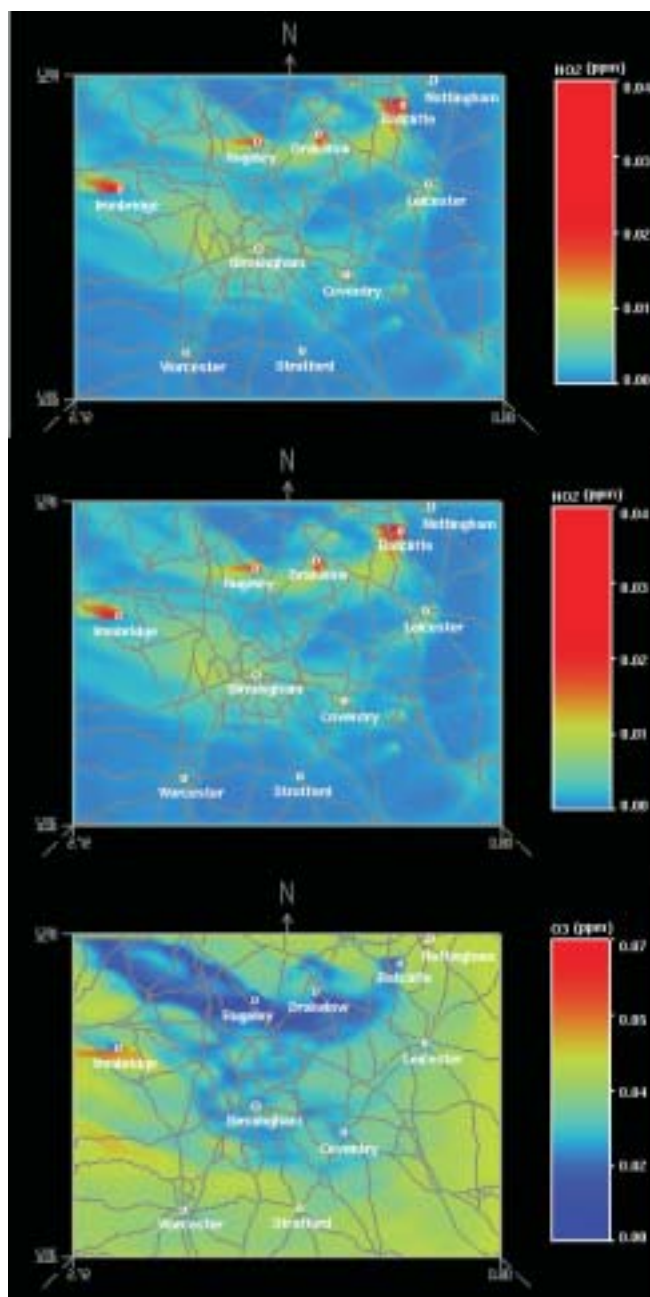


**Figure 5.37** Surface concentrations of NO, NO<sub>2</sub> and O<sub>3</sub> on 24th June 1999.



**583.** The work demonstrates that Eulerian modelling approach has considerable utility in predicting background concentrations of NO<sub>x</sub> within urban and rural areas. The model resolution is however insufficient to allow calculations for specific streets and urban hotspots.

## 5.6 Surface concentration mapping

### 5.6.1 Introduction

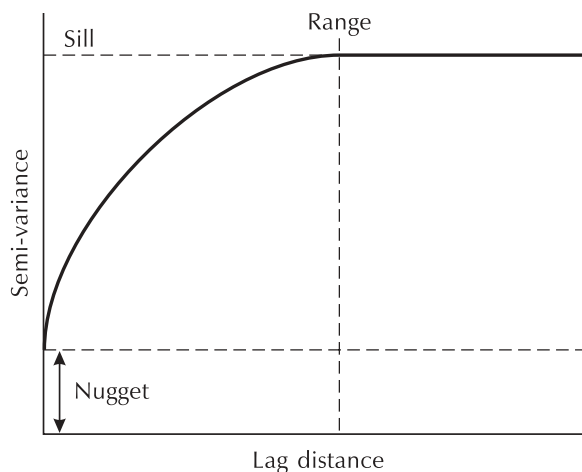
- 584.** Producing a spatial representation of NO<sub>2</sub> concentrations usually requires application of an interpolation procedure, i.e. the estimation of the concentration at an unsampled location using values at sampled locations (such as monitoring stations or dispersion model receptor points).
- 585.** A benefit of surface concentration modelling is the assessment of potential patterns of exposure to specific events, which can otherwise be difficult to estimate. Some techniques also enable generation of error and probability surfaces which can be used to assess the uncertainty in spatial estimates and/or the probability of concentrations exceeding air quality standards. Error estimations associated with an interpolated surface can help inform the location of new monitoring stations, which can in turn help provide a more accurate interpolated surface for future air quality assessments.
- 586.** Disadvantages to interpolation techniques include the difficulty of determining the 'best' interpolation procedure to use for a particular dataset and careful consideration of sample points to ensure that a valid air quality surface is produced. The main policy-related drawback is the lack of any direct future predication capability.

### 5.6.2 Techniques and characteristics

- 587.** Surface concentration modelling of NO<sub>2</sub> using interpolation assumes that the value of NO<sub>2</sub> at a particular point is likely to be more similar to the values at nearby sites than to the values at sites further away. The application of basic interpolation procedures only yields meaningful results if sample points have similar siting characteristics, and are not strongly influenced by specific local sources. It is therefore usual to use data relating to background sites as the basis of such an interpolation exercise. Resultant concentration surfaces indicate a 'broad brush' estimated pattern of background concentrations and do not estimate the influence of particular sources at individual locations, such as around major roads. The national maps produced using the methodology described in section 5.2 of this chapter provide greater spatial detail through the combination of interpolation techniques with other modelling procedures and additional datasets.
- 588.** This restriction does not necessarily apply to interpolating the output of dispersion models where surfaces are estimated from user-defined or automatically selected receptor locations. A regular sampling framework of an appropriate density or one which is developed to be sensitive to known patterns of change (for example, through specifying a higher density around major road links) enables estimates to be generated between points with reasonable confidence.
- 589.** There are numerous techniques available to interpolate monitoring data, each with different characteristics. The underlying interpolation algorithm selected always has an influence on the patterns of concentrations generated from the same input dataset (reference literature on GIS and geostatistics includes: Burrough and McDonnell, 1998; Isaaks and Srivastava, 1989). Although there is no universally accepted mechanism, there are a number of techniques that are commonly employed to map the spatial distributions of air quality data. Interpolation by kriging has been identified by a number of authors as a suitable technique (for example, Lefohn *et al.*, 1987; Phillips *et al.*, 1997).
- 590.** Kriging is a smoothing interpolator which uses regionalised variable theory. In its basic form it requires the spatial structure of the phenomenon under consideration to have the same patterns over the entire area being examined (stationarity). The nature of this pattern is

determined through analysis of a semi-variogram (Figure 5.38) which plots the difference in the magnitude of measured values between pairs of sample points as a function of the spatial separation of the points (the lag distance). If the data are spatially auto-correlated, the differences in values for sample pairs is less where the samples are closer together and higher where the sample pairs are further apart. Using the pattern of auto-correlation as a guide, a function is then fitted which best describes the observed relationship. This function will also help determine the range and the sill of the dataset, after which point differences are taken as random spatially uncorrelated noise. The data may also include a nugget value that represents uniform noise in the dataset, for example, as a result of measurement error.

**Figure 5.38** Characteristics of the semi-variogram



- 591.** Alternative standard interpolation methods include use of splines, which produce concentration surfaces where surface curvature is minimised between sample points, and inverse distance weighting in which values are estimated using samples in a specified neighbourhood, the nearer samples are the more weight they are assigned.
- 592.** Given that data patterns can exhibit large variability, as a result of source proximity, meteorology and chemical reactions, standard procedures may be inadequate due to an inability to account for different spatial structures within the same dataset. Consequently, variations of standard approaches have been developed (for example, Fuentes, 2001; Ionescu *et al.*, 2000)
- 593.** Exploratory data analysis is an important first stage of any interpolation exercise which helps to identify the statistical characteristics of the sample dataset and the presence of any outliers prior to surface generation. The results of interpolation procedures can be assessed in various ways, for example through a cross comparison of surfaces and their error statistics, or through a comparison of the relative influence of individual sample points. The former can help to identify the optimum surface from a set of possibilities, both in terms of different procedures and also in terms of other specific parameters such as the size and orientation of search neighbourhoods. The latter includes techniques such as cross validation of sample points using a leave-one-out procedure where predictions for known sample sites can be made through the application of the procedure with the remaining samples. This is useful to identify the particular influence of individual sites on the final surface and can be a further basis for the rejection of samples as outliers. Local knowledge can also be an important factor in the assessment of estimated surfaces.

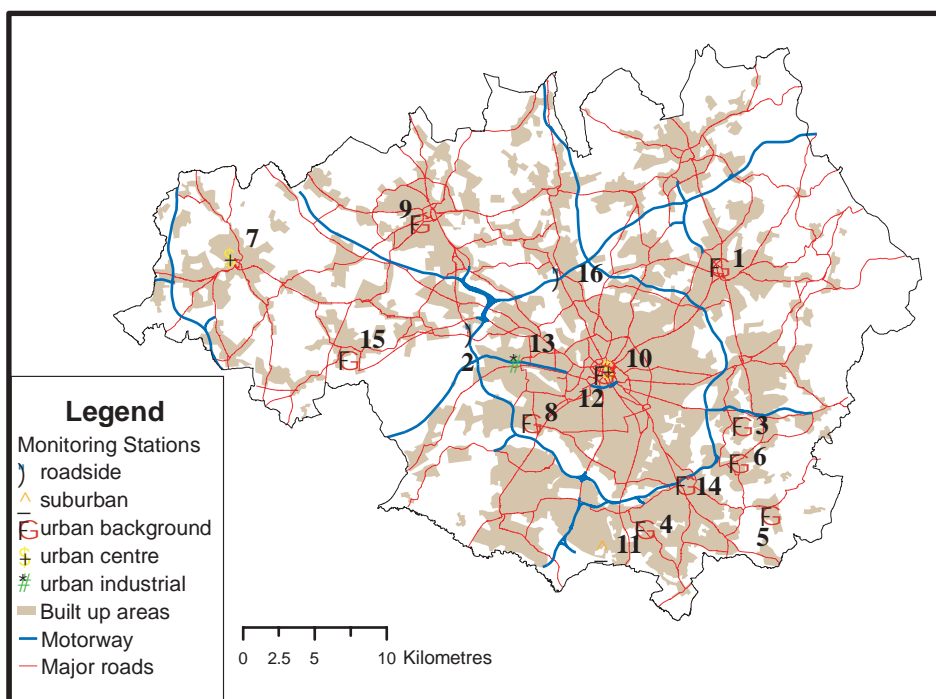
### 5.6.3. Urban scale interpolation

**594.** To illustrate some of the techniques and issues outlined above, concentration surfaces have been applied to the estimation of patterns of  $\text{NO}_2$  concentrations in the Greater Manchester conurbation, first during a winter-time episode in December 2001 and secondly for annual mean concentrations for 2001.

#### 5.6.3.1 Concentration modelling of episode conditions

**595.** As is discussed in section 6.5.3, elevated concentrations of hourly  $\text{NO}_2$  were experienced in a number of northern UK cities during the period of Tuesday 11th and Wednesday 12th of December 2001. In the conurbation of Greater Manchester, concentrations greater than  $200 \mu\text{g m}^{-3}$  were seen at many sites. A map of the location of sites is given in Figure 5.39. Peak hourly values and the time they were recorded for each site are shown in Table 5.9 and the full time series are shown in Figure 5.40. Although the peak value was experienced at the largest number of sites on the morning of the 12th December, the episode was characterised by a large range of values over relatively small spatial scales and short time periods. This makes the interpolation of concentration values particularly problematic.

**Figure 5.39** Location of automatic monitoring stations measuring hourly  $\text{NO}_2$  in Greater Manchester, 2001.



**596.** The sites to form the sample dataset, shown in Table 5.9, were selected primarily on the basis of their siting characteristics and the temporal patterns in concentrations over the period of interest. The urban industrial site at Salford Eccles is near to a relatively large point source of  $\text{NO}_x$  (which emitted 300 tonnes of  $\text{NO}_x$  during 2001) but since emissions from elevated sources are not likely to exert an influence during this type of winter-time, and the temporal pattern of concentrations was similar to neighbouring urban background sites (Figure 5.40(a) and (c)), this site was retained. Exploratory data analysis of specific hourly values suggested that the urban background sites of Stockport Bredbury (site no. 6) represents an extreme outlier for some of the hours during the time period and the temporal distribution of values was also found to be atypical compared to the remaining stations in the area. Although there is a strong case for exclusion of this site from the analysis it was included in the interest of completeness.

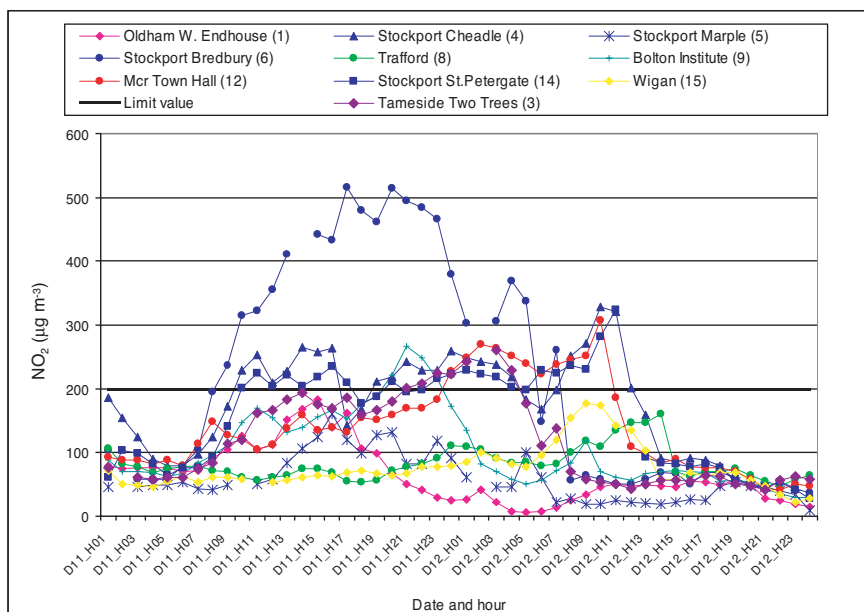
**597.** Three basic interpolation functions were used to assess the optimum function for surface generation: inverse distance weighting, splines and kriging. The very small number of sample data points in this case restricted the possibilities of using a more sophisticated approach. Since ordinary kriging requires normally distributed data for the generation of probability measures (but not for error and prediction surfaces), it was necessary to identify hours which showed a normal distribution (or which could be transformed to a normal distribution) for the creation of probability surfaces.

**Table 5.9** Peak hourly NO<sub>2</sub> concentrations 11/12/01 to 12/12/01 (µg m<sup>-3</sup>) monitored at AURN and Calclub+ sites in Greater Manchester.

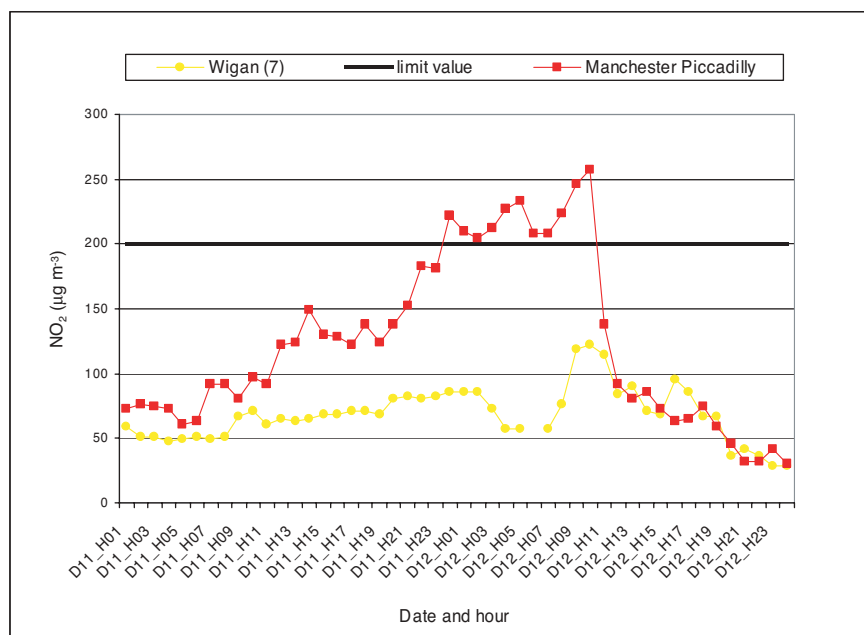
| Station | Siting           | District (Site name)      | Peak value | Peak hour   | No. hrs > 200 µg m <sup>-3</sup> | Modelled |
|---------|------------------|---------------------------|------------|-------------|----------------------------------|----------|
| 1       | Urban Background | Oldham (W. Endhouse) +    | 183        | 11/12 15:00 | 0                                | Y        |
| 2       | Roadside         | Salford (M60) +           | 275        | 12/12 11:00 | 9                                | N        |
| 3       | Urban Background | Tameside (Two Trees) +    | 262        | 12/12 15:00 | 7                                | Y        |
| 4       | Urban Background | Stockport (Cheadle) +     | 329        | 12/12 10:00 | 22                               | Y        |
| 5       | Urban Background | Stockport (Marple) +      | 160        | 11/12 16:00 | 0                                | Y        |
| 6       | Urban Background | Stockport (Bredbury) +    | 516        | 11/12 17:00 | 20                               | Y        |
| 7       | Urban central    | Wigan (Centre) +          | 122        | 12/12 10:00 | 0                                | Y        |
| 8       | Urban Background | Trafford (Background) +   | 160        | 12/12 14:00 | 0                                | Y        |
| 9       | Urban Background | Bolton (Institute)        | 267        | 11/12 21:00 | 4                                | Y        |
| 10      | Urban central    | Manchester (Piccadilly)   | 258        | 12/12 10:00 | 11                               | Y        |
| 11      | Suburban         | Manchester (South)        | 159        | 12/12 10:00 | 0                                | N        |
| 12      | Urban Background | Manchester (Town Hall)    | 308        | 12/12 10:00 | 11                               | Y        |
| 13      | Urban industrial | Salford (Eccles)          | 432        | 12/12 10:00 | 11                               | Y        |
| 14      | Urban Background | Stockport (St. Petergate) | 325        | 12/12 11:00 | 21                               | Y        |
| 15      | Urban Background | Wigan (Leigh)             | 178        | 12/12 09:00 | 0                                | Y        |
| 16      | Roadside         | Bury (M60)                | 311        | 11/12 23:00 | 10                               | N        |

**Figure 5.40** Time series of NO<sub>2</sub> concentrations across Greater Manchester 11th to 12th December 2001 at (a) urban background; (b) urban centre; and (c) other sites.

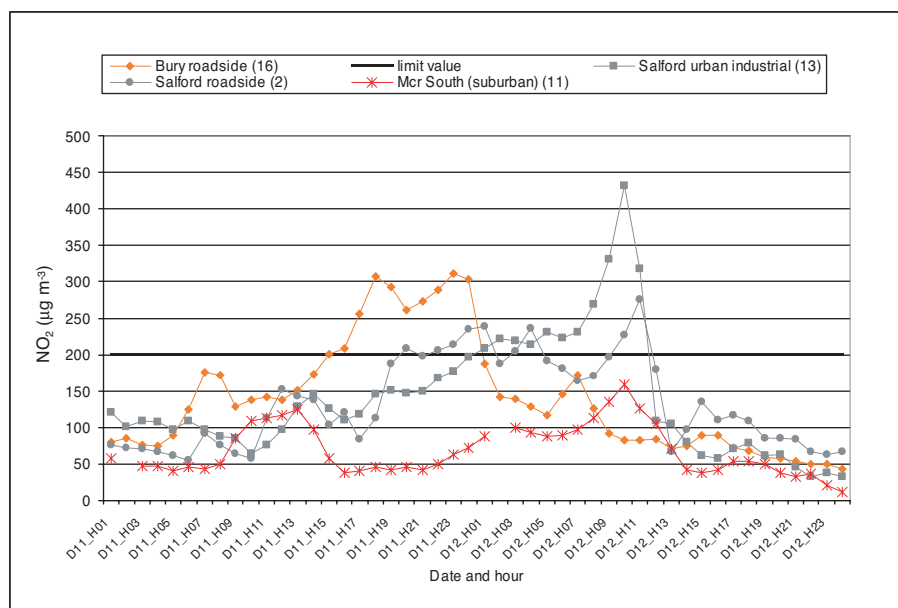
(a) urban background sites



(b) urban centre sites



## (c) Other sites

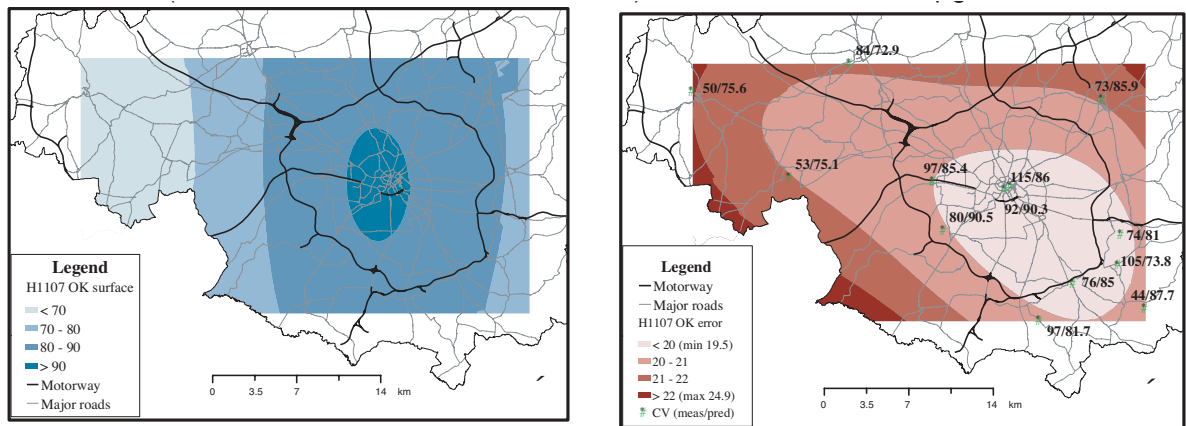


**598.** The results of a cross comparison of surfaces suggested that splines and ordinary kriging produced least overall error in the final surface estimates although the specific error and parameters in each case did vary according to the hour selected. In the interests of consistency, a time series of surfaces have been produced using ordinary kriging throughout, as this produced the optimum results for most of the hours tested. Examples of estimated  $\text{NO}_2$  concentration surfaces for 7 am, 2 pm, and 7 pm on 11th December and 7 am and 9 am on 12th December are shown in Figure 5.41. The morning of the 11th shows that Manchester city centre has the highest  $\text{NO}_2$  concentrations with a gradual fall-off towards the periphery of the conurbation, consistent with the annual average pattern of  $\text{NO}_2$  concentrations measured at the automatic sites in the area. By 2 pm concentrations of  $\text{NO}_2$  have increased considerably and begin to show a distinct pattern of high concentrations towards the south west. This pattern continues into the next day with very high concentrations by 9 am of the 12th. In the morning of the 12th there are also high concentrations in central Manchester which were less pronounced during the afternoon and early evening on the 11th. These surfaces only represent background concentrations. Concentrations of  $\text{NO}_2$  within 20-50 m of motorways and major roads (see section 6.3) are likely to be in excess of estimated background values whereas locations with a suburban characteristic are likely to exhibit lower concentrations.

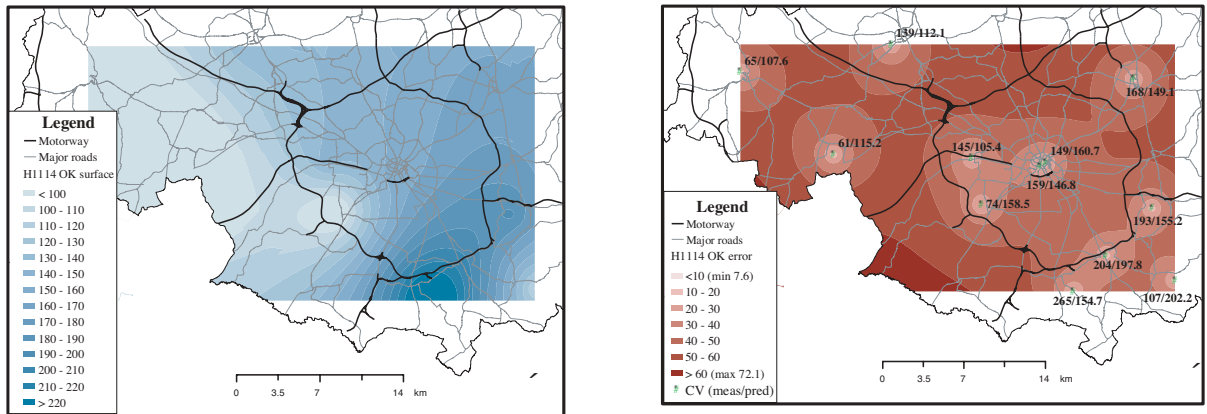
**599.** Figure 5.41 also provides error surfaces for each of the modelled hours. The most significant errors are associated with time periods with the highest concentrations. Cross-validation indicated large errors showing which particular stations have the most impact on the final surface generated.

**Figure 5.41** Selected hourly predicted NO<sub>2</sub> concentration (left-hand maps) and error surface concentration (right-hand maps). Cross validation values refer to measured/predicted values based on leave-one-out procedure.

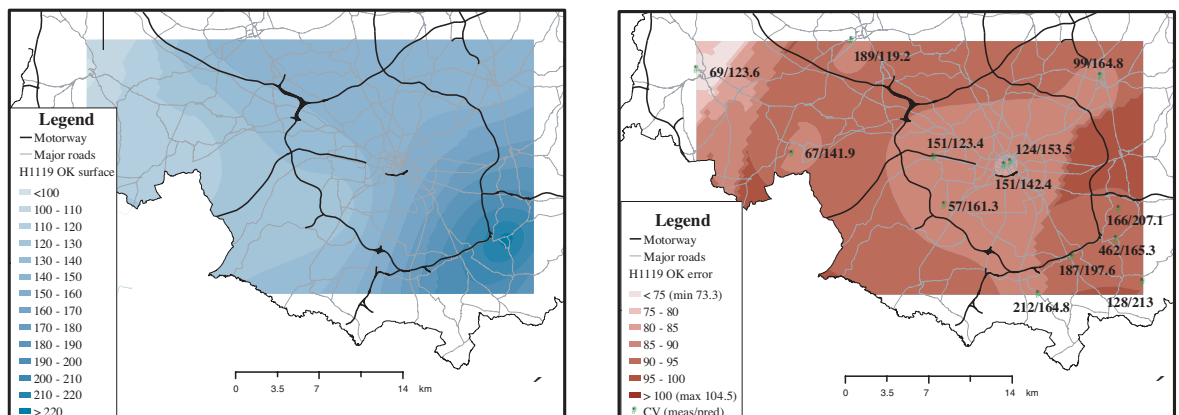
(a) 11th Dec 7am (monitored min 44, monitored max 115) – concentrations are in µg m<sup>-3</sup>.



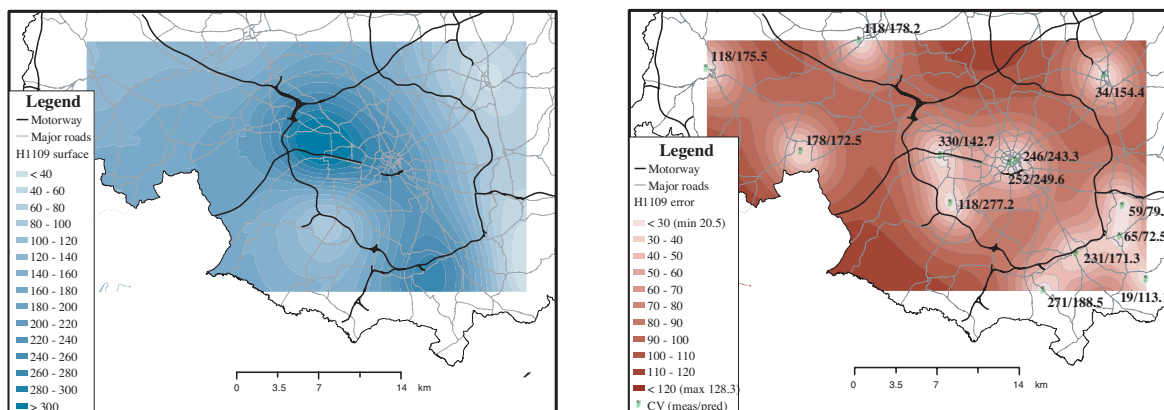
(b) 11th Dec 2pm (monitored min 61, monitored max 265). – concentrations are in µg m<sup>-3</sup>.



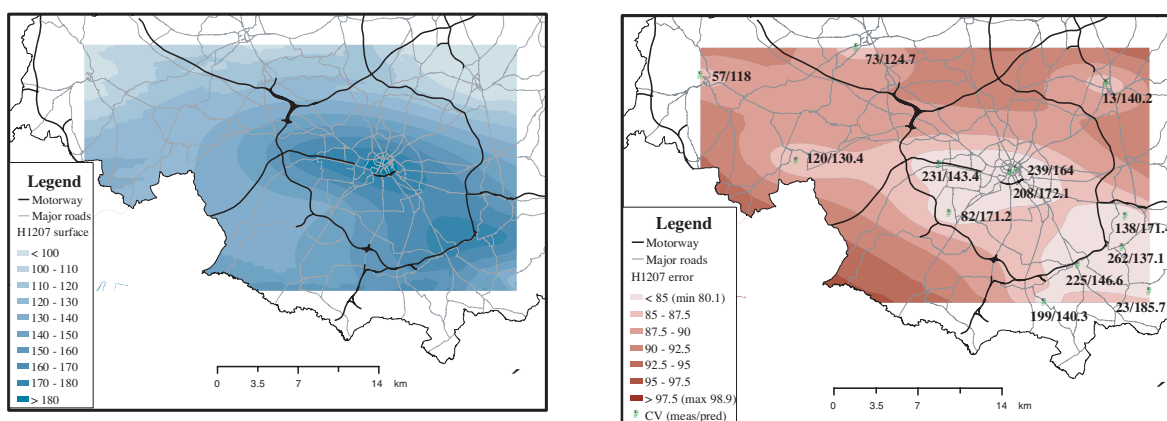
(c) 11th Dec 7 pm (monitored min 55, monitored max 210) – concentrations are in µg m<sup>-3</sup>.



(d) 12th Dec 7 am (monitored min 13, monitored max 262) – concentrations are in  $\mu\text{g m}^{-3}$ .



(e) 12th Dec 9 am (monitored min 19, monitored max 330) – concentrations are in  $\mu\text{g m}^{-3}$ .

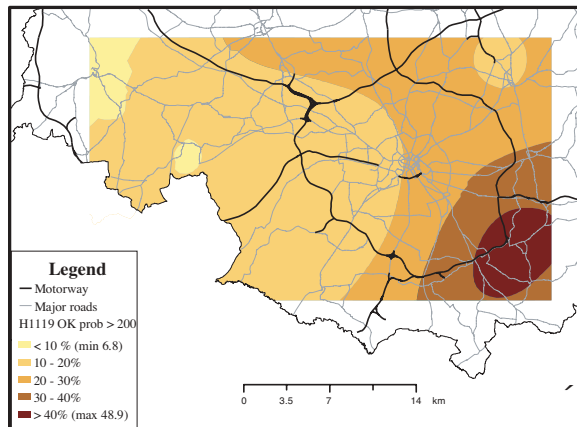
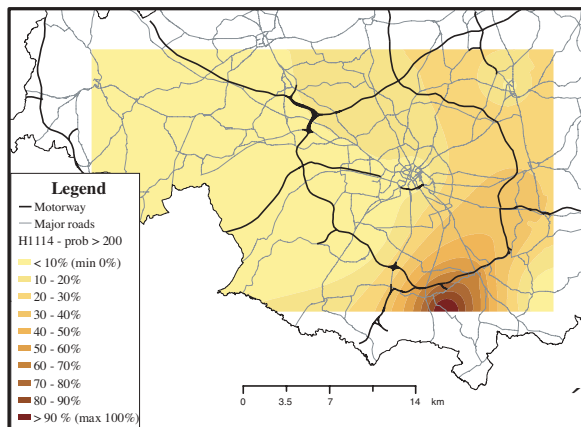


**600.** Illustrative probability maps for selected hours are shown in Figure 5.42, and indicate the estimated probability that  $\text{NO}_2$  concentrations exceeded  $200 \mu\text{g m}^{-3}$  at urban background locations over the conurbation at the times specified. As with the concentration maps, these probabilities do not relate to locations near to large local sources such as major roads and motorways.

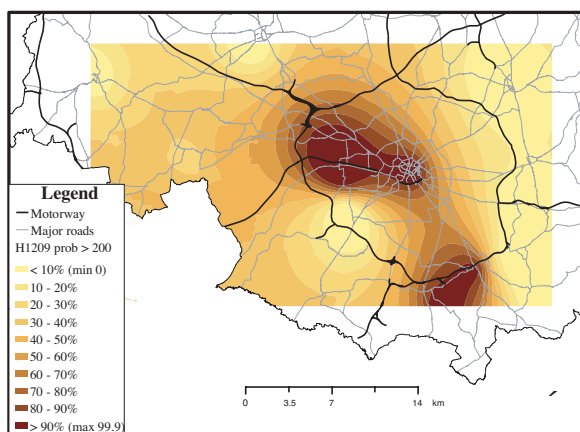
**Figure 5.42** Selected hourly probability surfaces for exceedence of  $200 \mu\text{g m}^{-3}$  during 11th and 12th December 2001 (%).

(a) 11th December 2pm

(b) 11th December 7pm



(c) 12th December 9am



**601.** This urban scale episode work has illustrated a number of issues raised in section 5.6.2 concerning the application of interpolation techniques to estimating surface concentrations of  $\text{NO}_2$ . The lack of sample points in this example restricts the level of sophistication with which procedures can be applied as well as the robustness of the data produced. The lack of points meant that it was not always possible to include anisotropy (directional) effects which can sometimes help to improve the robustness of predictions.

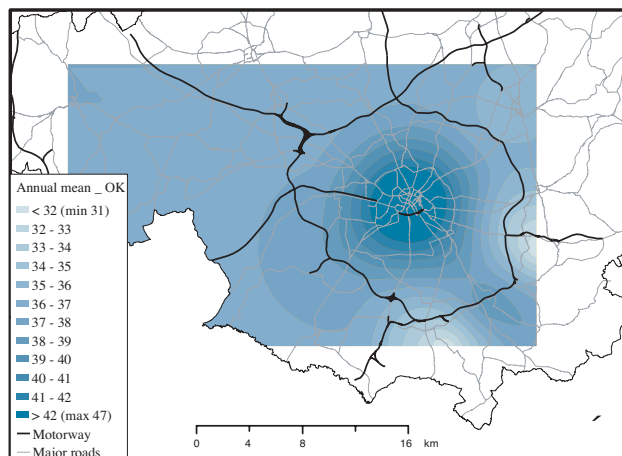
**602.** The very high variability in concentrations monitored at urban background locations in relatively close proximity (especially in Stockport in the south-west) suggests the strong influence of localised site characteristics (for example, proximity to source or topographic setting). The impact of these characteristics may be particularly important during winter-time episode conditions. Consequently the assumption of stationarity may not then hold for all the hours shown in this example.

### 5.6.3.2 Concentration modelling of annual means

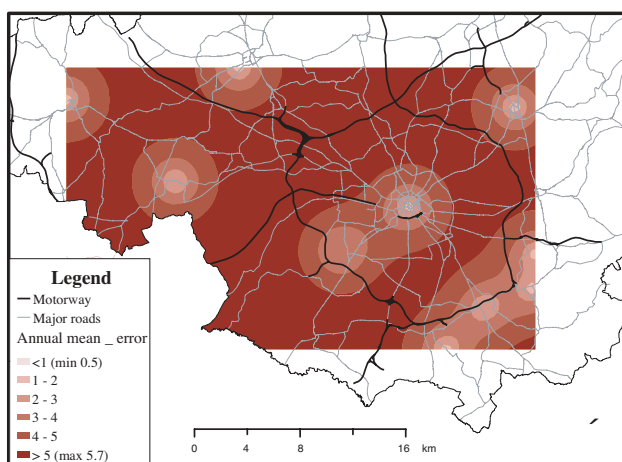
**603.** Spatial maps of annual average  $\text{NO}_2$  concentrations for the Greater Manchester have also been estimated for the sites indicated in Table 5.9 for 2001 using the same basic methodology described in the previous section. Prediction, error and probability surfaces are shown in Figure 5.43. These suggest that there was a very high probability that annual average concentrations of  $\text{NO}_2$  exceeded  $40 \mu\text{g m}^{-3}$  in many central Manchester locations in 2001. There is a higher overall confidence with annual mean data as can be seen from the error plots in Figure 5.43.

**Figure 5.43** Prediction, error and probability surfaces (exceedence of  $40 \mu\text{g m}^{-3}$ ) for annual average  $\text{NO}_2$  concentrations in Greater Manchester for the calendar year 2001.

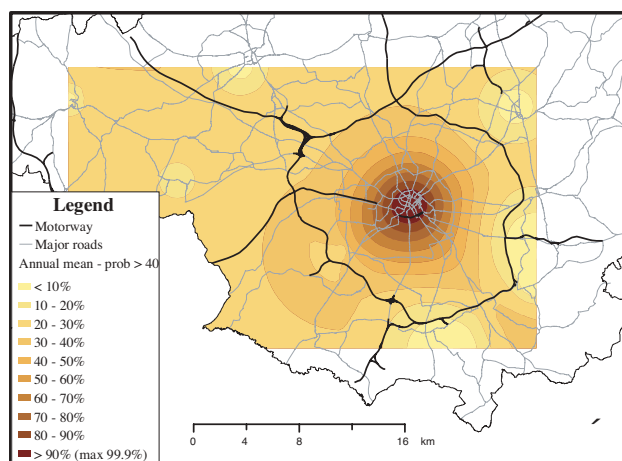
(a) Predictions – concentrations are in  $\mu\text{g m}^{-3}$



(b) error surface – concentrations are in  $\mu\text{g m}^{-3}$



(c) probability surface for exceedence of  $40 \mu\text{g m}^{-3}$  (%)



#### 5.6.4. National scale interpolation

- 604.** At the national scale, fine scale spatial variations are currently best represented with the dispersion model based semi-empirical techniques discussed earlier in this chapter.
- 605.** Measured annual mean concentrations of NO<sub>2</sub> at intermediate and urban background locations in the UK NO<sub>2</sub> Diffusion Tube Network have been routinely used by NETCEN to produce interpolated maps of urban background NO<sub>2</sub> concentrations produced throughout the UK, using a bilinear interpolation model (Loader *et al.*, 2002). The bilinear interpolation method creates a smoothed two-dimensional dataset from bilinear and quadratic functions on x, y, and z datasets. This interpolation method approximates existing points onto a grid (in this case 10 x 10 km), interpolates by linear interpolation, and then improves the estimation by computing gradients at the points using quadratic interpolations. It then refines the values using-distance weighting methods. The new surface smoothes the original data points, it will not necessarily pass through them.
- 606.** The same interpolation algorithm has been used since the network was commissioned in 1993, to ensure consistency for comparative purposes. As with the example of spatial mapping in the Manchester area, these maps only represent NO<sub>2</sub> concentrations at urban background locations and not at roadside or rural locations. Roadside measurements are not interpolated, as concentrations measured at such locations are likely to be representative of only very limited spatial areas.

#### 5.6.5. Summary and conclusions

- 607.** This section has provided an overview of interpolation procedures and their usage in terms of modelling surfaces of NO<sub>2</sub>. There are a variety of techniques available and no universally agreed methodology for application to air quality datasets. The examples have shown some of the specific considerations in applying interpolation to NO<sub>2</sub> values at the urban scale, many of which are directly applicable to surfaces produced for the national scale. These include a consideration of monitoring station siting characteristics as well as the extent, density and distribution of points in terms of monitored data or dispersion model receptor points. Although there are drawbacks and difficulties in the application of interpolation procedures, these are essential building blocks to many of the modelling procedures discussed in this chapter.